



URBAN DEVELOPMENT DIRECTORATE (UDD)

Government of the People's Republic of Bangladesh

**Geological Study and Seismic Hazard Assessment
Under
Preparation of Development Plan for Mirsharai Upazila, Chittagong
District: Risk Sensitive Landuse Plan (MUDP)**

Package No. 2 (Two)

Draft Final Report

August, 2018

Submitted by



Environmental & Geospatial Solutions (EGS)

Suite No.-6 ,12th Floor, 218, Sahera Tropical Center, Elephant Road, Dhaka-1205

EXECUTIVE SUMMARY

Urban Development Directorate (UDD) has decided to introduce suitable development plan for Mirsharai upazila. As such, UDD has initiated the project titled 'Preparation of Development Plan for Mirsharai Upazila, Chittagong District: Risk Sensitive Landuse Plan'. Geological Study and Seismic Hazard Assessment is one of the important development module of this project. In this development plan, subsurface geological and geotechnical information's consider as an important tool for a durable and sustainable urbanization.

In this project work, both the geophysical and geotechnical investigations have been conducted. The duration of the project is (19th December, 2017 to 18th September, 2018). In geotechnical survey 85 numbers of SPT boring (up to 30m) has been conducted in the field and the soil samples also collected from the field and laboratory tests have been completed. And in geophysical Survey, fifteen (15) Downhole Seismic (PS Logging), twenty (20) Multi-channel analysis of surface wave (MASW), and thirty (30) Microtremor (single array) have been investigated by using some sophisticated instruments.

However, subsurface 3D model of different layers has been developed through Geotechnical investigation, which will be updated eventually by integrating other data set. According to Standard Penetration Test's (SPT) N-value, layer 3 and layer 5 consider as a foundation layer. Moreover, the concern foundation layer contains velocity is more than 180m/s. According to MASW and Drownhole seismic test results S-wave velocity more than 180 m/s varies from 6.3m to 12.5m depth, which is suitable for foundation. Foundation depth should be varies from around 6m to 15m in overall Mirsharai Upazila.

This study is an attempt towards refinement in seismic hazard calculation of Bangladesh using PSHA methods. Results are presented in form of hazard maps and curves showing PGA and SA. Peak ground acceleration has been computed with 2% and 10% probability exceedance in 50 years. In this study both peak ground acceleration (PGA) and peak spectral acceleration (PSA) have been estimated considering with and without site effect. However, the ground motion has found much higher than all other previous studies. The reason might be due to the utilization of appropriate Ground Motion Prediction Equation for different fault zones and utilization of Vs30 information of Mirsharai to account for the site effect.

It should be noted that there is room for further improvement in tackling the uncertainties of many other source parameters and attenuation models. This study will contribute towards further seismic hazard assessments in Bangladesh and also facilitate in reducing seismic risk in structures by updating building codes in the country.

However, the project area Mirsharai is not that much landslide prone. Landslide susceptibility map is produced by the weight of evidence method in order to show the degree of influence of each causal factors with past landslide occurrence. Overall the area lies in low to moderate landslide susceptible prone area. Most of the area lies within very low to low landslide susceptible area (about 85%). The remaining project area is mostly in moderate landslide prone zone.

Nasim Ferdous

Nasim Ferdous

Team Leader and Coordinator
Engineering Geology and Geotechnical Unit
Email: ferdous.nasim1@gmail.com
Environmental & Geospatial Solutions (EGS)

Abbreviations

ASTM : American Society for Testing and Materials

AVS30 : Average Shear Wave velocity of 30 meter depth

BH: Borehole

MASW : Multi-Channel Analysis of Surface Wave

N value : Soil resistance or compactness

PGA : Peak Ground Acceleration

PS logging : Primary and Shear wave logging (Down-hole seismic test)

SA : Spectral Acceleration

SPT : Standard Penetration Tests

UDD: Urban Development Directorate

EGL : Existing Ground Level

GWL : Ground Water Level

PSHA: Probabilistic Seismic Hazard Assessment

CONTENTS

1. INTRODUCTION.....	4
1.1. Background	4
1.2. Location and Accessibility	5
1.3. Aims and Objectives	6
2. METHODOLOGY	6
2.1. Strategic Methodology	6
2.2. Detail Procedures Of Survey/Testing	8
2.2.1. Test Detail And Procedure Of Downhole Seismic Test (Ps Logging).....	9
2.2.2. Test Detail And Procedure Of Multi-Channel Analysis Of Surface Wave (MASW)...	15
2.2.3. Test Detail And Procedure Of Microtremor Measurement (Single Microtremor)	22
2.2.4. Standard Penetration Test (SPT) Method	23
3. GEOLOGY OF THE STUDY AREA	26
3.1. Surface Geology.....	26
3.2. Subsurface 3D model of different layers through Geotechnical investigation.....	29
3.3. Subsurface cross-section	33
4. SEISMIC HAZARD ASSESSMENT	39
4.1. Study Area.....	40
4.2. Methods.....	42
4.3. Results and Discussion.....	54
4.4. Engineering Geological Mapping	61
4.4.1 Shear Wave Velocity Estimation	62
4.4.2. Soil Type Determination based on Vs30	67
4.5. Building Height Map.....	70
5. LANDSLIDE SUSCEPTIBILITY ASSESSMENT	73
5.1. Methodology	76
5.1.1. Method Introduction	76
5.1.2. Landslide Inventory Preparation	77
5.2. Landslide Hazard Analysis	77
5.3. Landslide Susceptibility Mapping.....	91
5.4. Results and Discussions	94
6. CONCLUSION	98
7. REFERENCES.....	100

LIST OF FIGURES

FIGURE 1.1 LOCATION MAP OF THE PROJECT AREA	5
FIGURE 2.1 FIELD DATA ACQUISITION BY PS LOGGER	9
FIGURE 2.2 MAIN COMPONENT OF THE FREEDOM DATA PC	10
FIGURE 2.3 RECEIVER ORIENTATION IN SINCO CASING	10
FIGURE 2.4 CALCULATION OF SHEAR WAVE VELOCITY BY DOWN HOLE SEISMIC, WHERE R_1 =DISTANCE BETWEEN SOURCE TO TOP GEOPHONE AND R_2 =DISTANCE BETWEEN SOURCE TO BOTTOM GEOPHONE	10
FIGURE 2.5 TO SET THE WOODEN PLANK 1.0 METERS FROM A BOREHOLE	11
FIGURE 2.6 TO ATTACH THE TRIGGER TO A HAMMER.	11
FIGURE 2.7 TO CONNECT THE AIR PUMP WITH A BATTERY.	11
FIGURE 2.8 TO CONNECT THE COMPUTER WITH CABLES WHICH ARE CONNECTED TO THE GEOPHONE.	12
FIGURE 2.9 MAKE SURE THAT THE AIR BAG AT THE GEOPHONE WORKS. THEN, PUT THE GEOPHONE INTO THE BOREHOLE AND FIX THE SAFETY ROPE WITH THE HOLDER.....	12
FIGURE 2.10 HIT THE WOODEN PLANK IN 3 DIRECTIONS WHICH ARE ON THE LEFT, RIGHT AND VERTICAL DIRECTIONS..	13
FIGURE 2.11 TRIAXIAL GEOPHONE BEHAVIOR.	13
FIGURE 2.12 P WAVE AND S WAVE IN THE COMPUTER WINDOW	13
FIGURE 2.13 ARRIVAL OF S WAVE	13
FIGURE 2.14 FREEDOM DATA PC WITH P-SV DOWNHOLE SOURCE AND 1 TRI-AXIAL GEOPHONE RECEIVER USED IN CROSSHOLE SEISMIC INVESTIGATIONS	15
FIGURE 2.15 MASW DATA PROCESSING (PARK ET AL., 1999).....	16
FIGURE 2.16 RAYLEIGH WAVE DISPERSION IN LAYER MEDIA (RIX, 1988)	17
FIGURE 2.17 SCHEMATIC OF LINEAR ACTIVE SOURCE SPREAD CONFIGURATION	17
FIGURE 2.18 MASW FIELD DATA ACQUISITION	18
FIGURE 2.19 DISPERSION CURVE	19
FIGURE 2.20 ONE DIMENSIONAL VELOCITY STRUCTURE AND 2 D VELOCITY MODEL	20
FIGURE 2.21 DISPERSION CURVE FOR PASSIVE MASW	21
FIGURE 2.22 ONE DIMENSIONAL VELOCITY STRUCTURE FOR PASSIVE MASW.....	21
FIGURE 2.23 FUNDAMENTAL OF SINGLE MICROTREMOR OBSERVATION	22
FIGURE 2.24 FIELD DATA ACQUISITION OF SINGLE MICROTREMOR	23
FIGURE 2.25 THE SPT SAMPLER IN PLACE IN THE BORING WITH HAMMER, ROPE AND CATHEAD (ADAPTED FROM KOVACS, ET AL., 1981)	24
FIGURE 2.26 SPT SAMPLER AND DONUT HAMMER	25
FIGURE 3.1 SURFACE GEOLOGY MAP OF MIRSHARAI UPAZILA (SOURCE: AFTER GSB 2001)	26
FIGURE 3.2 (A) LEGEND AND LITHOLOGIC CHARACTERISTIC OF SUBSURFACE OF MIRSHARAI UPAZILA; (B) SUBSURFACE 3-D MODEL SHOWING NORTHEASTERN PART; (C) SUBSURFACE 3-D MODEL IN SOUTHWESTERN DIRECTION	30
FIGURE 3.3 FOUNDATION DEPTH OF MIRSHARAI UPAZILA.....	32
FIGURE 3.4 CROSS-SECTION A-A'	33
FIGURE 3.5 CROSS SECTION B-B'	34
FIGURE 3.6 CROSS SECTION C-C'	35
FIGURE 3.7 CROSS SECTION D-D'	36
FIGURE 3.7 CROSS SECTION E-E'	37
FIGURE 4.1 MAJOR SEISMOTECTONIC REGIMES IN AND AROUND BANGLADESH. IT HAS BEEN OVERLAID ON A HILLSHADED SRTM DIGITAL ELEVATION MODEL (DEM) OF 30M RESOLUTION (SOURCE: HTTPS://EARTHEXPLORER.USGS.GOV/) ADOPTED FROM WANG (2014).....	40

FIGURE 4.2 MAP SHOWING THE EARTHQUAKE EVENTS IN AND AROUND BANGLADESH BETWEEN 1505-2018	44
FIGURE 4.3 EVENTS AFTER DECLUSTERING USING GK METHOD.....	45
FIGURE 4.4 EVENTS AFTER DECLUSTERING USING MUSSON METHOD	46
FIGURE 4.5 BAR CHART SHOWING THE DEPTH DISTRIBUTIONS OF EARTHQUAKE EVENTS.....	47
FIGURE 4.6 STEP PLOTS OF COMPLETENESS MAGNITUDES FOR (A) GARDNER (B) MUSSON	49
FIGURE 4.7 GMPE LOGIC TREE	52
FIGURE 4.8 SOURCE LOGIC TREE FOR A- AND B-VALUES	53
FIGURE: 4.9 PGA MAPS FOR (A) 2% AND (B) 10% PROBABILITIES OF EXCEEDANCE IN 50 YEARS WITHOUT AND WITH SITE EFFECT.....	56
FIGURE: 4.10 PSA AT 0.2 SECONDS MAPS FOR (A) 2% AND (B) 10% PROBABILITIES OF EXCEEDANCE IN 50 YEARS WITHOUT AND WITH SITE CONDITION	57
FIGURE: 4.11 PSA AT 0.3S MAPS FOR (A) 2% AND (B) 10% PROBABILITIES OF EXCEEDANCE IN 50 YEARS WITHOUT AND WITH SITE EFFECT.....	58
FIGURE: 4.12 PSA AT 1.0S MAPS FOR (A) 2% AND (B) 10% PROBABILITIES OF EXCEEDANCE IN 50 YEARS WITHOUT AND WITH SITE EFFECT.....	59
FIGURE 4.13 HAZARD CURVES FOR MIRSHARAI UPAZILLA (WITHOUT AND WITH SITE EFFECT)	61
FIGURE 4.14 REGRESSION ANALYSIS BETWEEN MEASURED SPT-N VALUE AND SHEAR WAVE VELOCITY (Vs) OBTAINED FROM DOWN-HOLE SEISMIC TEST (PS LOGGING).....	64
FIGURE 4.15 SPT-N VALUE AND Vs EMPIRICAL RELATIONS FOR ALL SOILS IN STUDY AREA.....	64
FIGURE 4.16 ENGINEERING GEOLOGICAL MAP OF THE MIRSHARAI UPAZILA	66
FIGURE 4.17 SOIL CLASSIFICATION MAP OF MIRSHARAI ACCORDING TO NEHRP (STANDS FOR NATIONAL EARTHQUAKE HAZARD REDUCTION PROGRAM, USA) PROVISIONS BASED ON THE AVERAGE SHEAR WAVE VELOCITY DISTRIBUTION DOWN TO 30 M.....	69
FIGURE 4.18 BUILDING HEIGHT MAP OF MIRSHARAI UPAZILA.....	71
FIGURE 5.1 LANDSLIDE INVENTORY HAS BEEN OVERLAID THE HILL SHADE MAP	77
FIGURE 5.2 EXAMPLE OF SLOPE ANGLE.....	79
FIGURE 5.3 SLOPE MAP HAS BEEN PRODUCED FROM THE 10M RESOLUTION DEM.....	80
FIGURE 5.4 EXAMPLE OF ASPECT	81
FIGURE 5.5 EXAMPLE OF ASPECT CLASSES	81
FIGURE 5.6 ASPECT MAP OF THE STUDY AREA	83
FIGURE 5.7 NDVI DIFFERENCE MAP OF THE PROJECT AREA.....	85
FIGURE 5.8 EXISTING LAND COVER AND LAND COVER DIFFERENCE MAP	87
FIGURE 5.9 DRAINAGE AND DISTANCE FROM THE WATER BODY.....	88
FIGURE 5.10 ROAD AND DISTANCE FROM THE ROAD.....	89
FIGURE 5.11 FIGURE SHOWING AVERAGE RAINFALL (DATA SOURCE: BMD).....	90
FIGURE 5.12 DIGITAL ELEVATION MODEL	91
5.13 LANDSLIDE SUSCEPTIBILITY MAP OF THE PROJECT AREA	95
FIGURE 5.14 SUCCESS AND PREDICTION RATE.....	97

1. INTRODUCTION

1.1. Background

Bangladesh can earn money in local and also in foreign exchange by opening a tourist resort at Mirsharai. The spot, if properly developed will become an excellent holiday resort and tourist center. The rowing facility can be arranged easily; fishing and hunting facilities are already there. The success of developing Mirsharai as a tourist center and Special Economic Zone depends much on good communication facilities and availability of modern amenities. Moreover, the proposed Special Economic Zone would generate many industries related new activities including huge vehicular traffic such as air, rail, road and water. This phenomenon would have both positive and negative impacts on the socioeconomic condition and existing land use pattern of the region. The proposed planning package would guide such probable changes in the socio-economic condition and land use pattern of the region, and would also address the adverse impact of such changes.

Landuse planning is an impotent component for a modern urban development. But practicing urban development using a proper landuse plan is not developed in Bangladesh. Prior to landuse planning it is very essential to access surface and subsurface geological conditions and the relevant geological hazard and risk in and around the site of future urban development. Therefore a rigorous geological and geotechnical site characterization, including a potential risk analysis need to carry out for a risk resilient urban development.

Urban development is being increasing very fast in Bangladesh. The government has planned to develop Mirsharai as a tourist center and Special Economic Zone. However, risk sensitive urban planning is very important in such a disaster prone country like Bangladesh for a risk resilient urban development in these cities and surrounding area. In those cities Mirsharai is most disaster prone area because of this city is located near one of the most seismo-tectonically active zones of the earth. So this area covers the assessment and management of earthquake, landslide, and hydrometeorological hazards in pre-dominantly urban context. Considering the earthquake threat of the populated urban and rural areas of the project, UDD will have to be taken many initiatives for earthquake preparedness of the 16 (Sixteen) unions, including Ichhakhali, Wahedpur, Osmanpur, Karerhat, Katachhara, Khaiyachhara, Zorwarganj, Durgapur, Dhum, Maghadia, Mayani, Mithanala, Mirsharai, Saherkhali, Haitkandi and Hinguli Under Mirshari Upazila Development Plan (MUDP).

Slope stability assessment is very important for any development plan. While the study area is located near and/or in the hilly area, this assessment should be performed before any development plan. In this project our study area is along with hill track, slope stability assessment need to be conducted to protect slope failure and landslide. Geological, Geotechnical and DEM data should be compiled to accomplish this assessment.

Therefore the geological and geotechnical site characterization of the areas including potential seismic hazard and risk analysis is an important component for risk sensitive landuse planning of the populated urban and rural area. In here, Environmental & Geospatial Solutions (EGS) has been entrusted to conduct this project work.

1.2. Location and Accessibility

Mirsharai Upazila (CHITTAGONG DISTRICT) area 482.88 sqkm(BBS)/509.80sqkm, located in between 22°39' and 22°59' north latitudes and in between 91°27' and 91°39' east longitudes. It is bounded by TRIPURA state of India, CHHAGALNAIYA and FENI SADAR upazilas on the north, SITAKUNDA upazila and BAY OF BENGAL on the south, FATIKCHHARI upazila on the east, SONAGAZI and COMPANIGANJ (NOAKHALI) upazilas on the west. Mirsharai Thana was formed in 1901 and it was turned into an upazila in 1983. Mirsharai Upazila consists of 2 Municipality, 16 Union and 103 Mouza (Location of Project Area Figure 1.1).

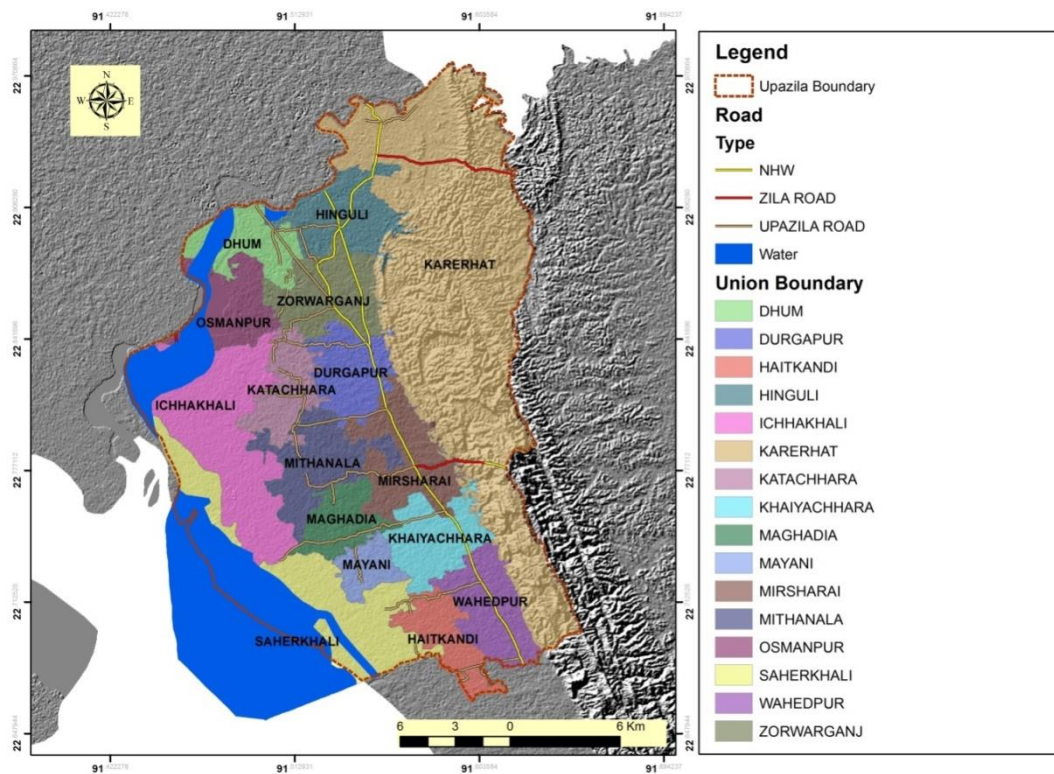


Figure 1.1 Location map of the project area

1.3. Aims and Objectives

The main objective of the research is to carry out a seismic hazard analysis of the 16 (Sixteen) unions, including Ichhakhali, Wahedpur, Osmanpur, Karerhat, Katachhara, Khaiyachhara, Zorwarganj, Durgapur, Dhum, Maghadia, Mayani, Mithanala, Mirsharai, Saherkhali, Haitkandi and Hinguli Under Mirshari Upazila Development Plan (MUDP). The main objective will be achieved through accomplishment of the following sub-objectives:

- i. Geological and geomorphologic map of the study area
- ii. Sub-surface lithological 3D model development
- iii. Soil classification map using geophysical and geotechnical investigations
- iv. Engineering geological map development based on AVS30
- v. Foundation layers delineation and developing engineering properties of the sub-soil
- vi. PGA, Sa (T) Maps of 0.2 and 1.0 second periods values of 10% exceedance probability during next 50 years for local site condition.
- vii. Risk Sensitive Building Height
- viii. Landslide vulnerable zones will be identified from the study.
- ix. Liquefaction potential index (LPI) map will be constructed from study data.
- x. Formulation of Policies and plans for mitigation of different types of hazards, minimizing the adverse impacts of climate change and recommend possible adaptation strategies for the region.

2. METHODOLOGY

2.1. Strategic Methodology

The methodology consists of both field and laboratory investigations. To conduct this project work, geomorphological, geotechnical and geophysical data of soil will be collected, analysed and interpreted. Geomorphological data will be collected from image of the study area to prepare a geomorphological map. Geotechnical data will be collected from field investigations *i.e.*, boring, standard penetration test (SPT), and laboratory investigations *i.e.*, soil physical properties test, consolidation test, direct shear test and triaxial test of undisturbed soil sample. Geophysical data will be collected from down-hole seismic test (PS

logging) and Multi-channel analysis of surface wave (MASW) and Singles Microtremor survey. The total works will be conducted by the following methodology-

2.1.1. Geophysical Investigation

Field geophysical investigation is conducted to achieve the purpose of seismic risk and damage assessment. Seismic site characterization by analyzing seismic wave propagation velocity from acquired shallow seismic wave form data is the main objective. P-S logging, Multi Channel Analysis of Surface Wave (MASW) and Microtremor tools are involved in geophysical investigation.

General purposes of the geophysical survey:

- To estimate shear wave velocity and measure soil/rock properties (i.e. shear modulus, bulk modulus, compressibility, and Poisson's ratio)
- Engineering geological map development based on AVS30
- To Seismic site response study
- Risk Sensitive Building Height
- Characterization of strong motion sites
- Utilize this information for seismic hazard analysis

2.1.2. Geotechnical Investigation

Geotechnical investigations have become an essential component of every construction to ensure safety of human beings and materials. It includes a detailed investigation of the soil to determine the soil strength, composition, water content, and other important soil characteristics.

Geotechnical investigations are executed to acquire information regarding the physical characteristics of soil and rocks. The purpose of geotechnical investigations is to design earthworks and foundations for structures, and to execute earthwork repairs necessitated due to changes in the subsurface environment. A geotechnical examination includes surface and subsurface exploration, soil sampling, and laboratory analysis. Geotechnical investigations are also known as foundation analysis, soil analysis, soil testing, soil mechanics, and subsurface investigation. The samples are examined prior to the development of the location. Geotechnical investigations have acquired substantial importance in preventing human and material damage due to the earthquakes, foundation cracks, and other catastrophes.

Geotechnical investigations can be as simple as conducting only a visual assessment of the site or as detailed as a computer-aided study of the soil using laboratory tests.

General purposes of the geotechnical survey:

- Sub-surface lithological 3D model development
- Foundation layers delineation and developing engineering properties of the sub-soil
- Landslide vulnerable zones will be identified from the study
- Liquefaction susceptibility or Liquefaction potential index (LPI) map will be constructed from study data

Following investigations given in Table that have been conducted for the preparation of engineering geological maps for rural part of MUDP Project area:

Name of Union	Name of investigations			
	Borelog with SPT (upto 30m)	PS logging (30m depth)	MASW (30m depth)	Single Microtremor
Ichhakhali, Wahedpur, Osmanpur, Karerhat, Katachhara, Khaiyachhara, Zorwarganj, Durgapur, Dhum, Maghadia, Mayani, Mithanala, Mirsharai, Saherkhali, Haitkandi and Hinguli	85	15	20	30

2.2. Detail Procedures Of Survey/Testing

The methodology consists of both field and laboratory investigations. To conduct this project work, geomorphological, geotechnical and geophysical data of soil will be collected, analysed and interpreted. Geomorphological data will be collected from satellite image of the study area to prepare a geomorphological map. Geotechnical data will be collected from field investigations i.e., boring, standard penetration test (SPT), and laboratory investigations i.e., soil physical properties test, consolidation test, direct shear test and triaxial test of undisturbed soil sample. Geophysical data will be collected from down-hole seismic test (PS logging) and Multi-channel analysis of surface wave (MASW) and Singles Microtremor survey. The total works will be conducted by the following methodology-

The method of testing/surveying, application, Instrumentation and previous works of Geophysical and Geotechnical investigation are given below-

2.2.1. Test Detail And Procedure Of Downhole Seismic Test (Ps Logging)

Seismic down hole test is a direct measurement method for obtaining the shear wave velocity profile of soil stratum. The seismic down hole test aims to measure the travelling time of elastic wave from the ground surface to some arbitrary depths beneath the ground. The seismic wave was generated by striking a wooden plank by a 7kg sledge hammer. The plank was placed on the ground surface at around 3 m in horizontal direction from the top of borehole. The plank was hit separately on both ends to generate shear wave energy in opposite directions and is polarized in the direction parallel to the plank.

The shear wave emanated from the plank is detected by a tri-axial geophone. The geophone was lowered to 1 m below ground surface and attached to the borehole wall by inflating an air bladder. Then, the measurements were taken at every 1 m interval until the geophone was lowered to 30 m below ground surface. For each elevation, 9 records were taken and then used to calculate the shear wave velocity. The first arrival time of an elastic wave from the source to the receivers at each testing depth can be obtained from the downhole seismic test.



Figure 2.1 Field Data Acquisition by PS logger

Two geophones are lowered in the hole by keeping them 1.5m apart. There exists two ways of moving geophone either upward or downward. Say, if the hole is 30m then the bottom geophone is kept at 30m and then the top geophone will be at 28.5m and then we bring these geophones upward by taking reading after each meter and for downward is vice versa. In

Downhole Seismic, an accelerometer mounted to a wooden plank source is used to trigger data collection.



Figure 2.2 Main Component of the Freedom Data PC

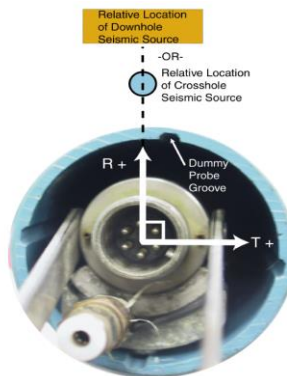


Figure 2.3 Receiver Orientation in Sinco casing

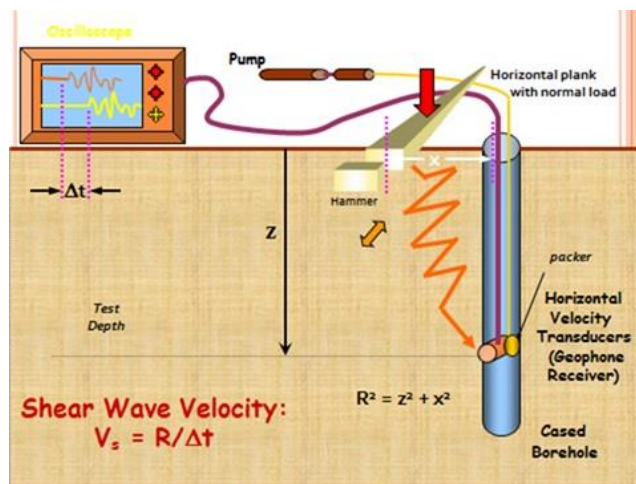


Figure 2.4 Calculation of Shear Wave Velocity by Down hole Seismic, where R_1 =Distance between source to top geophone and R_2 =Distance between source to bottom geophone



Figure 2.5 To set the wooden plank 1.0 meters from a borehole



Figure 2.6 To attach the trigger to a hammer.



Figure 2.7 To connect the air pump with a battery.



Figure 2.8 To connect the computer with cables which are connected to the geophone.



Figure 2.9 Make sure that the air bag at the geophone works. Then, put the geophone into the borehole and fix the safety rope with the holder



Figure 2.10 Hit the wooden plank in 3 directions which are on the left, right and vertical directions.

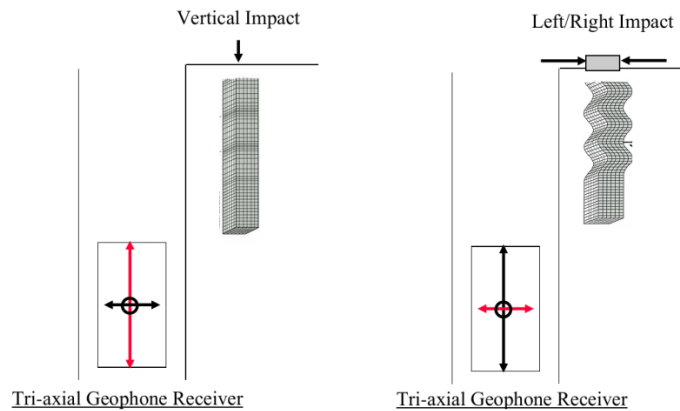


Figure 2.11 Triaxial geophone behavior.

Analysis and Calculation from PS Logging

P-wave travel time is calculated by the first arrival of either peak or trough in the seismic trace and P-wave is characterized by higher frequency and lower amplitude. On the other hand, shear wave is characterized by lower frequency but high amplitude.

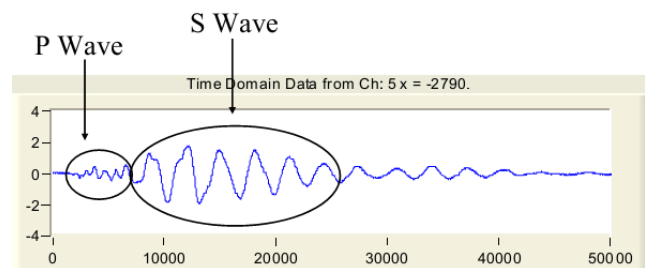


Figure 2.12 P wave and S wave in the Computer Window

S wave travel time is calculated from the first cross as we hit in both direction of the wooden plank so there generate opposite phase shear waves in radial and transverse direction and cross at some points.

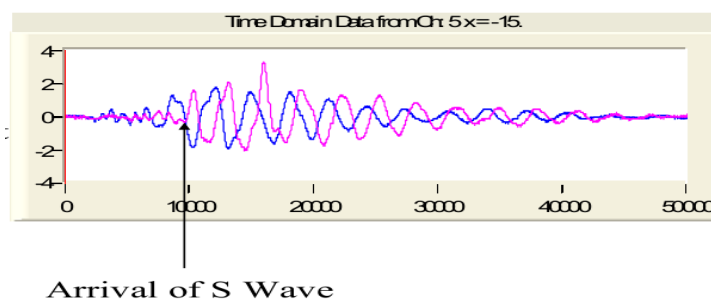


Figure 2.13 Arrival of S wave

Moreover, bounty of engineering geological parameters of soil can be determined whenever shear wave and compressional wave velocity is known. The Shear Modulus (G), Constrained Modulus (M) , Poisson Ratio (ν) and Young Modulus(E) of the soil profiles are calculated using the following formula:

$$\begin{aligned}G &= \rho V_S^2 \\M &= \rho V_P^2 \\ \nu &= [0.5(\frac{V_P}{V_S})^2 - 1] / [(\frac{V_P}{V_S})^2 - 1] \\ E &= 2G(1 + \nu)\end{aligned}$$

Where, ρ is the local soil mass density (unit weight divided by gravity) obtained from the boring log information is taken 2 gm/cc for based on SPT results.

Besides, the average shear wave velocity upto 30 m depth has been determined using the following equation.

$$T_{30} = \sum \frac{H_i}{V_i}$$

$$AVS_{30} = \frac{30}{T_{30}}$$

Where, H_i : Thickness of i th layer and $30 = \sum H_i$
 V_i : S-wave velocity of i th layer

Instrument List

The PS logging test equipments are listed below-

1. One Freedom NDT PC
2. Two High Sensitive Tri-axial Geophones.
3. Two set Cable/Air line Spool
4. Wooden Plank.
5. 7kg weight Hammer.



Figure 2.14 Freedom Data PC with P-SV Downhole Source and 1 Tri-axial Geophone Receiver used in Crosshole Seismic Investigations

Application of PS Logging Test

Downhole Seismic (PS Logging) system is useable for providing information on dynamic soil and rock properties for earthquake design analyses for structures, liquefaction potential studies, site development, and dynamic machine foundation design. The investigation determines shear and compressional wave depth versus velocity profiles. Other parameters, such as Poisson's ratios and moduli, can be easily determined from the measured shear and compressional wave velocities. The PS Logging is a downhole method for the determination of material properties of soil and rock.

2.2.2. Test Detail And Procedure Of Multi-Channel Analysis Of Surface Wave (MASW)

MASW utilizes the frequency dependent property of surface wave velocity, or the dispersion property, for V_s profiling. It analyses frequency content in the data recorded from a geophone array deployed over a moderate distance.

The processing of MASW is schematically summarized in Figure 2.15. The principle MASW is to employ and arrange a number of sensors on the ground surface to capture propagating Rayleigh waves, which dominates two-thirds of the total seismic energy generated by impact sources. If the tested ground is not homogeneous, the observed waves will be dispersive, a phenomenon that waves propagate towards receivers with different phase velocities depending on their respective wavelength (see Figure 2.16).

From field observation, the data in space-time domain (for instance, the left plot in Figure 3.19) is transformed to frequency-velocity domain by slant-stack and Fast Fourier transform using

$$S(\omega, c) = \int e^{-i\frac{\omega}{c}x} U(x, \omega) dx$$

where $U(x, \omega)$ is the normalized complex spectrum obtained from the Fourier transform of $u(x, t)$, ω is the angular frequency, c is the testing-phase velocity and $S(\omega, c)$ is the slant-stack amplitude for each ω and c , which can be viewed as the coherency in linear arrival pattern along the offset range for that specific combination of ω and c . When c is equal to the true phase velocity of each frequency component, the $S(\omega, c)$ will show the maximum value. Calculating $S(\omega, c)$ over the frequency and phase-velocity range of interest generates the phase-velocity spectrum where dispersion curves can be identified as high-amplitude bands. The dispersion curve is, then, used in inversion process to determine the shear wave velocity profile of the ground.

In theory, a phase-velocity spectrum can be calculated for a known layer model \mathbf{m} and the field setup geometry. This process is called forward modeling. The inversion process tries to adjust assumed layer model as much as possible through several iterations in order to make the calculated spectrum looks similar to the dispersion curve obtained from the field test. Once the algorithm can match the calculated with the measured one, the assumed model will be considered as the true profile.

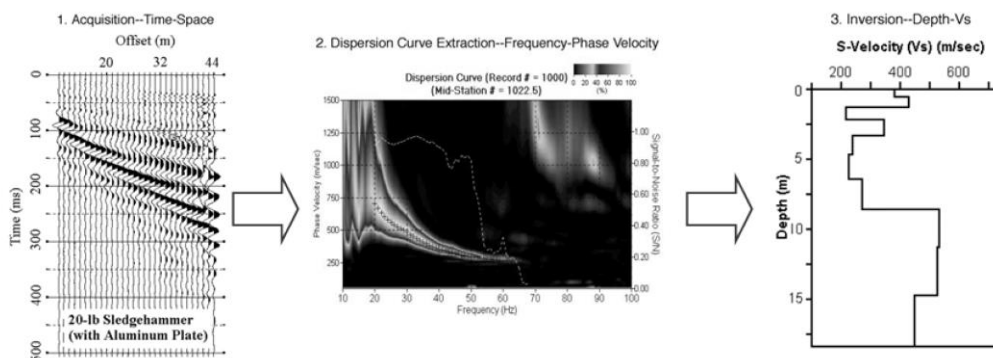


Figure 2.15 MASW data processing (Park et al., 1999)

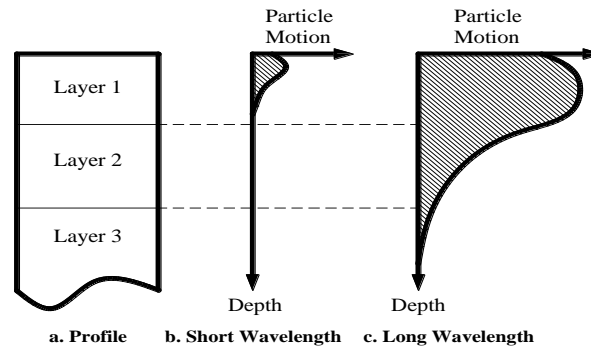


Figure 2.16 Rayleigh wave dispersion in layer media (Rix, 1988)

Active Source Data Acquisition

The active MASW method was introduced in GEOPHYSICS in 1999. This is the most common type of MASW survey that can produce a 2D VS profile. It adopts the conventional mode of survey using an active seismic source (e.g., a sledge hammer) and a linear receiver array, collecting data in a roll-along mode. It utilizes surface waves propagating horizontally along the surface of measurement directly from impact point to receivers. It gives this VS information in either 1D (depth) or 2D (depth and surface location) format in a cost-effective and time-efficient manner. The maximum depth of investigation (z_{max}) is usually in the range of 10–30 m, but this can vary with the site and type of active source used.

Seismic energy for active source surface wave surveys can be created by various ways, but we used a sledgehammer to impact a striker plate on the ground since it is a low-cost, readily available item. To signal to the seismograph when the energy has been generated, a trigger switch is used as the interface between the hammer and the seismograph. When the sledgehammer hits the ground, a signal is sent to the seismograph to tell it to start recording.

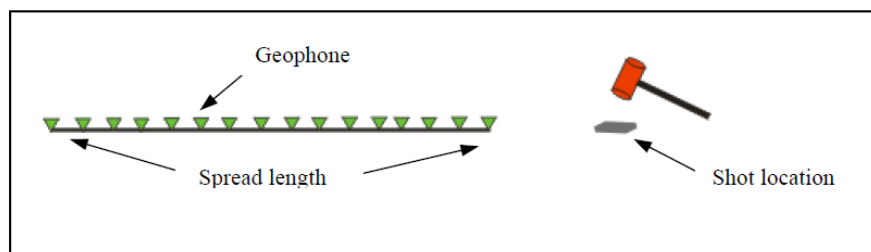
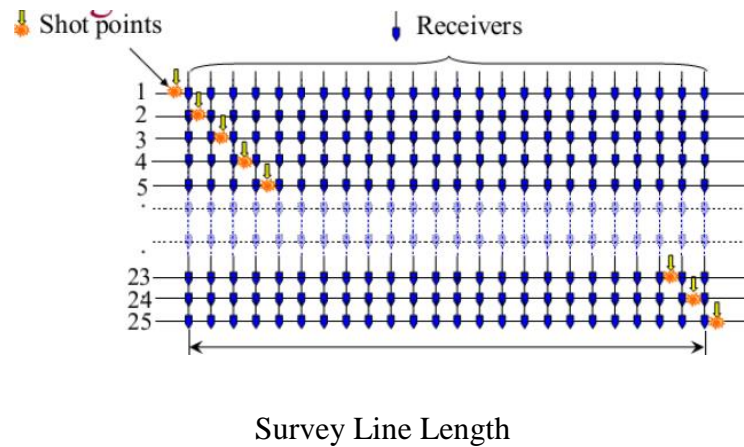


Figure 2.17 Schematic of linear active source spread configuration

During our field work we used 12 channels with 3m interval, 1.5 m source (sledge hammer) offset, 1 ms sample interval, 2 seconds record length and auto trigger option. Natural frequency of Geophone is 10 Hz. And the active source spread configuration for the station 20 was like below:



(Number of Sources= Number of Receivers + 1)



Figure 2.18 MASW Field Data Acquisition

At every station one data was acquired by stacking (3 times hammer hit) to enhance the data quality.

Analysis of MASW

In the phase velocity analysis, SPAC (Spatial Autocorrelation) method (Okada, 2003) is employed. Okada (2003) shows Spatial autocorrelation function $\rho(\omega, r)$ is expressed by Bessel function.

$$\rho(\omega, r) = J_0(\omega r / c(\omega)) \text{ -----}(1)$$

Where, r is the distance between receivers, ω is the angular frequency, $c(\omega)$ is the phase velocity of the waves, J_0 is the first kind of Bessel function. The phase velocity can be obtained at each frequency using equation (1). Figure 2-19 shows an example of dispersion curve of the survey, the frequency range between 15 and 50 Hz.

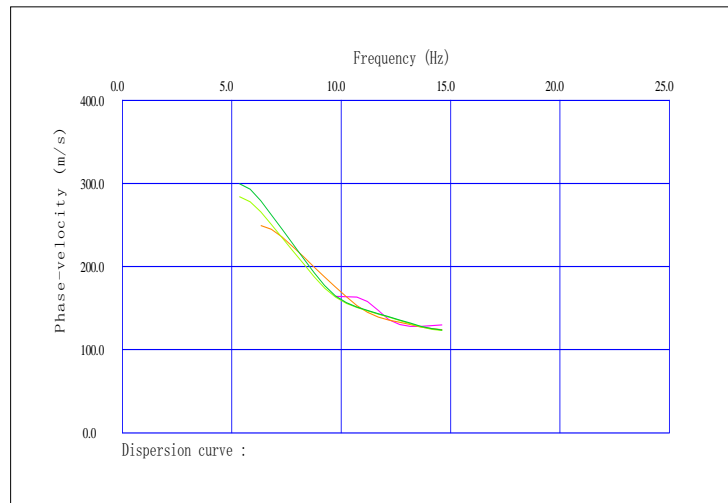


Figure 2.19 Dispersion Curve

A one-dimensional inversion using a non-linear least square method has been applied to the phase velocity curves. In the inversion, the following relationship between P-wave velocity (V_p) and V_s (Kitsunezaki et. Al., 1990):

$$V_p = 1.29 + 1.11V_s \text{ -----}(2)$$

Where V_p and V_s are the P-wave velocity and S-wave velocity respectively in (km/sec).

These calculations are carried out along the measuring line, and the S-wave velocity distribution section was analyzed, then summarized to one dimensional structure; SeisImager software can also give a 2-D velocity model (for active), a sample of which is shown in Fig. 2.20.

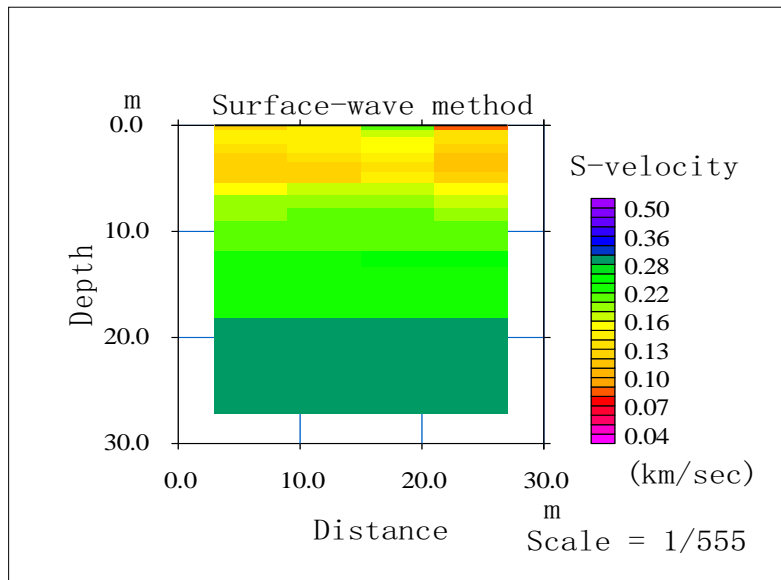
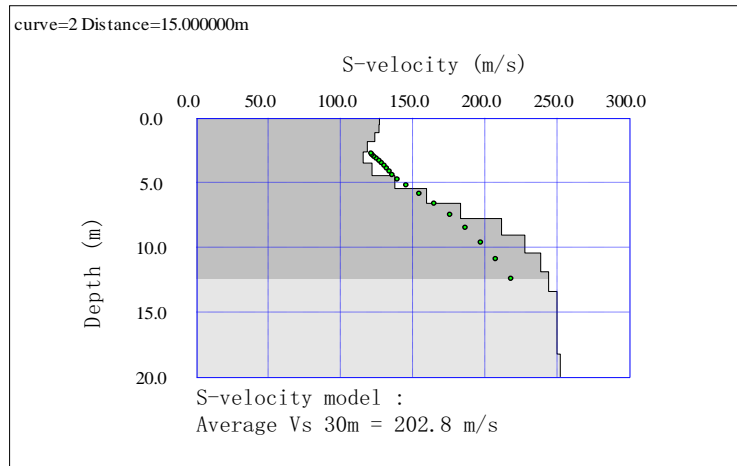


Figure 2.20 One dimensional Velocity Structure and 2 D velocity Model

Figure 2.21 shows an example of dispersion curve for passive MASW and phase velocity versus frequency as a sample. A one dimensional inversion using a non-linear least square method has been applied to the phase velocity curves and one dimensional S-wave velocity structures down (Figure 2.22).

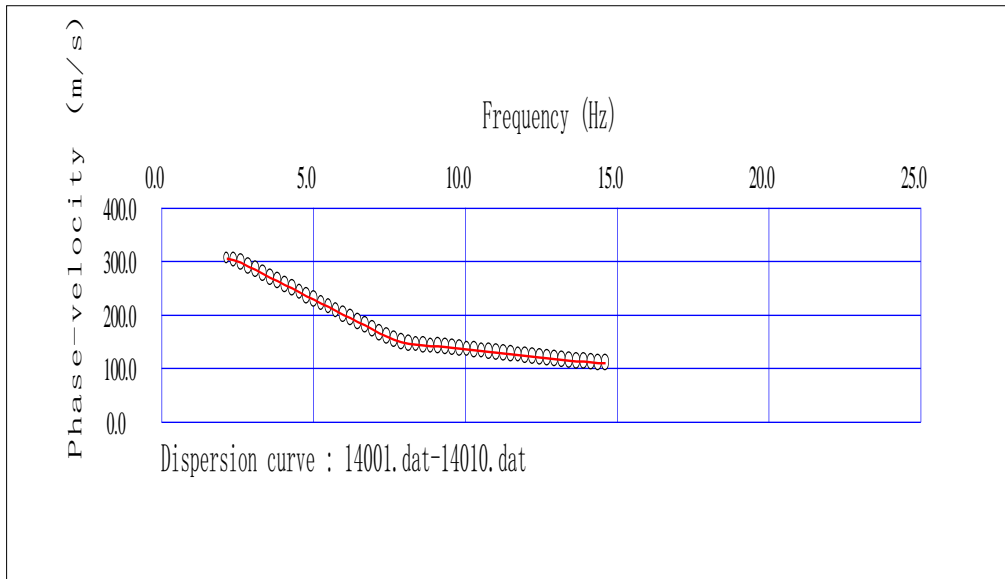


Figure 2.21 Dispersion Curve for Passive MASW

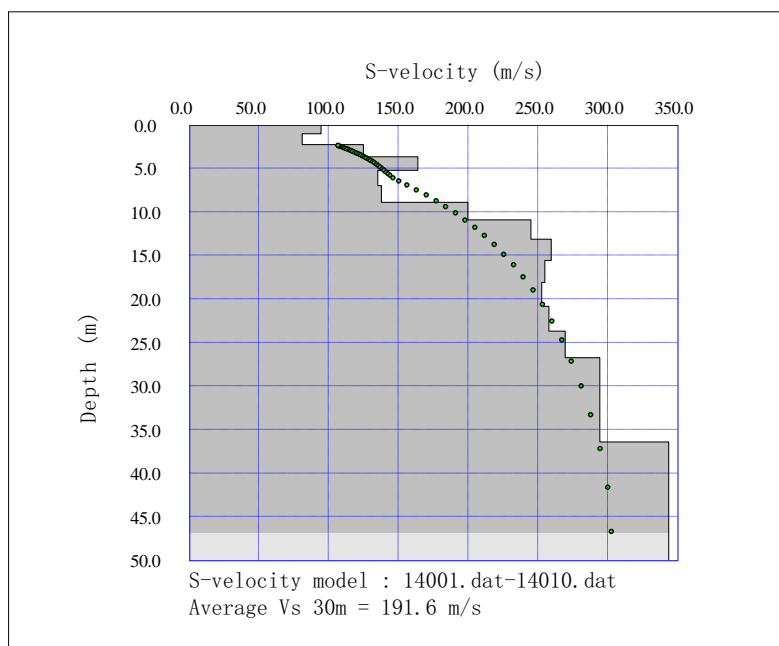


Figure 2.22 One dimensional velocity structure for Passive MASW

Calculation of AVS 30

The AVS30 can be calculated as follows:

$$T_{30} = \sum(H_i/V_i)$$

$$AVS\ 30 = (30 / T_{30})$$

Where, H_i = Thickness of the i th layer and $\sum H_i = 30$

V_i = S wave velocity of the i th layer

2.2.3. Test Detail And Procedure Of Microtremor Measurement (Single Microtremor)

Microtremor method is a practical and economical seismic survey since it has potential to explore deep soils without a borehole. Microtremors are the phenomenon of very small vibrations of the ground surface even during ordinary quiet time as a result of a complex stacking process of various waves propagating from remote man-made vibration sources caused by traffic systems or machineries in industrial plants and from natural vibrations caused by tidal and volcanic activities. Observation of microtremors can give useful information of dynamic properties of the site such as predominant period, amplitude, peak ground acceleration and shear wave velocity.

Single Microtremor observation

Method

1) The transfer function of surface layer

$$S_T = \frac{\text{Hor. spectrum at surface}}{\text{Hor. spectrum at base}} = \frac{S_{HS}}{S_{HB}}$$

2) Vertical component of MT is affected by Rayleigh wave at surface, but no effect at base and no amplification of vertical waves. Define the effect of Rayleigh wave as;

$$E_S = \frac{\text{Ver. spectrum at surface}}{\text{Ver. spectrum at base}} = \frac{S_{VS}}{S_{VB}}$$

3) To eliminate the effect of Rayleigh wave, define new transfer function as;

$$S_{TT} = \frac{S_T}{E_S} = \left(\frac{S_{HS}}{S_{VS}} \right) \times \left(\frac{S_{VB}}{S_{HB}} \right) = \left(\frac{S_{HS}}{S_{VS}} \right)$$

$$\frac{H/V \text{ spectrum}}{H/V} = \frac{H_S}{H_V} = \frac{\sqrt{F_{NS} \times F_{EW}}}{F_{UD}}$$

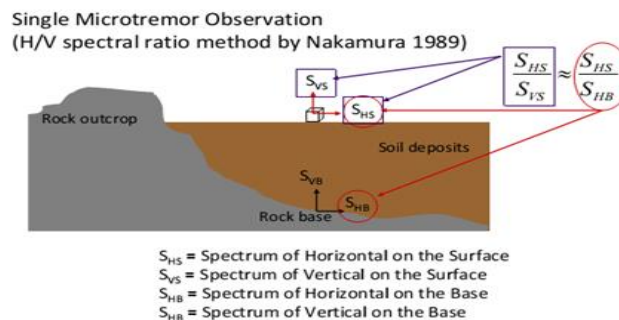


Figure 2.23 Fundamental of Single Microtremor observation

Field Data Acquisition System

Microtremor observations are performed using portable equipment, which is equipped with a super-sensitive sensor, a wire comprising a jack in one site and USB port in another site, and a laptop computer is also used. The microtremor equipment has been set on the free surface on the ground without any minor tilting of the equipment. The N-S and E-W directions are properly maintained following the directions arrowed on the body of the equipment. The sampling frequency for all equipments is set at 200Hz. The low-pass filter of 40Hz is set in the data acquisition unit. Like the seismometer or accelerometer, the velocity sensor used can measure three components of vibrations: two horizontal and one vertical. The natural period of the sensor is 2 sec. A global positioning system (GPS) is used for recording the coordinates of the observation the available frequency response range for the sensor is 0.5-20Hz. sites. The length of record for each observation was 10~20 min. In all fields of this project this data acquisition system has be applied.



Figure 2.24 Field data acquisition of Single microtremor

2.2.4. Standard Penetration Test (SPT) Method

The Standard Penetration test (SPT) is a common in situ testing method used to determine the geotechnical engineering properties of subsurface soils. The test procedure is described in the British Standard BS EN ISO 22476-3, ASTMD1586. A short procedure of SPT N-value test is described in the following paragraph.

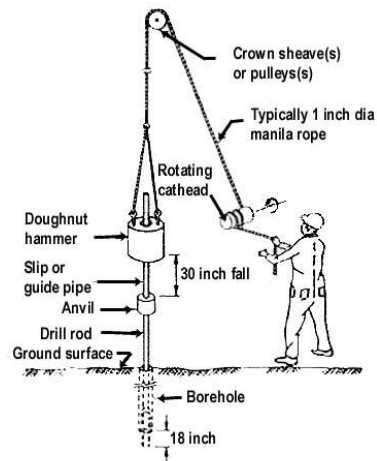


Figure 2.25 The SPT sampler in place in the boring with hammer, rope and cathead (Adapted from Kovacs, et al., 1981)

The test in our field uses a thick-walled sample tube, with an outside diameter of 50 mm and an inside diameter of 35 mm, and a length of around 650 mm. This is driven into the ground at the bottom of a borehole by blows from a slide hammer with a weight of 63.5 kg (140 lb) falling through a distance of 760 mm (30 in). The sample tube is driven 150 mm into the ground and then the number of blows needed for the tube to penetrate each 150 mm (6 in) up to a depth of 450 mm (18 in) is recorded. The sum of the number of blows required for the second and third 6 in. of penetration is termed the "standard penetration resistance" or the "N-value". In cases where 50 blows are insufficient to advance it through a 150 mm (6 in) interval the penetration after 50 blows is recorded. The blow count provides an indication of the density of the ground, and it is used in many empirical geotechnical engineering formulae.

The main objective of SPT is as follows:

- a) Boring and recording of soil stratification.
- b) Sampling (both disturbed and undisturbed).
- c) Recording of SPT N-value
- d) Recording of ground water table.

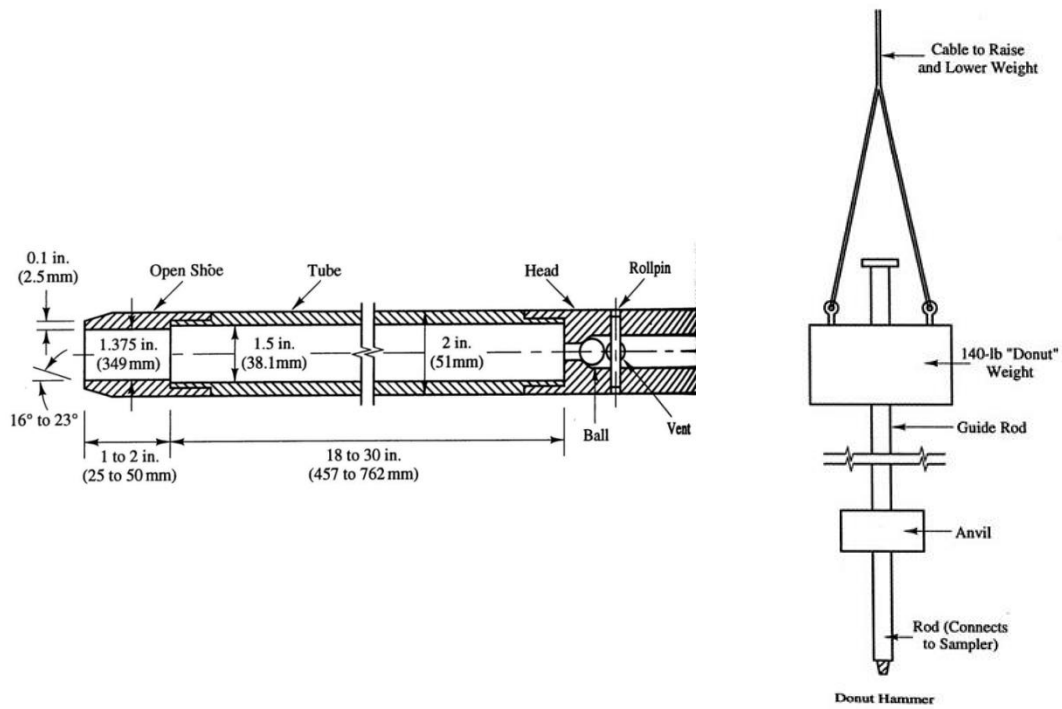


Figure 2.26 SPT Sampler and Donut Hammer

3. GEOLOGY OF THE STUDY AREA

3.1. Surface Geology

Geology focuses on the nature and properties of rocks and sediments. A good knowledge on the geology of the rocks and sediments is indispensable to understand the nature and properties of the parent materials. It is essential to understand the processes of formation of major soils of the country. Geomorphological knowledge is also important to visualize the processes and methods well. Bangladesh lies in an active seismic location. Moreover being a riverine country, the sediments are much affected by the combination of river process and seismic activity. The rivers are the most significant features of Bangladesh geology. They constantly change course, sometimes so rapidly that it cannot be predicted. As a result the topological features of Bangladesh are ever changing and it gives a spectacular feature of Surface geology (Figure 3.1).

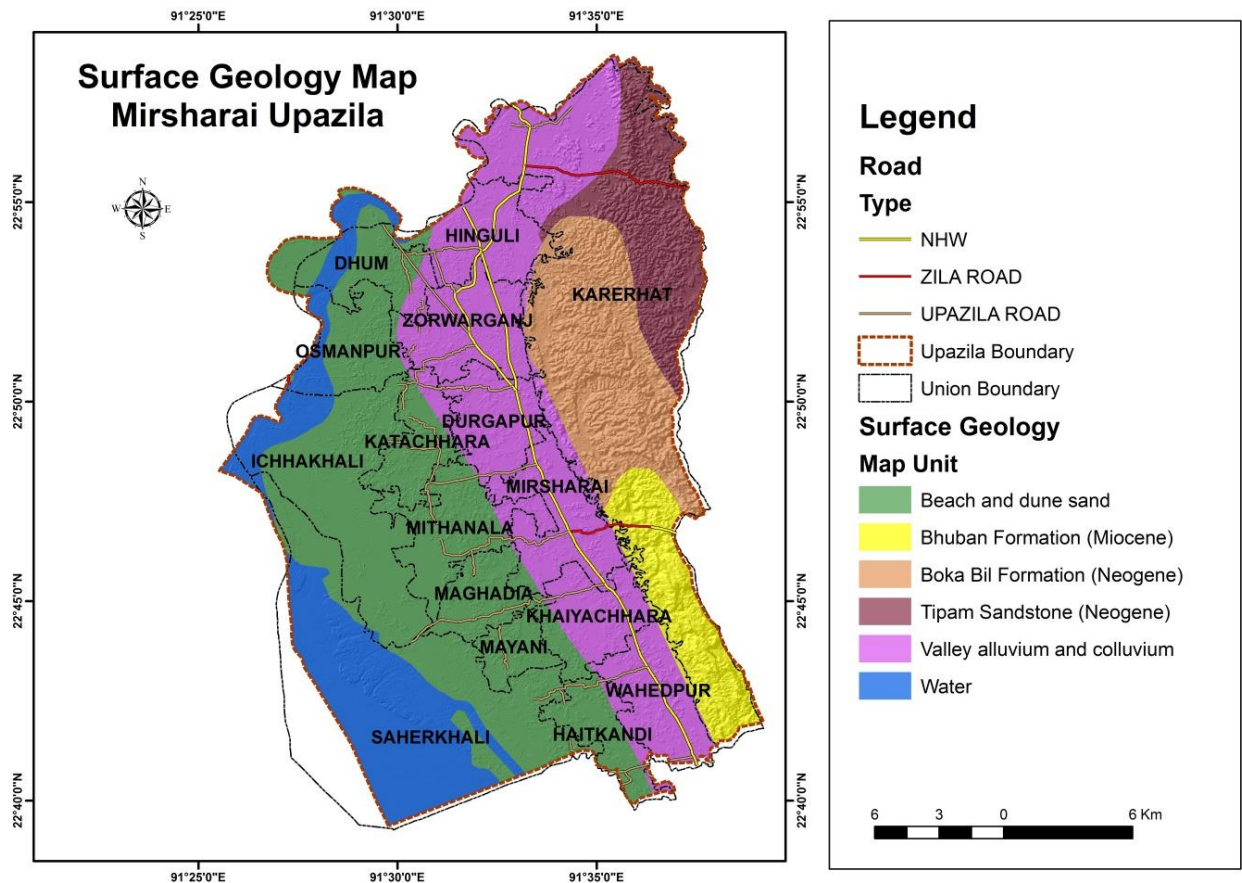


Figure 3.1 Surface Geology Map of Mirsharai Upazila (Source: After GSB 2001)

Bhuban Formation:

Bhuban Formation a Miocene body of rock identified by its lithic characteristics. The lower unit of P Evans (1932) Surma Group was designated by him as the Bhuban Stage after the Bhuban Range of Assam, India (Source: Banglapedia).

Bhuban subgroup is further divided into three subdivisions in the Bengal Basin .they are:

- i. Upper Bhuban Formation: This formation underlies conformably the Boka Bil Formation. The contact in most cases is gradational. Consists of massive, brownish, soft friable, medium grained sandstone with some fragments of shales.
- ii. Middle Bhuban Formation: It overlies the Upper Bhuban Formation conformably the contact being gradational. The rock formation is predominantly argillaceous sandstone with shale, mudstone and siltstone.
- iii. Lower Bhuban Formation: It comprises mostly of grayish, fine to very fine grained well bedded, compact, massive sandstone interbedded with thinner bands of siltstone and shale.

The oldest rocks, the Lower Bhuban Formation are outcropped in the cores of the easternmost anticlines near the Indian border. Based on foraminifera test and hystrichospherids encountered in the shaly sequences of this member indicate deposition in a marine to brackish environment. Rocks of the Middle Bhuban Member are also confined to the cores of the anticlines in the eastern part of the Chittagong Hill Tracts indicating a deltaic to near shore depositional environment. The Upper Bhuban Member crops out in most of the anticlines throughout the Chittagong Hill Tracts. The study area does not have such extensive exposure of the unit. The Upper Bhuban Member is dominated by gymnospermous pollen. This indicates that the orogenies in the region were already so highly elevated that the climatic conditions were favorable for the growth of gymnospermous plants in this zone.

Bokabil Formation:

The Bokabil Formation conformably overlies the Bhuban Formation and is unconformably overlain by the Tipam Sandstone Formation. It was named by Evans (1932) as Bokabil stage after a locality in the Hailakandi valley, northern Cachar, Assam, India (Source: Banglapedia). The unit is mainly composed of silty shale, shale, siltstone and sandstone. The silty shale is gray to bluish, laminated to thinly bedded, compact and highly jointed. The shale is Greenish gray to bluish gray, very thinly to thickly laminated. Siltstone is

predominantly yellowish gray to bluish gray, moderately hard, laminated, sometimes shows ripple marks. Sandstone is gray to yellowish gray, moderately hard and compact, thin to thick bedded and medium to fine grained. Sandstone commonly shows planar cross-bedding with abundant flaser lamination. (Ismail Hossain, Md. Sultan-Ul- Islam, 2013).

The formation is exposed in the hill ranges of greater Sylhet, Chittagong district and the Chittagong Hill Tracts. From the Boka Bil Formation, more than 100 fossil species have so far been identified from two localities of the Garo Hills. Most of them belong to Pelecypoda and Gastropoda. Different species of Foraminifera have been recorded, such as *Chiloguembelina globigera*; *Globigerina bulloides*; *G. falconensis*-*G. cf bradyi* and *G. quinqueloba*. In the Sitakunda hills the Bokabil Shale contains *Ostrea digitalina*, *O. gryphoides* and numerous plates of *Bolanus*, fragments of *Arca*, *Pecten*, *Trochus*, *Oliva* and Corals. The formation may have been deposited under shallow marine to deltaic and estuarine environments. (Banglapedia).

Tipam Sandstone Formation:

The Tipam Sandstone Formation is mainly coarse-grained sandstone. It is composed of mainly grey-brown to pale-grey, coarse-grained, cross bedded, massive sandstone alternation with grey shale. The sandstones are mainly lithic arkose, arenaceous in nature. Sandstone composed of quartz. Tipam Sandstone deposits occur throughout the Frontal Fold Belt of Bengal Basin. From the southern part of Chittagong hill tracks to the western part of Indian state Mizoram and Tripura. In the Frontal Folded Belt area this formation is often seen in the anticlinal trends, forming steep cliffs (Source: Banglapedia). But in the study area small strips are exposed.

On the Surma basin of Sylhet area Tipam sandstone is divided into three parts: Lower, Middle and Upper Tipam Sandstone. Lower Tipam is usually Yellowish brown to dark brown with very little gray colored clay. Middle Tipam alteration of grayish fine grained ripple laminated sandstone with grey colored parallel laminated silty shale. The Upper Tipam is consists of grey colored medium to very fine grained sandstone with siltstone, silty shale and shale. (Dhiman kumar Roy, Md. Mostafizur Rahman, Sarmin Akter, 2006).

Valley Alluvium and Colluvium:

Valleys are low-lying areas within uplifted lands. Usually rivers run through the valleys. River deposits are generally found in valleys. Colluvium is a general term applied to any

loose, heterogeneous, and incoherent mass of soil material or rock fragments deposited by rain-wash, sheet-wash, or slow, continuous downslope creep, usually collecting at the base of gentle slopes or hillsides. Here the colluviums in this zone is associated to river borne or rain wash deposit.

Alluvium and Colluvium deposits are a mixture of sand, silt and clay sized loose materials deposited mainly by river borne deposit. They are recent one and hence not compacted and unconsolidated. The sediments are mainly gray colored with less micaceous substance and clay rich dominantly. Easily weathered materials are altered to clay in this deposit (Feldspar to clay).

Beach and Dune Sand:

Sand is considered any loose, granular material having grains which are 0.05 to 2.0 millimeters in diameter. Sand dunes are mounds of windblown sand which vary greatly in size, from less than one meter to tens of meters high. The size depends upon the supply of sand. There is even greater variation in the area covered by dunes. Many of the more recognizable dune forms are ridges or complexes of mounds or crescents.

3.2. Subsurface 3D model of different layers through Geotechnical investigation

According to 250m × 250m grid pattern, Standard penetration test locations are selected and drilling for identifying the geological characteristic of sub-surface soft sedimentary rocks. Description of different layer of the soil, its sedimentary characteristics, structure, and lithology are reflected in 3D model. Engineering properties of different soil layer: SPT value, soil strength and foundation layer etc are also being described. Computing all the results of soil properties and geotechnical properties preparation of 3D model for sub surface information of different layers of the area can be done by using GIS.

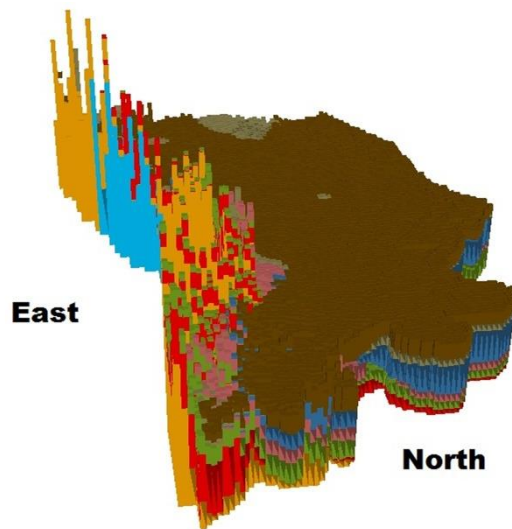
Lithological succession encountered in the boreholes reveals that geologically the study area is very complex as the eastern part is high terrace zone on the other hand western part is flat land area which finally ended up in bay of bangle. The borelogs encompasses eight distinct lithofacies, denoted as layers1 to layer8 and each layer has distinct lithological characteristics and standard penetration test blow counts (SPT-N) as described in Figure-3.2a.

a.

Lithological Description

- Layer-1: Brownish Gray Soft to Stiff Clayey SILT/Silty CLAY with Very Fine Sand
- Layer-2: Gray Loose to Medium Dense Very Fine to Fine SAND with Silt
- Layer-3: Gray Medium Dense Medium to Fine SAND
- Layer-4: Brown to Gray Medium to Very Stiff Clayey SILT with Very Fine Sand
- Layer-5: Brown to Gray Medium Dense to Very Dense Medium to Fine SAND
- Layer-6: Brown to Gray Very Stiff Clayey SILT
- Layer-7: Reddish Brown to Gray Dense to Very Dense Medium to Fine SAND
- Layer-8: Brownish Gray Very Hard CLAY/SHALE

b.



c.

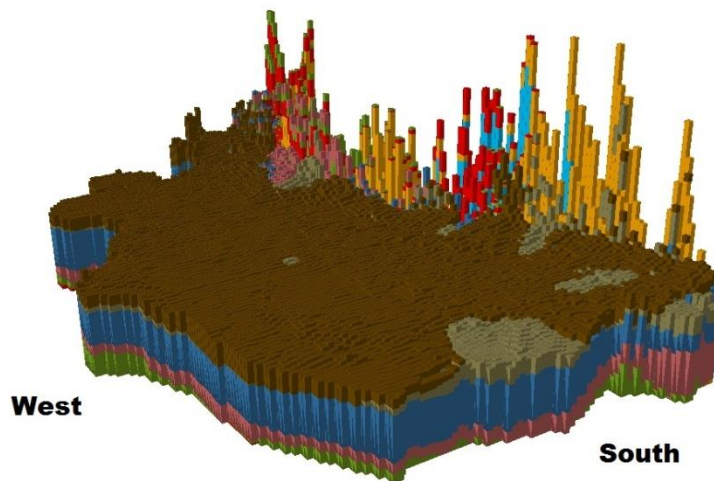


Figure 3.2 (a) Legend and Lithologic characteristic of subsurface of Mirsharai Upazila; (b) Subsurface 3-D model showing Northeastern part; (c) Subsurface 3-D model in Southwestern direction

Subsurface 3D model was prepared showing Northeastern part and along Southwestern direction using ArcGIS to elucidate the subsurface geological conditions of the study area as shown in Figure 3.7 b & c respectively. All 85 boreholes of 30m depth were carefully examined to delineate the spatial distribution of the subsurface lithological units of the area.

Among 8 layers; layer 1 to layer 5 is mostly present at the flat landed areas and layer 6 to layer 8 is mainly present at hilly regions of the study area. From the Figure 3.7 b & C, it can observe that Layer 1 is present at the top of the study area. However the layer is absent at the hilly regions and southern part of the flat lands of study area. A thin layer of layer 2 is present almost throughout the flat landed areas of the study area. Layer 3 which is considered as the foundation layer is the thickest layer within the flat land zone and thickness increases gradually toward southwestern part of the area. Thickness of Layer 4 gradually decreases toward western part of the study area. Layer 5 is also considered as foundation layer where layer 3 is absent especially at Karerhat Union. Thickness of the layer gradually increases toward north of the area. Layer 6 is discretely present within the area and thickness of the layer increases toward northeastern part of the area. Layer 7 and 8 mainly encountered at the eastern part of the area. Both the layers are present within the hilly regions of the study area and could not be encountered within the 30m depth zone of flat land regions. Thickness of layer 7 increases abruptly toward northeastern part of the area and the thickness of layer 8 increases abruptly toward eastern part of the area.

Based on N-value (soil resistance) layer 3 and layer 5 consider as a foundation layer. Among them layer 3 cover almost all area of Mirsharai Upazila. Only northern part of the Karerhat union and surrounding area reflect layer 5 as a foundation layer. Northern part of the Karerhat union, central part of Zorwarganj, South-eastern part of Durgapur and Wahedpur, Eastern part of Mirsharai and Khaihachhara and South-western part of Mithanala union reflect shallow foundation depth (3m), which need to be verified with allowable bearing capacity. Foundation depth of overall area of Mirsharai Upazila varies 3m to 10m (Figure-3.3). Very few areas consider their foundation depth more than 10m. This analysis might be updated while other test result will integrate.

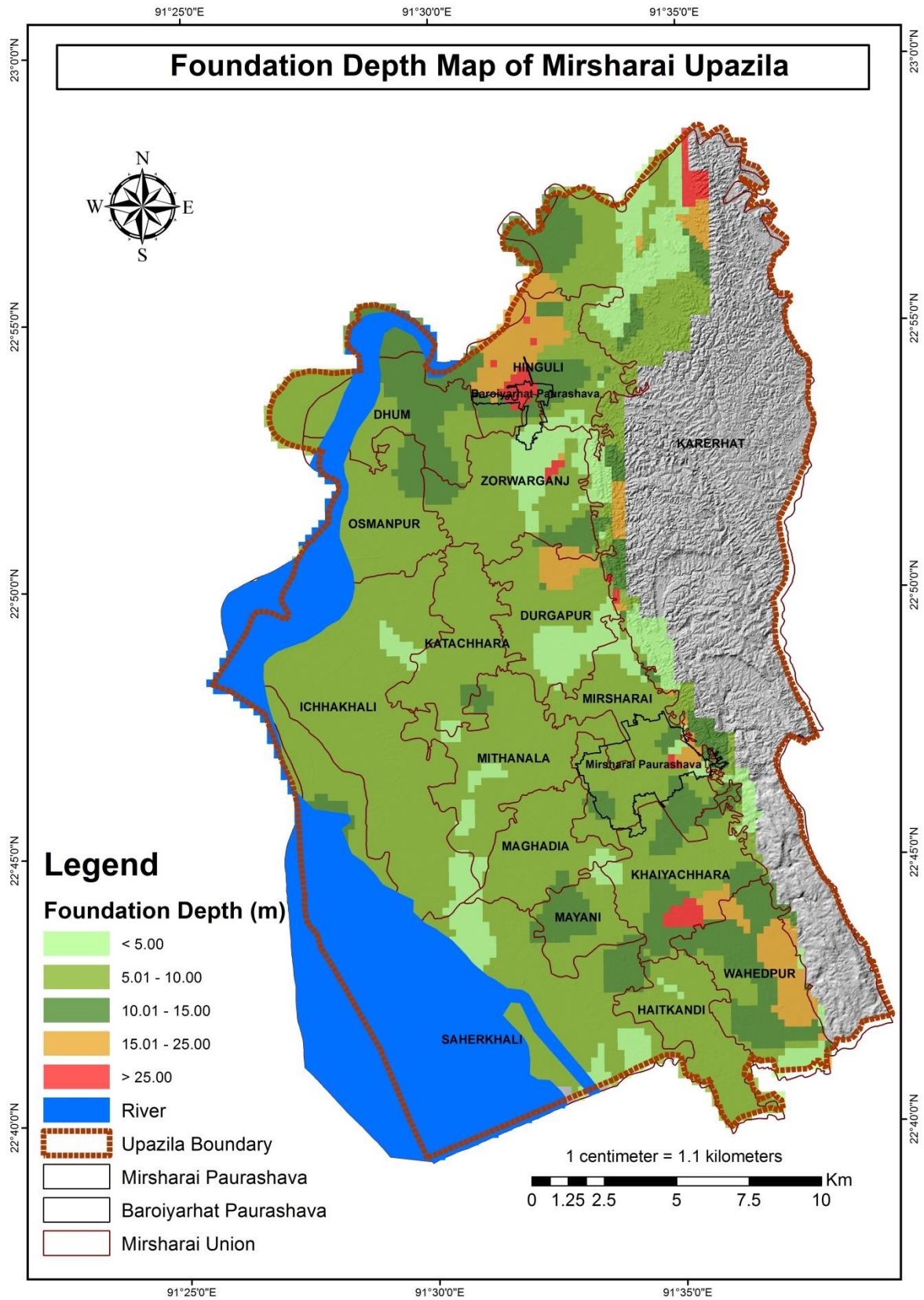


Figure 3.3 Foundation depth of Mirsharai Upazila

3.3. Subsurface cross-section

Five cross-sections were prepared, two roughly in North-south direction, one East west, one North-east and one North-west direction. Each cross section covers several boreholes and many boreholes that are very close to the section line. There are 8 different facies assemblages encountered in this area by borehole, where most of the layers are inconsistent.

Cross-section A-A'

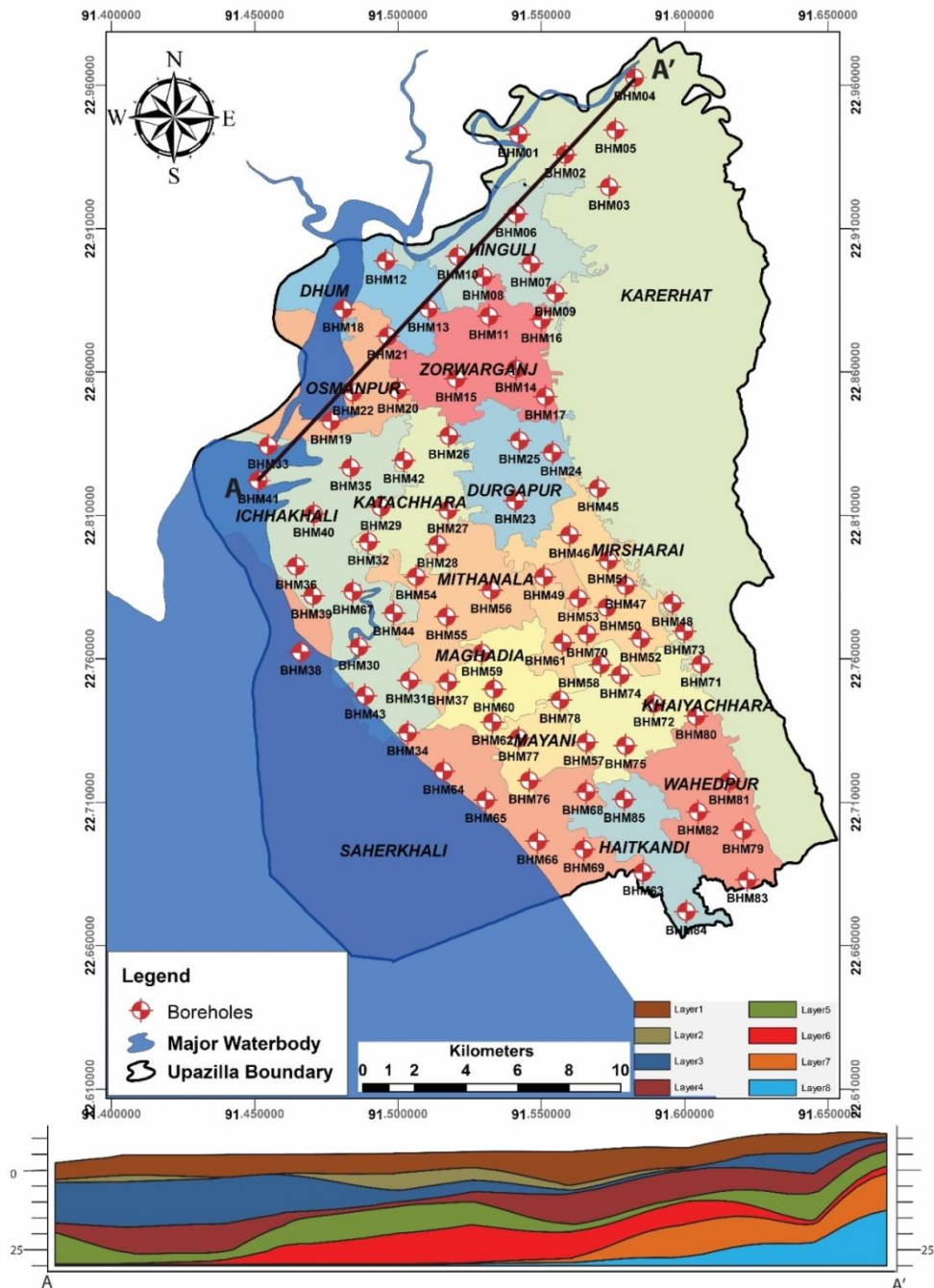


Figure 3.4 Cross-section A-A'

Cross-section A-A' is drawn in northern portion of the studied area in N-W direction that cover approximately 20.766 km from BH_M41 to BH_M4. It encounters BH_M 21, BH_M 6, BH_M 2 and has a close proximity to BH_M33, BH_M19, BH_M13, BH_M10, BH_M5. In this section all layers was encounter but varies in thickness.

Cross-section B-B'

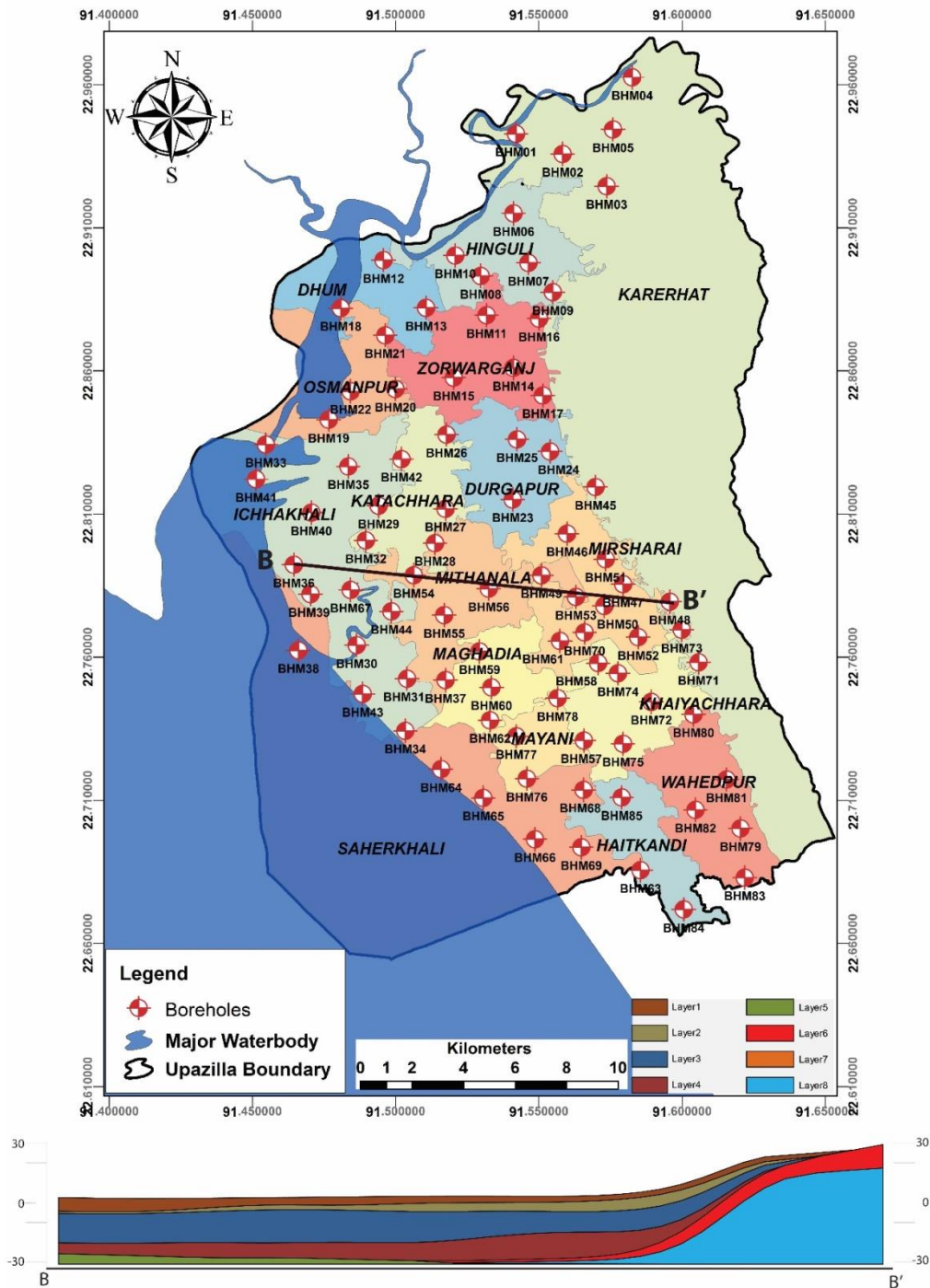


Figure 3.5 Cross section B-B'

Cross section B-B' is drawn along the middle portion of the studied area that cover approximately 12.88 km from BH_M36 to BH_M48, where It encounters BH_M28 and

BH_M53as well. Layer Thickness in almost uniform from 36 to 47, noticeably layer1 have 1to 5m, Layer2 have 1-4, Layer3 have 10-15m Layer 4 have 5-6m thickness. Layer 2 pinched out near 36 and Layer5 was found at the base of Layer4 but. It also pinched out near 48 along with other layers such as 1,2,3,4. Layer 7 was not encountered in any of this borehole. Highest thickness of the Layer 6 found in 48 and also Thickness of the Layer 8 at and near 48 was about 30m and its base was not found.

Cross-section C-C'

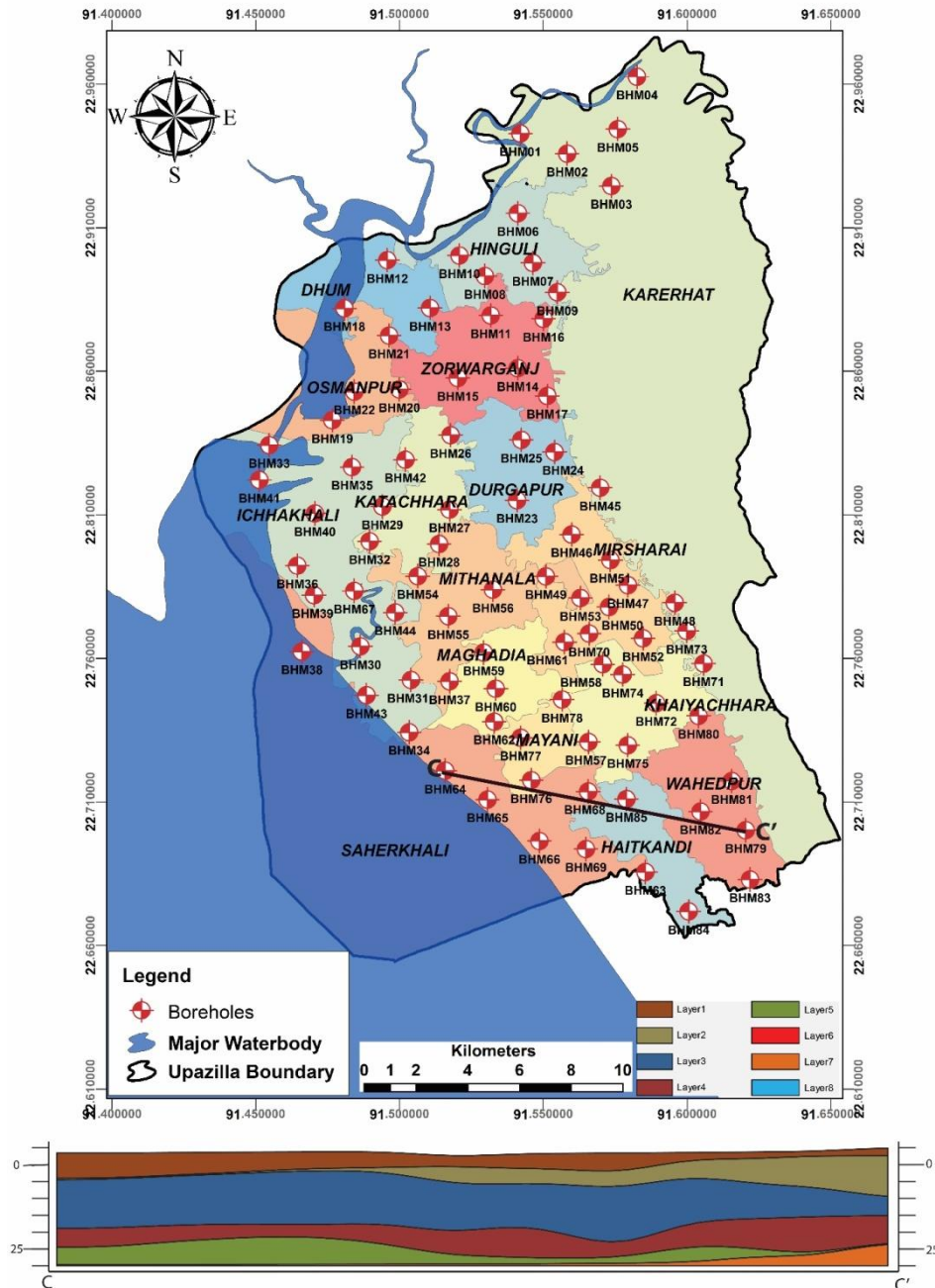


Figure 3.6 Cross section C-C'

Cross section C-C' is drawn in the southern portion of the studied area in NWW direction that cover approximately 10.976 km from BH_M64 to BH_M79. It encounters BH76 68 85

82 . At 64 Layer1 is about 5 to 6 m , Layer 3 is 15-16m, Layer 4 is about 4-5m and Layer6 is about 5 to 8 m in thickness.Layer 2 is absent here but near 76 its thickness is 2-3 m and it increased toward 79 and become 10-12m while layer1 become 1-2m in thickness. Layer 4 Varies from 4 to 8 m in thickness throughout the section. Layer 7 was found in bore 79 but it was very thin. Layer-8 was absent in this section.

Cross-section D-D'

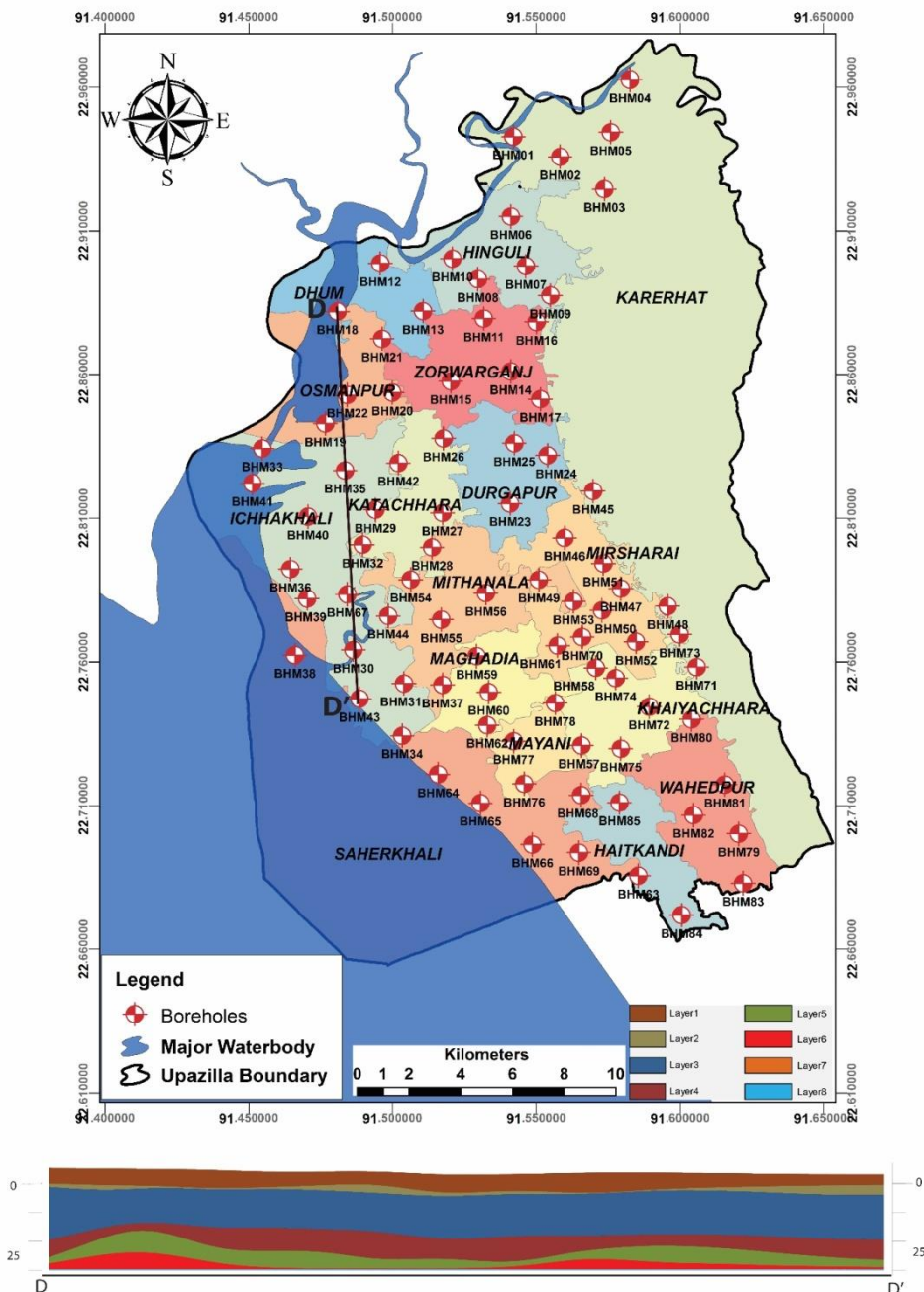


Figure 3.7 Cross section D-D'

Cross section D-D' is drawn along the middle portion of the studied area that cover approximately 14.924 km from BH_M18 to BH_M43. It encounters BH_M 22, BH_M19 BH_M35 BH_M67 BH_M30. Layer 1 is 1-6m in thickness where layer 3 is 15-20m in

thickness throughout the section. Layer 4 is about 8-10 m in thickness but decreased near 22 and 67. Layer5 is mostly thin in this section but have 5-8m thickness near 22. Layer 6 also has the same condition as the Layer5. Layer7 and Layer 8 was found in this section.

Cross-section E-E'

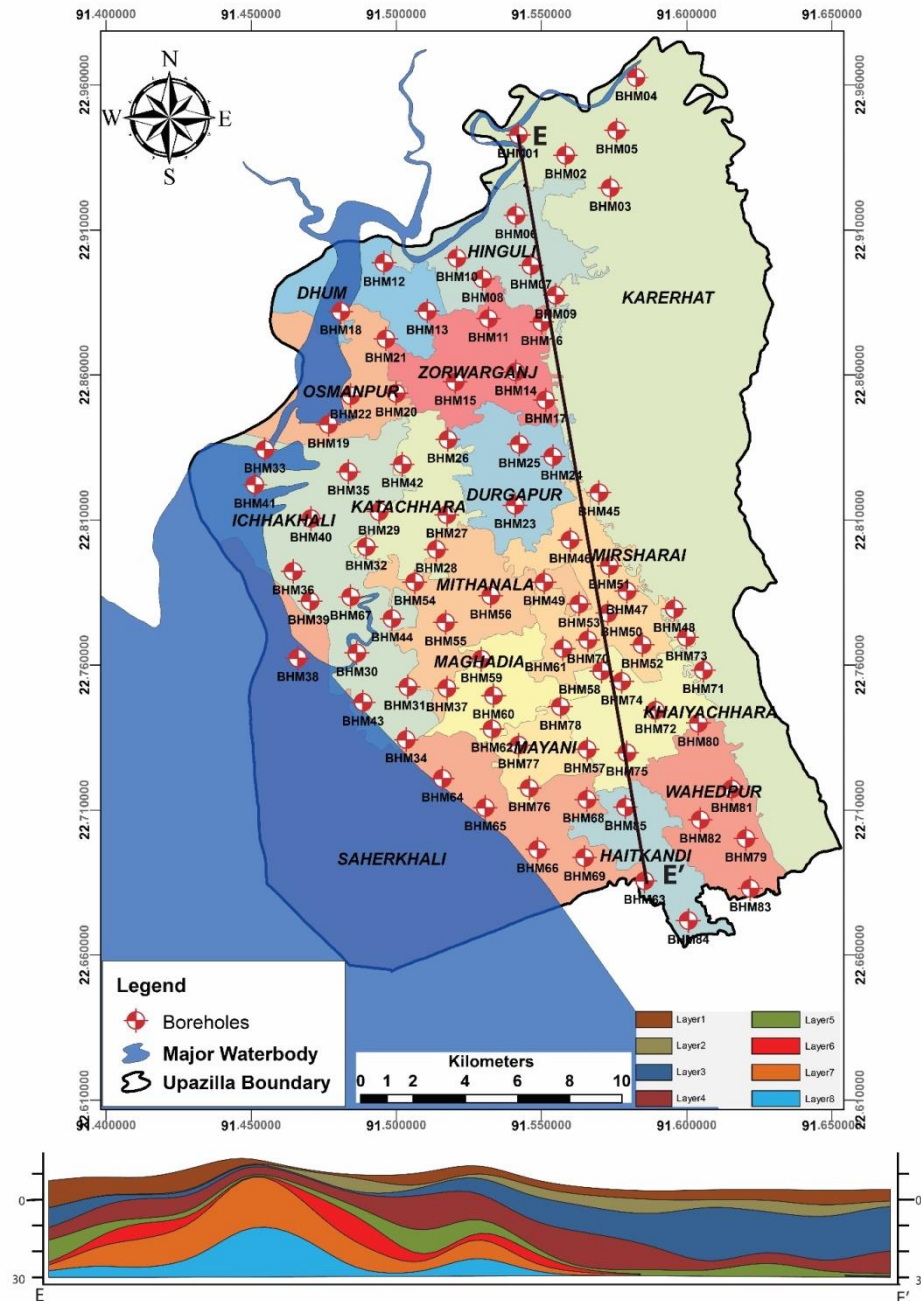


Figure 3.7 Cross section E-E'

Cross section E-E' is drawn along the middle portion of the studied area that cover approximately 27.69km from BH_M1 to BH_M69. In the east portion layer 1,2,3,4 have average thickness of 5m, 3m, 20m, 10m respectively. Near the borehole No. BH_M 9 to

BH_M 45 these layers pinched and layer 7 and 8 have thickness of about 15m each. In the southern part of the cross-section represents nearly 20 m thick layer 3.

4. SEISMIC HAZARD ASSESSMENT

Seismic hazard is a broad term used in a general sense to refer to the potentially damaging phenomena associated with earthquakes, such as ground shaking, liquefaction, landslides, and tsunami. In the specific sense, seismic hazard is the likelihood or probability of experiencing a specified intensity of any damaging phenomenon at a particular site or over a region in some period of interest. The methodology for assessing the probability of seismic hazards grew out of an engineering need for better designs in the context of structural reliability (Cornell, 1968; Cornell, 1969), since such assessments are frequently made for the purpose of guiding decisions related to mitigating risk. However, the probabilistic method has also proven to be a compelling, structured framework for the explicit quantification of scientific uncertainties involved in the hazard estimation process. Uncertainty is inherent in the estimation of earthquake occurrence and the associated hazards of damaging ground motion, permanent ground displacements, and in some cases, seiche and tsunami. The process begins with the characterization of earthquake occurrence using two sources of data: observed seismicity (historical and instrumental) and geologic. The occurrence information is combined with data on the transmission of seismic shaking to form the seismotectonic model. Since uncertainty is inherent in the earthquake process, the parameters of the seismotectonic model are systematically varied via logic trees, Monte Carlo simulation, and other techniques, to provide the probabilistic seismic hazard model's results. The results may be disaggregated (also known as deaggregation) to identify specific contributory parameters to the overall results. The results must also consider the site-specific soil properties.

However, there remains gaps and a lack of understanding in the existing seismic studies of the country such as limited consideration for site effects, uncertainties in source parameters and zonation, lack of a complete catalogue, selection of region appropriate GMPEs amongst others. Consequently, an updated seismic hazard model for the country is imperative and necessitated by new data, recent findings, and improved methodologies. In this study we attempt to perform a new probabilistic seismic hazard analysis (PSHA) of Bangladesh addressing some of the existing shortcomings. This includes using revised seismic source zones based on the recent study of Wang (2014), declustering the events with two different established methods, tackling uncertainties with the logic-tree approach as well as applying different GMPEs and accounting for the site conditions throughout the country. As the project is very much concerned with the future development of Mirsharai Upazaila, this report particularly focus on the seismic hazard scenario of the project area. This report

contains the PGA (peak ground acceleration) and PSA (peak spectral acceleration) information with 2% and 10% probability of occurrence in 50 years.

4.1. Study Area

The area of concern for this study is the tectonic regime in and around Bangladesh and detailed seismology, geodesy, and tectonics study has revealed that Bangladesh is surrounded by five major potentially active seismotectonic regimes (Wang et al. 2014). The complex interaction of Indian plate with Eurasian and Burma Silverplate, results in a great threat of earthquakes for Bangladesh. The country has experienced five major destructive earthquakes with Richter magnitude 7.0 and above (ADPC and OYO 2009; Ambraseys 2004; Bilham 2004) over the past 150 years.

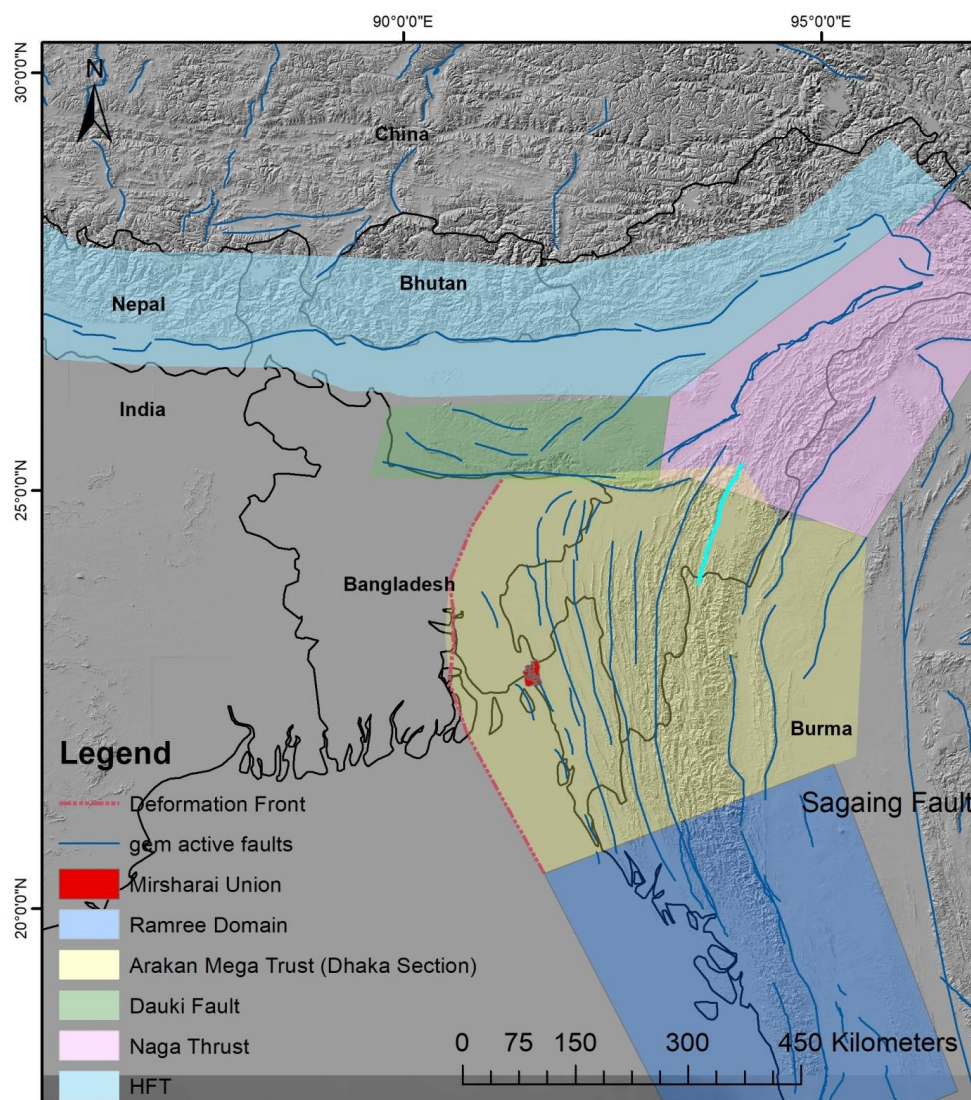


Figure 4.1 Major Seismotectonic regimes in and around Bangladesh. It has been overlaid on a hillshaded SRTM Digital Elevation Model (DEM) of 30m resolution (Source: <https://earthexplorer.usgs.gov/>) Adopted from Wang (2014).

The Himalayan Thrust Fault (HFT) marked by the collision between Indian plate and Eurasian plate in the north, extends to almost 2000km from the Kashmir in the west to the Himalayan syntaxes in the Assam (Yu & Sieh 2013). Just south of the HFT lies the 270km long north dipping reverse Dauki fault running along the southern flank of Shillong plateau. Arakan megathrust runs as concave folded thrust belt on the other side of Bangladesh from south to northeast. The Ramree domain is characterized by sustained convergence and pronounced seismicity in the northern part as opposed to its southern counterpart and is 450km long (Wang et al. 2014). This tectonic regime has produced a deformation belt that increases its width from about 170km in the south to about 250km in the north. The north of Ramree domain, the Dhaka section (~500km long & ~400km maximum width) of Arakan Mega Thrust is formed due to the collision of Burma silver plate and thick sediment laden Ganges-Brahmaputra delta (Wang et al. 2014). Recent studies by Steckler et al. (2016) have revealed the presence of locked megathrust deformation front boundary underneath the Dhaka, the densely populated capital of the country. Numerous thrust faults exist in the Chittagong Tripura Folded Belt (CTFB) of this region. A 430km long and 160-240km wide section of the NE and SW trending Naga Thrust regime is present between the Shilling plateau and Himalayan syntaxis, formed by the Indo-Burman plates collision (Wang et al., 2014). In addition, the 1400 km long Sagaing fault system is another likely source of major earthquake and it lies between Andaman sea ridge spreading zones in the south to the eastern Himalayan syntaxes in the north.

The probability of occurrence of a major earthquake and the recurrence interval for each tectonic regime from the fault zone length and slip rate has been estimated by Yu & Sieh (2013). The Arakan megathrust (Dhaka section), HFT and Ramree show the highest potentiality of generating major earthquake. The maximum magnitude earthquake that can be generated from each of the source regimes has also been estimated. The relationship of Strasser et al. (2010) used is as follows:

$$M_w=4.868+1.392\log(L)$$

Here L is the length of fault path that would produce anticipated earthquake and M_w refers to moment magnitude converted from seismic moment using Hanks & Kanamori (1979) relation,

$$\log(M_o)=1.5M_w+16.1, \text{ where } M_o= \mu AD$$

Here the recurrence intervals are just a coarse approximation of the time between maximum sized earthquakes for the five major faults (Yu & Sieh 2013).

Some of the important source parameters of the five tectonic regimes are given in Table 4.1 which have been inferred from the study of Wang et al. (2014). A rake value of 90 degrees is assumed for reverse faults.

Table 4.1 Source Zone Parameters

	Length(km)	Dip	Rake	Strike	Hypocentral Depth(km)	M _{max}	Slip Rate	Recurrence Interval
CTBF	~500	<10	90	345	20	8.6	10	Unknown, perhaps 1548
HTF	~500	~10	90	90	20	8.6	21	1100 (?)
Dauki	~270	~45	75	90	35	8.3	11	1897
Naga	~400	~23	90	48	20	8.5	5	Unknown
Ramree	~500	~16	90	325	30	8.6	23	1762

Source: Yu & Sieh (2013)

4.2. Methods

The PSHA is carried out following the Hazard Modelers Toolkit (Weatherill 2014) of OpenQuake engine developed by Global Earthquake Model (GEM). This is a free and open source software written in the Python programming language for calculating seismic hazard and risk at variable scales (from single sites to large regions) (Silva et al. 2014). The steps followed are discussed below.

Earthquake Catalogue and Magnitude Homogenization

The initial step involves gathering seismicity data from earthquake catalogue for in and around Bangladesh. The records of 3296 events, within a geographical limit of 18.021°-30.031° latitude and 85.034°-96.987° longitude, between years 1505 and 2018 has been collected from

the USGS, GEM-ISC, BSSA, and BMD (Bangladesh Meteorological Department) catalogue. All the events are arranged in a chronological order and checked for redundancy.

Since the catalogue contains different magnitude scales such as surface-wave magnitude (M_s), body-wave magnitude (M_b), local or Richter scale Magnitude (M_l) and moment magnitude (M_w), magnitude conversion for all the events is performed to homogenize the unit of measurement. The magnitudes are all expressed as moment magnitude, M_w , because it does not tend to saturate for large events (Hanks & Kanamori 1979). The conversion relations between different types of magnitudes ($M_s/M_b/M_l$) and moment magnitude that are used is given below and a map showing all the events is shown in figure 4.2.

Table 4.2: Magnitude conversion empirical relations

Magnitude	Magnitude Range	Magnitude Conversion Relation	References
M_s	3.0 to < 6.2	$M_w = 0.67 M_s + 2.07$ ($\sigma = 0.17$)	(Scordilis 2006)
	6.2 to 8.2	$M_w = 0.99 M_s + 0.08$ ($\sigma = 0.20$)	(Scordilis 2006)
M_b	3.5 to 5.5	$M_w = 0.85 m_b + 1.03$ ($\sigma = 0.20$)	(Scordilis 2006)
	5.5 to 7.3	$M_w = 1.46 m_b - 2.42$	(Sipkin 2003)
M_L	$M_L \leq 6$	$M_w = M_L$	(Heaton & Tajima 1986)

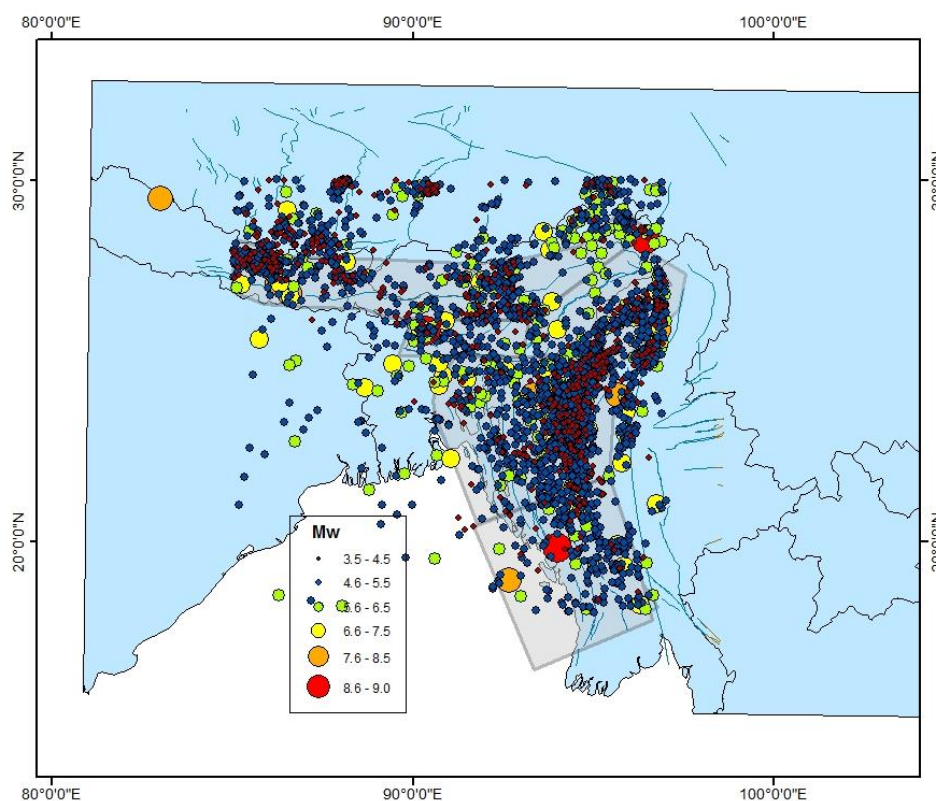


Figure 4.2 Map showing the earthquake events in and around Bangladesh between 1505-2018

Declustering

This catalogue is then declustered because PSHA based on the Cornell (1968) approach assumes a Poissonian process, where seismic events are considered temporally independent. Thus the dependent events (foreshocks, aftershocks or swarms) are separated from the mainshocks. In this study, two different algorithms for declustering are applied to the catalogue separately, namely the

Garnder & Knopoff (1974) method and the algorithm used in AFTERAN program (Musson 1999).

Gardner and Knopoff (1974)

In the first method, the events are sorted in descending order of magnitude and dependent events within fixed temporal and spatial windows which depend on the magnitude of the events are identified. The algorithm thus identifies foreshocks and aftershocks by considering the windows forwards and backwards in time from the main shock. Garnder & Knopoff (1974) are approximated by:

$$\left. \begin{array}{l} \text{distance (km)} \\ \text{time (decimal years)} \end{array} \right\} = \begin{cases} 10^{0.1238M+0.983} \\ 10^{0.032M+2.7389} & \text{if } M \geq 6.5 \\ 10^{0.5409M-0.547} & \text{otherwise} \end{cases}$$

There have been some modifications to the original window and while declustering using the GK algorithm, in this study we apply the one proposed by Uhrhammer [1986] which is as follows:

$$\text{distance (km)} = e^{-1.024+0.804M}$$
$$\text{time (decimal years)} = e^{-2.87+1.235M}$$

Out of total 3296 events, the GK declustering method leaves us with 2450 events. Among these events, 1936 (i.e. 59% of the total events) of them are only considered finally because the rest fall outside the five seismic source zones (as shown in table 4.2 and figure 4.3).

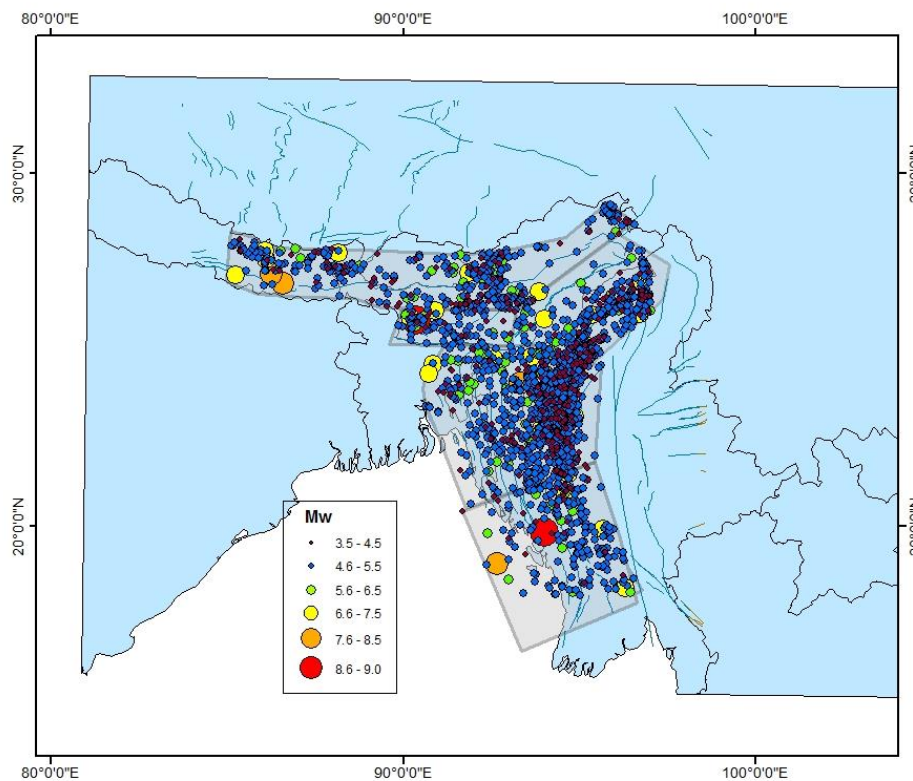


Figure 4.3 Events after declustering using GK method

AFTERAN (Musson 1999)

The AF approach is a modification of the GK approach but is slightly more computationally complex. Here, instead of a fixed time window, a moving-time window is used. At first the

events are arranged into their magnitude-descending order after which the events within fixed distance windows are identified using a moving time window of T days. The events which fall both within the distance window and the T days' time-window are declared as dependent ones. The time window is then shifted to the next event, and the process is repeated. In this study, in order to retain a significant number of events and also ensure a Poissonian process, the AF algorithm with a GK distance window and 100 days' time-window is used to decluster the catalogue.

This procedure leaves us with a total of 3197 events out of the initial 3296. Again, we only consider the events which lies within the perimeters of the five source zones and that filters out a final of 2477 events which constitutes 75% of the original dataset (shown in table 4.3 and figure 4.4).

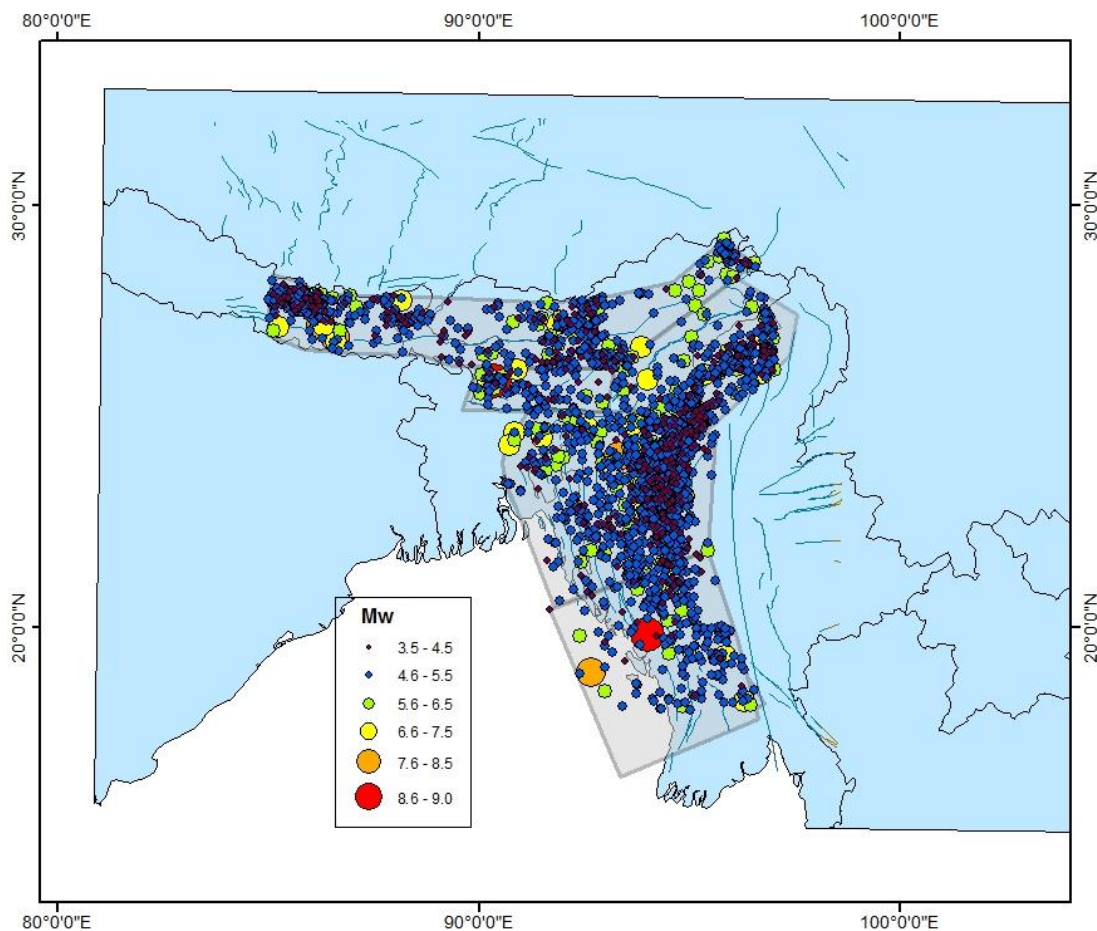


Figure 4.4 Events after declustering using Musson method

Table 4.3 Summary of seismic events

	Before Declustering	After Declustering
Gardener and Knopoff	3296	1936
AFTERAN (Musson)		2477

Both the methods resulted in different number of events for each of the five seismic zones as shown in table 4.4

Table 4.4 Number of events in each seismic zone after declustering

	GK	Musson
CTFB	872	980
Dauki	89	91
HTF	383	711
Naga	382	455
Ramree	210	240
Total	1936	2477

Depth distribution of the events from both methods of declustering is shown in figure 3.4.

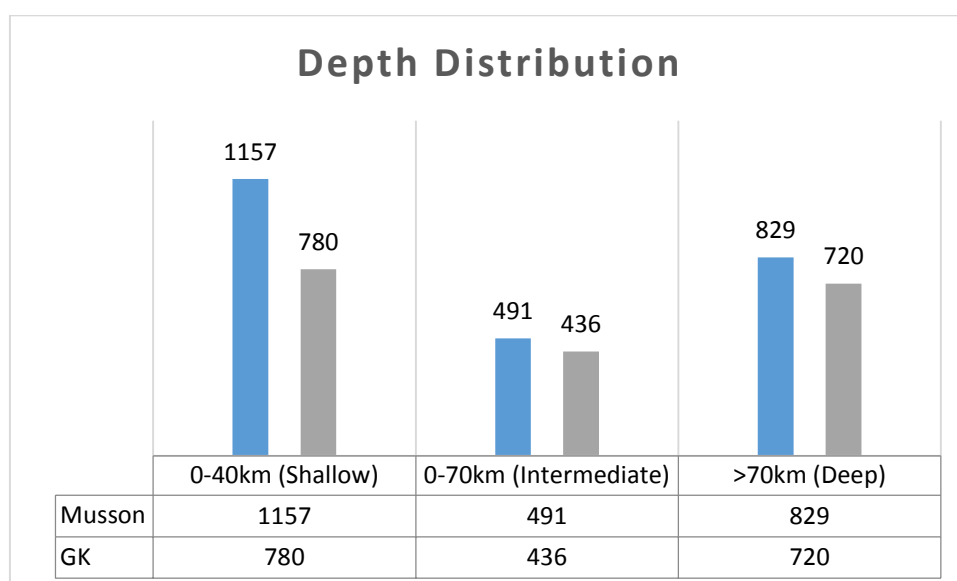


Figure 4.5 Bar chart showing the depth distributions of earthquake events

Catalogue Completeness

The completeness of the catalogue is estimated using the Stepp (1972) method to determine the smallest magnitude at which all of the earthquakes in space and time have been detected (i.e. magnitude of completeness, M_c). The Stepp (1972) method uses the standard deviations of empirical annual occurrence rates of events of different magnitudes classes for different

time intervals, identifying the M_c when the observed rate of earthquakes above M_c starts to show deviation from the expected rate.

The unbiased estimate of the mean rate of events per unit time interval of a given sample, if time interval, T_i is taken and Poissonian distribution of events assumed, is:

$$\lambda = \frac{1}{n} \sum_{i=1}^n T_i$$

with variance $\sigma_i^2 = \lambda/n$. For unit time interval of 1 year, the standard deviation of the estimate of the mean is

$$\sigma_\lambda = \sqrt{\lambda}/\sqrt{T}$$

where T is the sample length.

Identification of the M_c is a very crucial step for seismic hazard analysis because incomplete catalogues can affect the recurrence parameters of the source zones which in turn may significantly impact the estimation of hazard at a site. The following magnitude and years are considered to be complete in the earthquake catalogue and the Stepp plots for both methods are shown in Figure 4.6.

Table 4.5 Years of Magnitude Completeness

Completeness Magnitude	Year of Completeness	
	Gardner	Musson
3.0	1982	1987
4.0	1982	1987
5.0	1966	1974
6.0	1939	1913
7.0	1820	1815

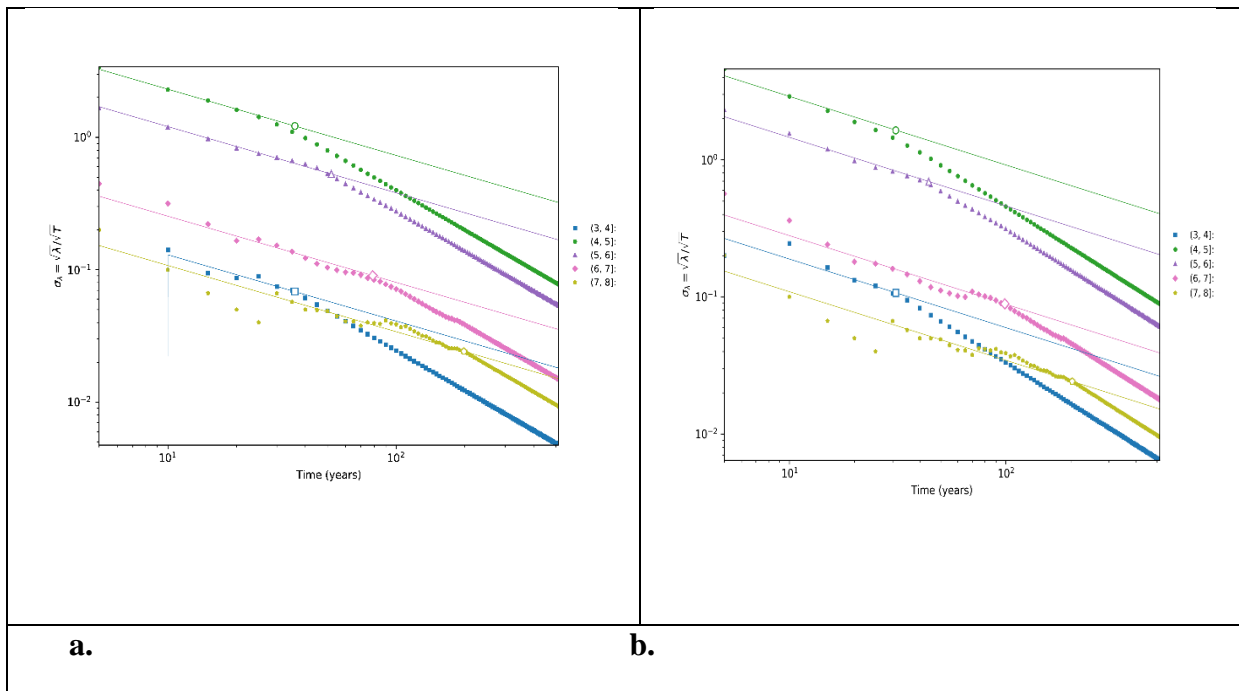


Figure 4.6 Step plots of completeness magnitudes for (a) Gardner (b) Musson

It is clear that events of small magnitudes are complete from recent years (around 40 years ago) most likely due to lack of devices to detect them while events of larger magnitudes are completed from a longer period of time as they were easier to detect.

Recurrence Relationships

Gutenberg-Richter (GR) recurrence relationship for each source zones in obtained the form:

$$\text{Log}_{10}(N) = a - bM$$

where, N represents the cumulative number of earthquakes above magnitude M , and a and b are two constants (Gutenberg & Richter 1944). Constant b is the measure of the relative abundance of large to small shocks. The GR parameters for the zones were estimated by the Maximum Likelihood (ML) method in this study. This method is an adjustment of the Aki (1965) and Bender (1983) approach to incorporate for time variation in completeness. The catalogue is divided into S sub-catalogues, where each sub-catalogue corresponds to a period with a corresponding M_c . The mean of the a - and b -values of each sub-catalogue, weighted by the number of events in each sub-catalogue, is taken to give the average a and b -values along with their uncertainties.

The a (intercept) and b -values (slope) of the magnitude-frequency for the five sources is shown in the table 4.6 below

Table 4.6 Recurrence ‘a’ and ‘b’ values for each zone

	GK		Musson	
	a-value	b-value	a-value	b-value
CTFB	3.41	0.68	3.90	0.71
HTF	3.20	0.61	2.52	0.36
Dauki	3.96	0.89	3.74	0.84
Naga	4.41	0.83	3.99	0.74
Ramree	3.52	0.67	2.90	0.54

The b value is usually 1 for seismically active regions. Higher values of b denotes that smaller magnitude events are more abundant than the larger ones for that particular region.

Maximum Magnitude

The source parameter maximum magnitude, M_{max} , simply defined as the largest possible earthquake that can occur in a certain region is associated with considerable epistemic uncertainties due to the evident limitations in its observability (Cornell 1968). For this study, the cumulative moment method is employed to estimate the maximum magnitude. This method has been adapted from the cumulative strain energy release method for estimating M_{max} which was initially proposed by Makropoulos & Burton (1983) where the M_{max} is derived from a plot of cumulative moment release against time.

The table below shows the M_{max} values for the five seismogenic source zones in this study. Generally, intraplate regions have maximum moment magnitudes varying between 6.5 and 7.0 whereas, for plate boundary regions it is between 8.0 and 9.0. The resulting M_{max} values are compared with those obtained from the magnitude-scaling relationships of Strasser et al. (2010) and consistency is found for most of them. For both declustering methods similar maximum magnitudes were obtained.

Table 4.7 Maximum magnitudes for each zone using cumulative moment method

	Maximum Magnitude
CTFB	8.3
HTF	7.9
Dauki	8.7
Naga	7.5
Ramree	8.8

Ground Motion Prediction Equation (GMPEs)

Selection of appropriate ground motion prediction equations to account for the attenuation of seismic energy is a rather challenging task which depends on the regional tectonic characteristics of the site of interest. Generally, three GMPEs are developed for three broad categories of regions, namely, shallow crustal events in active tectonic regimes (e.g. Western North America), shallow crustal earthquakes in stable continental regions such as that in Central and Eastern North America and finally for subduction zones (e.g. Pacific Northwest). Attenuation models relate the effect Y at a site to magnitude and distance, so that in general

$$Y=Y(M,r)$$

Where M is usually moment magnitude and 'r' can refer to the various types of distances. Some models use epicentral distance (R_{epi}), some use closest distance to fault rupture (R_{rup}), and some models use Joyner-Boore distance (R_{JB}).

No specific GMPE has been developed for Bangladesh which is why GMPEs used in neighboring regions or those in areas having similar geologic and tectonic attributes are used in the study. For active shallow crustal zones, Abrahamson & Silva (1997) and Boore & Atkinson (2008) relations have been used while for subduction zones, Youngs et al (1997) and Atkinson & Boore (2003) have been applied. In stable continental crusts, Atkinson & Boore (2006) and Campbell & Bozorgnia (2003) empirical relationships are used.

Site Effects

Taking site effects into account is a very important requirement for accurate estimation of seismic ground motion at site. For this study, V_{s30} which is the average shear wave velocity at 30m depth is considered. This has been measured for various locations throughout the

country using PS-logging and other methods. Most of the country falls under site class SC (V_{s30} ranging from 180-360 m/s) or site class SD (V_{s30} less than 180 m/s) (BNBC 2015). The relation between $Z_{1.0}$ and V_{s30} given by Chiou & Youngs (2008) is used to estimate the depth to shear wave velocity $V_S = 1.0$ km/s ($Z_{1.0}$) and while depth to $V_S = 2.5$ km ($Z_{2.5}$) is assigned 2 km following and Chowdhury (2016) and Boore & Atkinson (2008.)

Logic Tree Formulation

Logic tree approach has been used to tackle the epistemic uncertainties within certain source parameters (a and b- values of recurrence relationships) as well as for different GMPEs that were used for different tectonic regimes. Equal weights have been assigned to all branches because no concrete reason appeared to prefer one option over the other. The GMPE and source logic trees are shown in figure 4.7 and 4.8, respectively.

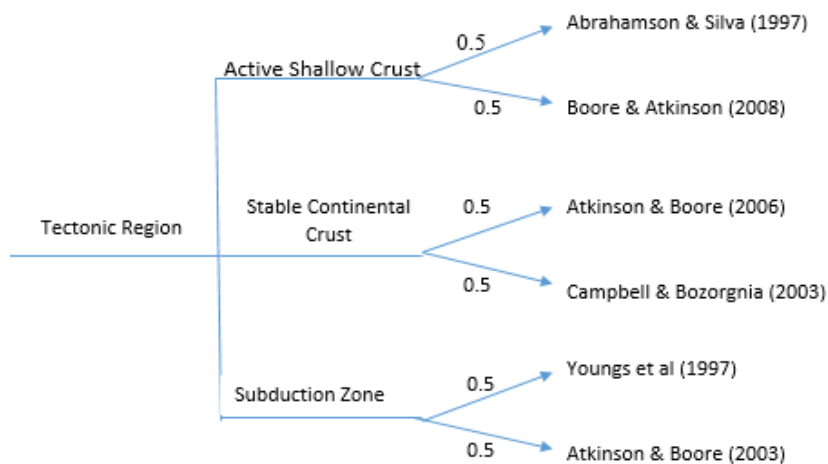


Figure 4.7 GMPE Logic Tree

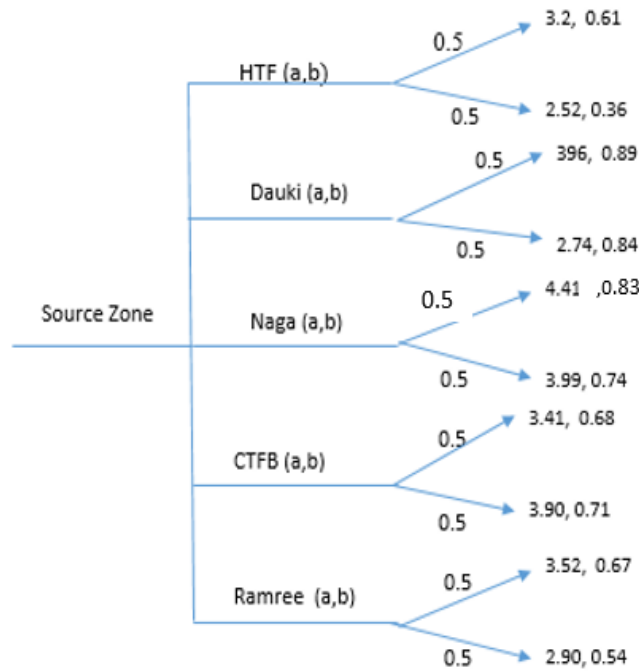


Figure 4.8 Source Logic Tree for a- and b-values

PSHA calculation

In the probabilistic seismic hazard assessment (PSHA) method, the ground motion at a site is estimated for a specified probability of being exceeded in a given time period (Cornell 1968). The results of PSHA can be expressed in many ways all of which involves some level of probabilistic computations combining uncertainties in earthquake size, distance, frequency and effects to estimate seismic hazard. A common approach involves the development of hazard curves which indicate the annual probability of exceedance of a ground motion parameter, which can then be used to calculate the probability of exceeding that parameter in a specific period of time. The standard Cornell-McGuire approach which is the basic calculation to find the probabilities is as follows:

$$E(z) = \sum_{i=1}^{N_s} V_i \int_{r=0}^{\infty} \int_{M_{min}}^{M_{maxi}} f_m(m) f_{ri}(r) P(Z>z | m,r) dr dm$$

where,

$E(z)$ = mean annual rate of exceedance of ground motion level “z” during a specified time period “t”;

N_s = number of seismogenic sources;

v_i = mean rate of occurrence of earthquakes between lower/upper bounds magnitude “m” being considered for the “ith” source

$f_{m_i}(m)$ = probability density distribution of magnitude within the “ith” source, which is obtained using the Gutenberg-Richter relationship;

$f_{r_i}(r)$ = probability density distribution of epicentral distance “r” between various locations within source “ith” and the site where hazard is estimated;

$P(Z > z | m, r)$ = probability that a given earthquake of magnitude “m” and epicentral distance “r” will exceed ground motion level “z”, which is obtained employing the selected attenuation relationships.

In this study, the OpenQuake software is used to perform classical PSHA calculations for Bangladesh by specifying the region grid coordinates. Hazard maps, curves and uniform hazard spectra are investigated for 50 years’ time period and calculated at 10% and 2% probabilities of exceedance. Spectral accelerations are computed for periods ranging from 0 to 2.0 seconds. Region grid-spacing of 15km is used to obtain a balance between the precision and computational demand and time. A pragmatic truncation value of 3 sigma (σ) for GMPEs is used because it was seen that values less than 3 were inappropriate (e.g. Strasser et al. (2010) and Bommer & Abrahamson (2006)).

4.3. Results and Discussion

The seismic hazard maps for Bangladesh are presented in figures below displaying spatial distribution of PGA and PSA at 0.2s, 0.3s and 1sec computed for 10% and 2% probability of exceedance in 50 years, which correspond to 475 and 2475 years recurrence interval respectively. These return periods are considered because they are the most commonly used parameters to express the PGA values which makes it easier for comparison while calculation of spectral accelerations at 0.2s, 0.3s and 1s periods for return periods of 475 and 2,475 years is consistent with building codes.

The results show that the PGA estimates in Bangladesh range from 0.097g to a maximum of 0.72g for 10% probability of exceedance. The south-eastern and north-eastern regions (including Chittagong and Sylhet) exhibit the highest PGA values of greater than around 0.5g, while the central regions (including Dhaka) have values ranging from 0.2g to 0.4g and the south-western sides have the least PGA values. As the return period increases to 2,475 years so does the PGA values, with the lowest being 0.18g and reaching up to 1.27g. The

distribution pattern is similar for both return periods. The level of high hazard in the southwestern zone can be attributed to the presence of the subduction zones of Ramree domain and CTFB which depict high seismicity. The stable continental crust zones have relatively less PGA values.

The maps for the peak spectral accelerations also show high values in the southeast and northeast regions as well as the northern tip of the country which may be due to the influence of the Himalayan Thrust Fault. The values for period 0.2 seconds are the highest with a maximum of 2.20g for 2% probability of exceedance. The spatial distribution of PSA at 0.2s is similar to that of the PGA distribution however, that of 1.0s and 2.0s shows some variation. This difference in pattern was also found in the studies of Al-Hussaini & Al-Noman (2010).

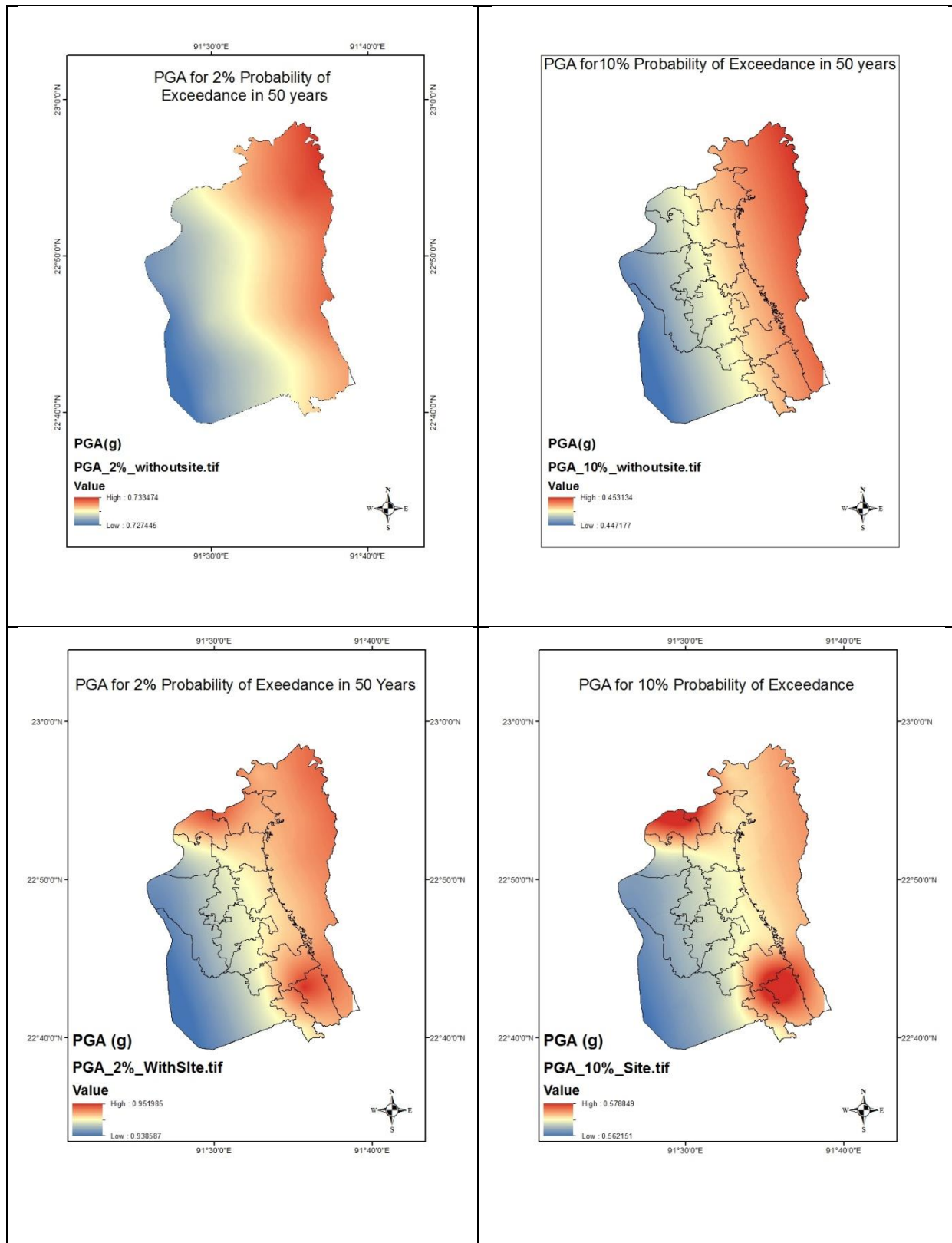


Figure: 4.9 PGA maps for (a) 2% and (b) 10% probabilities of exceedance in 50 years without and with site effect

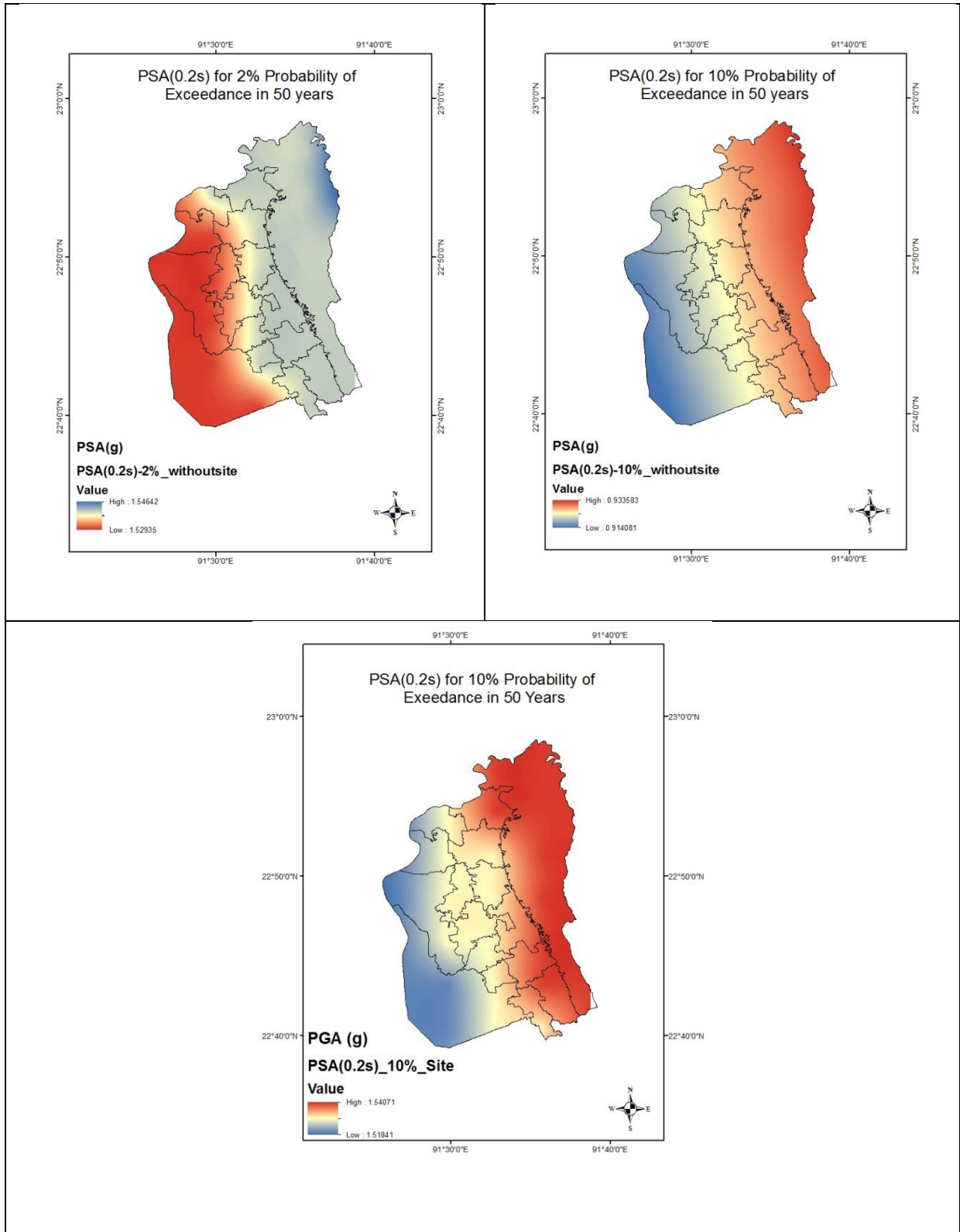


Figure: 4.10 PSA at 0.2 seconds maps for (a) 2% and (b) 10% probabilities of exceedance in 50 years without and with site condition

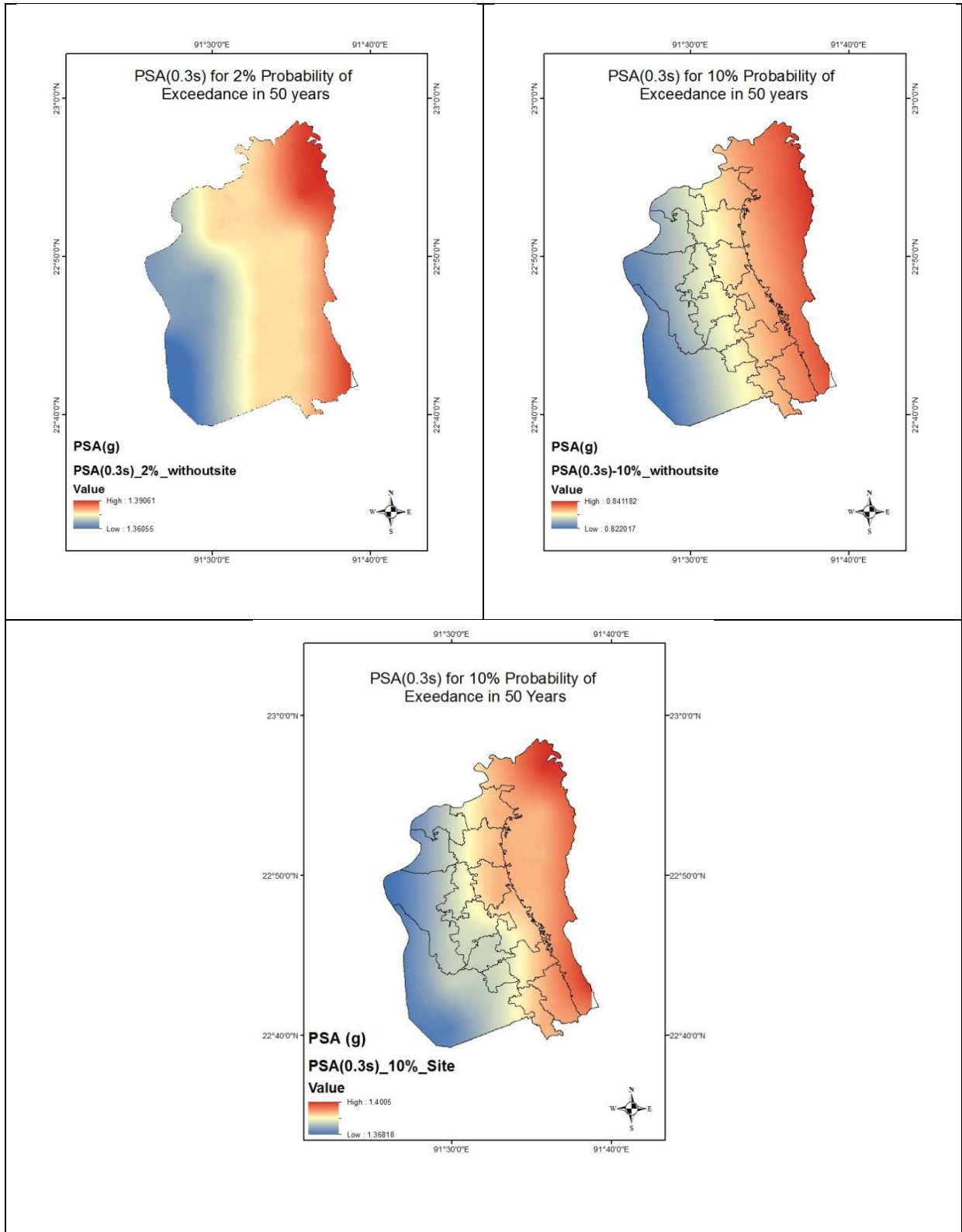


Figure: 4.11 PSA at 0.3s maps for (a) 2% and (b) 10% probabilities of exceedance in 50 years without and with site effect

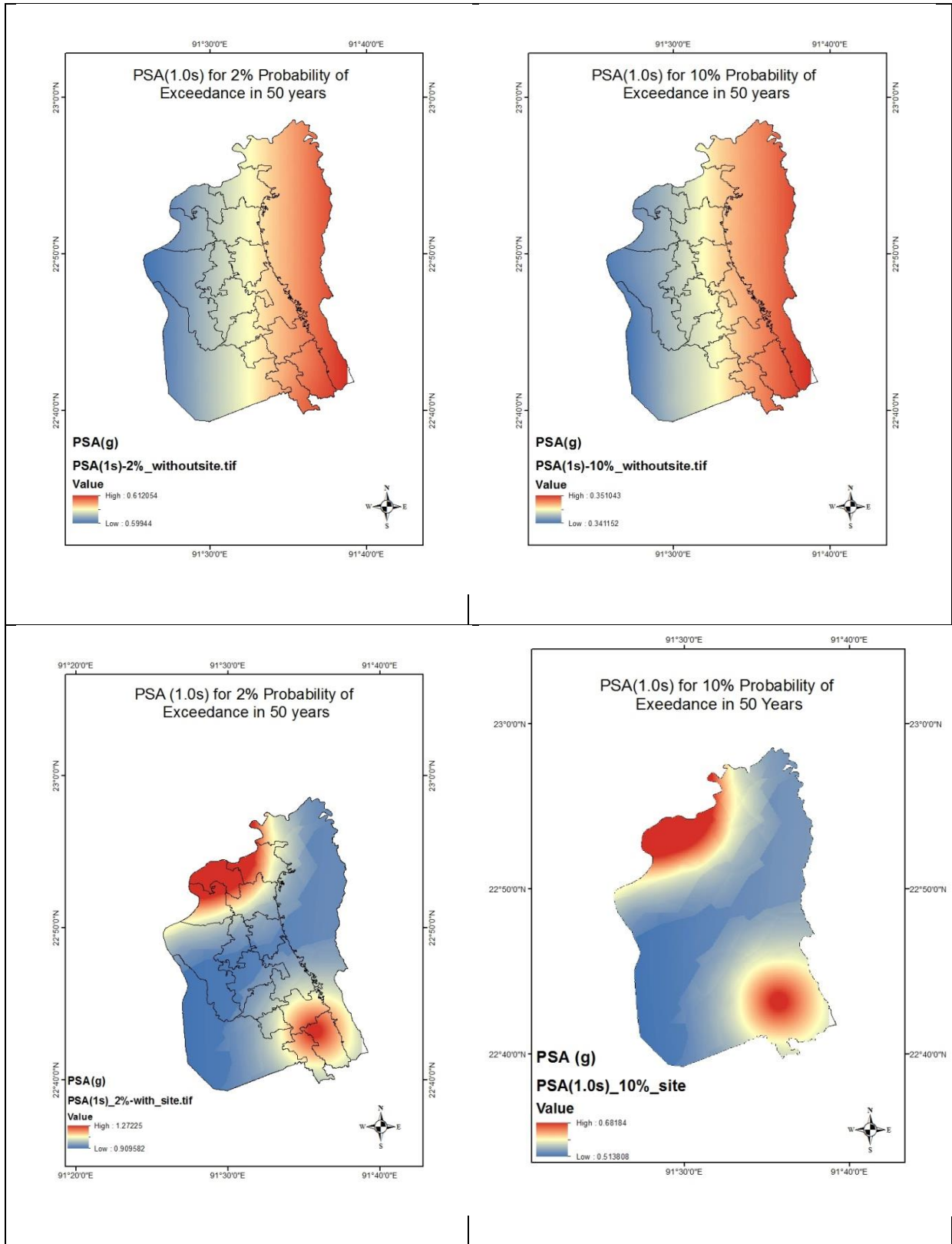
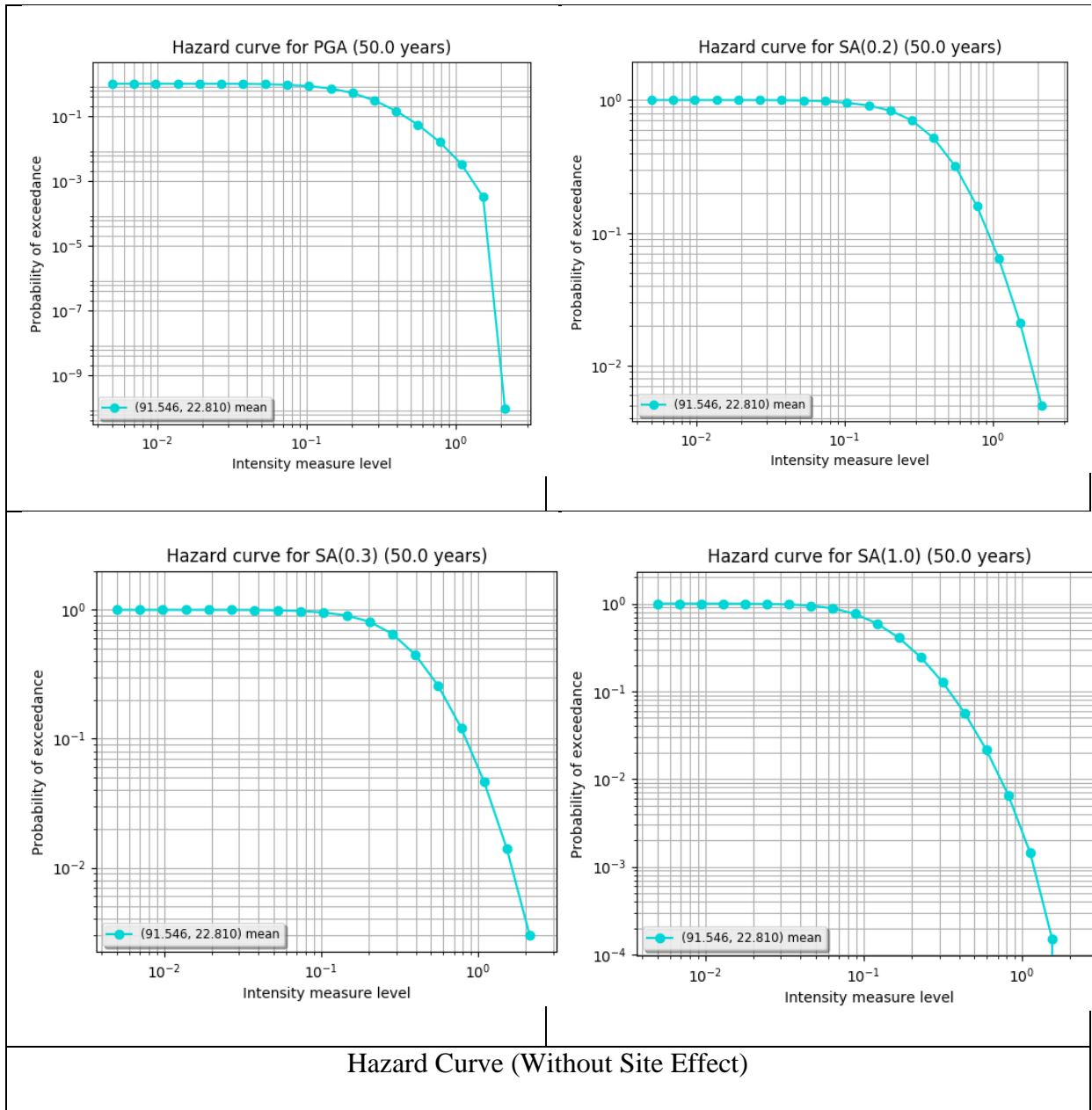


Figure: 4.12 PSA at 1.0s maps for (a) 2% and (b) 10% probabilities of exceedance in 50 years without and with site effect

Hazard curves showing the probability of exceedance against intensity measure levels (PGA and SA) for 50 years return period for Mirshari Upazilla.



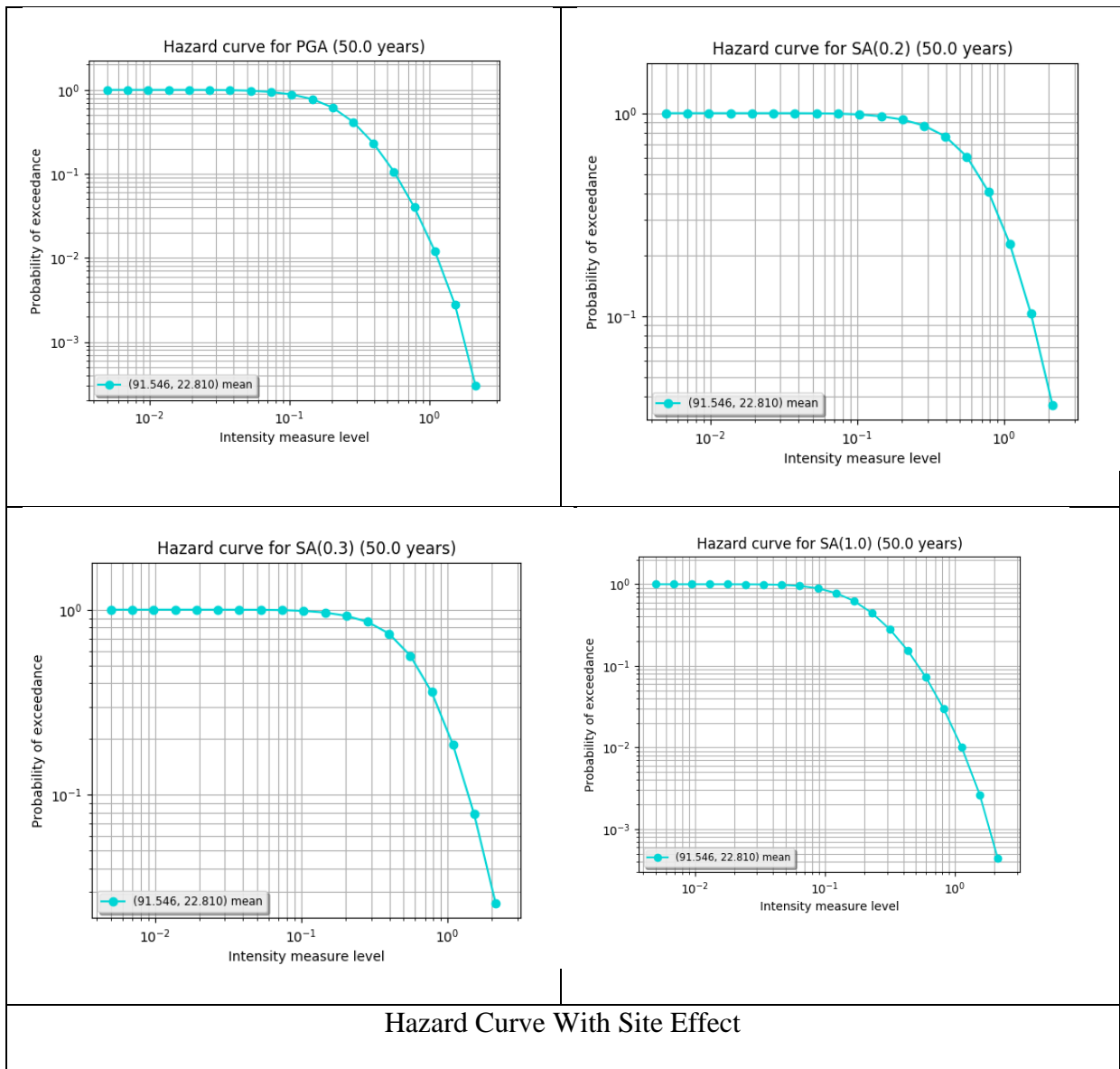


Figure 4.13 Hazard Curves for Mirsharai Upazilla (without and with site effect)

For all the hazard curves, it is clear that as the probability of exceedance decreases (i.e. the return period increases) the level of intensity measure subsequently increases.

4.4. Engineering Geological Mapping

There are many types of “Engineering Geological Map” depending on intended purpose. For instance, when the target is to know suitable foundation soil layer for a planned building, an engineering geology map should have a property of some geotechnical strength, in another

case, when it is necessary to know groundwater potential for a water resource development, a map is created on the basis of permeability of soil as a focal point.

In this study, the target is estimation/evaluation of earthquake phenomenon; so seismic and engineering characteristic of soil is required for the engineering geology map to analyze seismic hazard. Basic information needed for seismic hazard assessment is ground motion at the ground surface; the ground motion can be usually calculated using S-wave velocity. Hence, the engineering geological map is created on the basis of S-wave velocity.

It is notable that in seismic ground motion analysis, especially calculation of amplification of soil, is examined by an empirical method that uses average S-wave velocity of ground in the top 30m depth (hereinafter referred to as “ V_{s30} ”), because the limited point data that is boring/PS logging data should be expanded to the study area in order to make ground model. Therefore, “soil type map based on V_{s30} ” is defined as the “Engineering Geological Map” in this study.

4.4.1 Shear Wave Velocity Estimation

Estimation of shear wave velocity (V_s) and mapping is a way to characterize varying site conditions, and it can also be used to model earthquake-related ground shaking. Estimation of V_s aims to generate a map of estimated average shear wave velocities for the upper 30m of the subsurface, AV_{s30} . Field measurement of V_s of near surface layers implying near surface seismic surveys alike Downhole seismic test (PS Logging) and multi channel analysis of surface wave (MASW) can serve the purpose. V_s of subterranean layers can be obtained by another mean — determination of shear wave velocity from SPT N value from empirical relation between V_s and N value. Because of near surface seismic tests are expensive and so conducted in limited number while SPT tests could be done more extensively, a probabilistic correlation between V_s obtained from near surface seismic and SPT tests are used for to depict extrapolated gestalt picture of AV_{s30} distribution throughout the study area from point data (AV_{s30} at each borehole). The resulting velocities can be more confidently used for AV_{s30} mapping. Further this map can be used for seismic site response analysis i.e., to determine peak ground acceleration (PGA) and spectral acceleration (SA) values of both bedrock and ground surface.

As a part of engineering geological or AV_{s30} mapping, as mentioned earlier, of the Mirsharai Upazila, shear wave velocity (V_s) of the local near surface geological units were obtained by PS Logging, Multi channel analysis of surface wave (MASW) and SPT test. The shear wave velocity is a fundamental parameter required to define the dynamic properties of soils. A

viable formula for velocity determination at the project area was adopted by probabilistic correlation between V_s yielded from PS Logging and SPT tests. Then the AV_{s30} categories assigned to the generalized geologic units were used to generate a AV_{s30} map. Finally, the hybridized AV_{s30} map has been used for seismic site response analysis — PGA and SA mapping, which is hopefully believed to pave the way to the structural engineers and planners to sustainable infrastructure development at Mirsharai Upazila.

N Value and V_s Correlation

Correlations between SPT resistance and shear wave velocity have been proposed for a number of different soil types (Ohba and Toriumi,1970; Imai and Yoshimura, 1970; Fujiwara, 1972; Ohsaki and Iwasaki, 1973; Imai, 1977; Ohta and Goto, 1978; Seed and Idriss, 1981; Imai and Tonouchi, 1982; Sykora and Stokoe, 1983; Jinan, 1987; Lee, 1990; Sisman, 1995; Iyisan, 1996; Kayabalı, 1996; Jafari et al., 1997; Pitilakis et al., 1999; Kiku et al., 2001; Jafari et al., 2002; Andrus et al., 2006; Hasańcebi and Ulusay, 2007; Hanumantharao and Ramana, 2008; Dikmen, 2009). A summary of empirical relationships between SPT resistance and V_s in the literature is presented in for different soil types. In these relationships, SPT- N_{60} blow count is mostly considered. It should be noted that nearly all of the empirical relationships listed in Appendix II use a power-law relationship between V_s and SPT N-value. In these relationships, the values of the exponent, which control the curvature of the relationship, are more consistent than the constant that controls the amplitude. This accounts for the generally similar shapes of the curves.

The shear wave velocity of the Mirsharai upazila soil has been determined from down-hole seismic (PS Logging) method at 15 point and MASW at 20 point. The average shear wave velocities (AV_{s30}) determined from SPT blow counts (N) and down-hole seismic tests are considered during the development of empirical relationship. During the development of empirical relationship 15 PS logging data and 20 MASW data were used in this study area. The following power-law expression based on regression was obtained to derive V_s from N (red dashed line in Figure).

$$V_s = 100.29N^{0.2573} \dots\dots\dots (4.1)$$

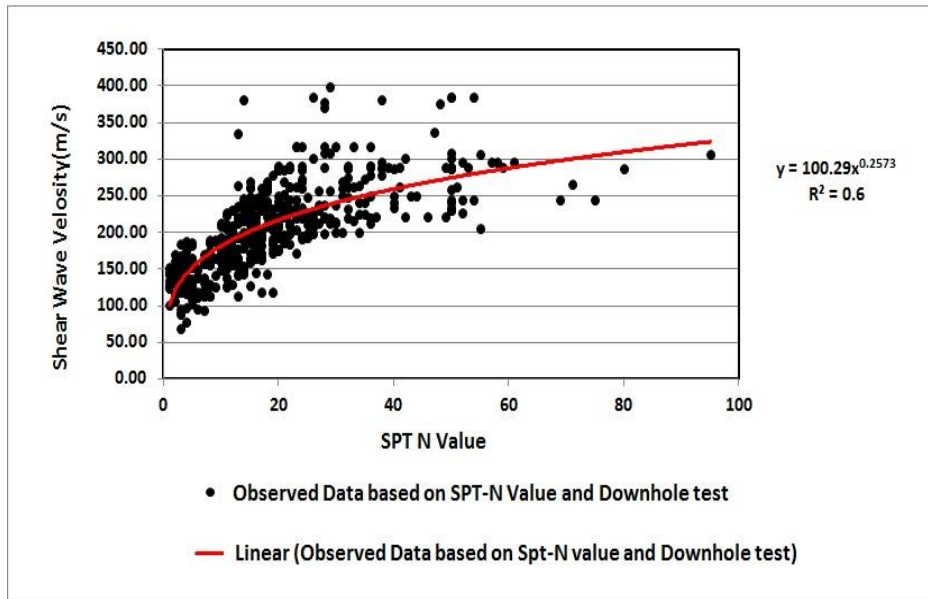


Figure 4.14 Regression analysis between measured SPT-N value and shear wave velocity (Vs) obtained from down-hole seismic test (PS Logging)

The shear wave velocities measured in down-hole tests can be compared with those estimated using empirical models for different soil types. The relationship proposed for Mirsharai upazila soil in this study (red dashed line in Figure) is quite compatible with the following equation (Equation – 4.2), which has similar trend, introduced by Ohba and Toriumi (1970) (blue bold line in Figure).

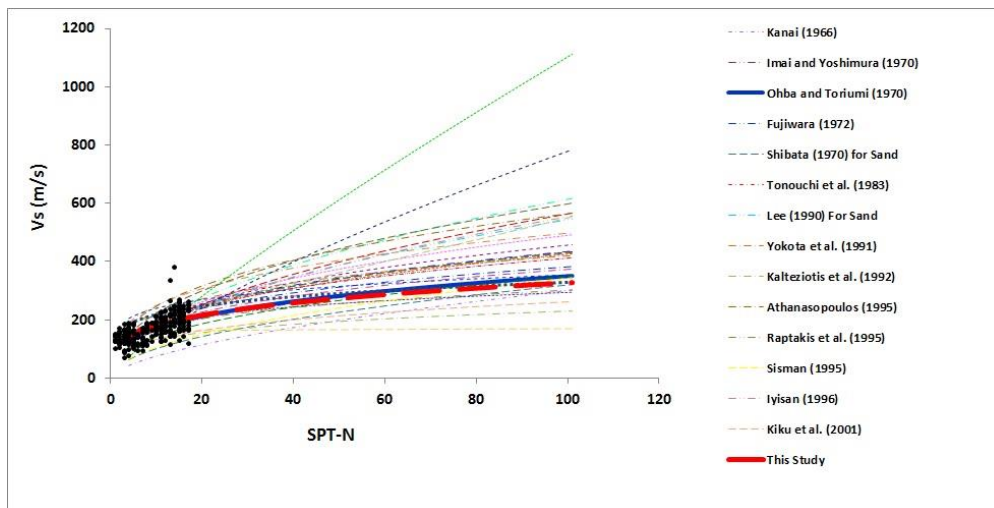


Figure 4.15 SPT-N value and Vs empirical relations for all soils in study area

The distribution of the shear wave velocity data with respect to SPT-N value at the same depth with SPT application and SPT-based down-hole test is considered in the interpretations.

$$V_s = 84N^{0.31} \dots\dots\dots (4.2)$$

Based on this equation 4.2, shear wave velocity (V_s) at every 1.5m interval was calculated at every boreholes drilled in the project area.

Vs 30 Calculation

Near surface shear wave velocity is crucial for earthquake-hazard assessment studies (Wald & Mori 2000; Kanli et al. 2006). The average shear wave velocity of the upper 30 m (AV_{s30}) can be computed in accordance with the following expression:

$$V_s^{30} = \frac{30}{\sum_{i=1}^N (h_i / v_i)} \dots\dots\dots(4.3)$$

where h_i and v_i denote the thickness (in meters) and shear-wave velocity of the i^{th} formation or layer respectively in a total of N existing in the top 30 m. V_{s30} was accepted for site classification in the USA (NEHRP) by the UBC (Uniform Building Code) in 1997 (Dobry et al, 2000). Using the aforementioned equation 5.6, AV_{s30} at every borehole was calculated. Figure represent AV_{s30} map of the Mirsharai upazila.

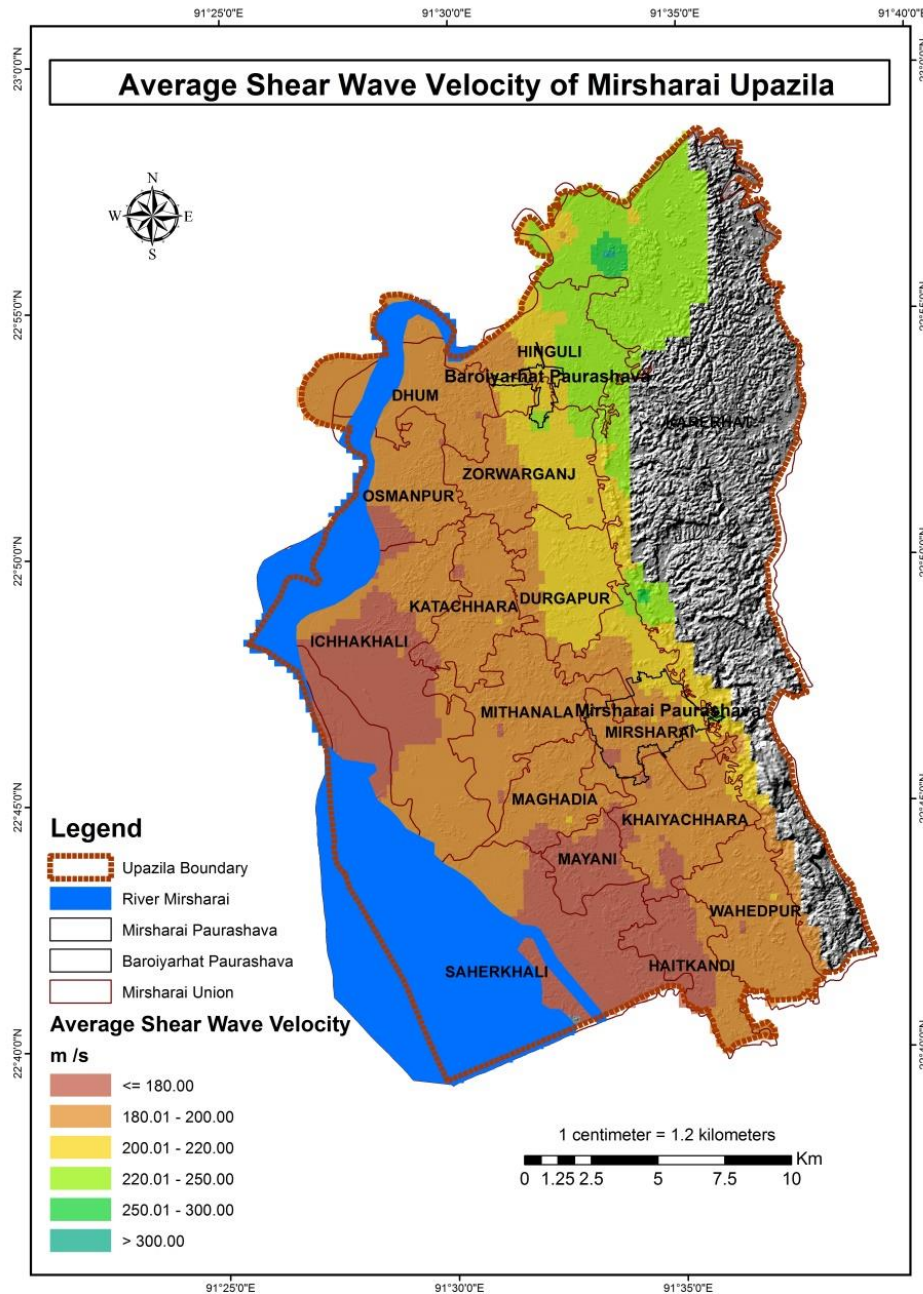


Figure 4.16 Engineering geological map of the Mirsharai Upazila

The Average Shear Wave Velocity (AVs30) within the area ranges from 160.13 to 308.78 m/s. From the figure it can be clearly visualized that the brown colored areas of Mayani, Haitkandi, Saherkhali, Ichhakhali, Osmanpur union represents average shear wave velocity less than 180 m/s. The orange colored zones Hinguli, Dhum, Zorwarganj, Osmanpur, Wehedpur, Haitkandi, Saherkhali, Magadia, Khaiyachara, Mirsharai, Mirsharai Paurashava, Mithanala, Ichhakhali, Katachhara and Durgapur union represents average shear wave velocity between 180 – 200 m/s. The yellow colored zones of Hinguli, Baraiyarhat Paurashava, Durgapur, Zorwarganj, Mirsharai and Karerhat Union represents shear wave velocity ranges

from 200 to 220 m/s; the light green colored areas of Karerhat and Hinguli union represents shear wave velocity ranges from 220 to 250 m/s and the rest of the area have higher velocity than 250 m/s. AVs30 of soil is a very use full tool for soil type classification.

4.4.2. Soil Type Determination based on Vs30

An important part of this study is the soil classification of the project area. The area has been investigated and classified according to a method provided by NEHRP (stands for National Earthquake Hazard Reduction Program, USA) Provisions. NEHRP Provisions describes; at first to define the site class based on AV_{s30} , and secondly to set the amplification factors by the selected site class, as shown in Table .

Table 4.8: Definition of site class based on Vs30 — according to NEHRP (National Earthquake Hazard Reduction Program, USA) provisions.

Site Class	Site class description	Shear wave velocity (m/sec)	
		Minimum	Maximum
A	HARD ROCK Eastern United States only	1500	
B	ROCK	760	1500
C	VERY DENSE SOIL AND SOFT ROCK Unstrained shear strength $u_s > 2000\text{psf}$ ($u_s \geq 100\text{kPa}$) or $N \geq 50$ blows/ft	360	760
D	STIFF SOILS Stiff soil with undrained shear strength $1000\text{psf} \leq u_s \leq 2000\text{psf}$ ($50\text{KPa} < u_s < 100\text{KPa}$) or $15 \leq N \leq 50$ blows/ft	180	360
E	SOFT SOILS Profile with more than 10 ft (3m) of soft clay defined as soil with plasticity index $PI > 20$, moisture content $w > 40\%$ and undrained shear strength $u_s < 1000\text{psf}$ (50kpa) ($N \leq 15$ blows/ft)		180
F	SOILS REQUIRING SITE SPECIFIC EVALUATIONS 1. Soils vulnerable potential failures or collapse under seismic loading:		

	<p>e.g., liquefiable soils, quick and highly sensitive clays, collapse weakly connected soils.</p> <p>2. Peats and/or highly organic clays: (10ft (3m) or thicker layer)</p> <p>3. Very high plasticity clays: (25ft (8m) or thicker layer with plasticity index > 75)</p> <p>4. Very thick soft/medium stiff clays: (120ft (36m) or thicker layer)</p>		
--	---	--	--

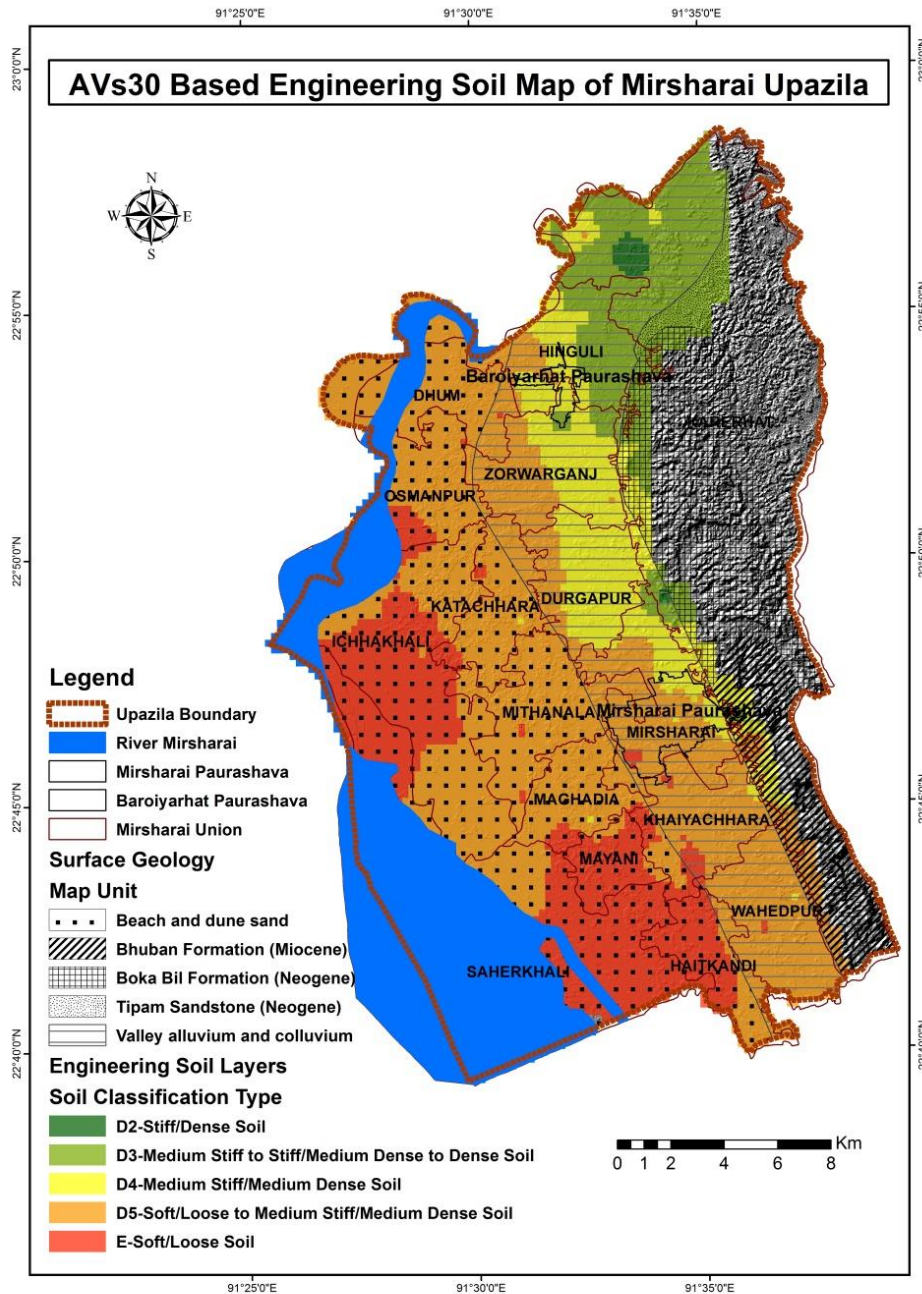


Figure 4.17 Soil classification map of Mirsharai according to NEHRP (stands for National Earthquake Hazard Reduction Program, USA) provisions based on the average shear wave velocity distribution down to 30 m

Velocity range of the soils of the project area is 160 to 300 m/s i.e., they belong to the class D and E according to the provision. Further class D has been categorized these soils into D1 to D5 sub-classes based on their V_{s30} velocity range, shown in Table .9.

Table 4.9: Sub soil, Vs30 based classification of the soils applied in this study.

Ground Class	V _{s30}	Soil Type
C	360 - 760 m/sec	Very Dense/ Hard Soil and Soft rock
D1	300 - 360 m/sec	Stiff / Dense to very dense/Hard Soil
D2	250 - 300 m/sec	Stiff / Dense Soil
D3	220 - 250 m/sec	Medium Stiff to Stiff / Medium Dense to Dense Soil
D4	200 - 220 m/sec	Medium Stiff / Medium Dense Soil
D5	180 - 200 m/sec	Soft/Loose to Medium Stiff /Medium Dense Soil
E	< 180 m/sec	Soft / Loose Soil

The soils at the project area fall mainly into 5 category (D2, D3, D4, D5 and E). From the Figure it can be observed that, the dark green colored areas of Karerhat unions belongs to category D2 which means the soil types of those areas are stiff/dense. The light green shaded areas of Hinguli, Baraiyarhat Paurashava, Zorwargonj and Karerhat union belongs to category D3 which means the soils types are medium stiff/medium dense to stiff/dense soil. The yellow colored areas of Hinguli, Baraiyarhat Paurashava, Zorwargonj, Durgapur, Mirsharai Paurashava and Mirsharai union shows that the soil types of the zones are D4 suggesting the soils are medium stiff/ medium dense. The orange colored areas suggest the soils are D5 type which means the soils are soft/loose to medium stiff/medium dense and the rest of the area belongs to category E suggesting soft/loose soils as shown in the Figure .

4.5. Building Height Map

Peak spectral acceleration (PSA) is an important tool for determining the building height of an area. Here PSA for 1.0 and 0.2 sec is used for identifying the appropriate location for high rise and low rise building respectively. A building height map is produced for the study area using PSA 1.0 and 0.2 sec (Figure 4.18).

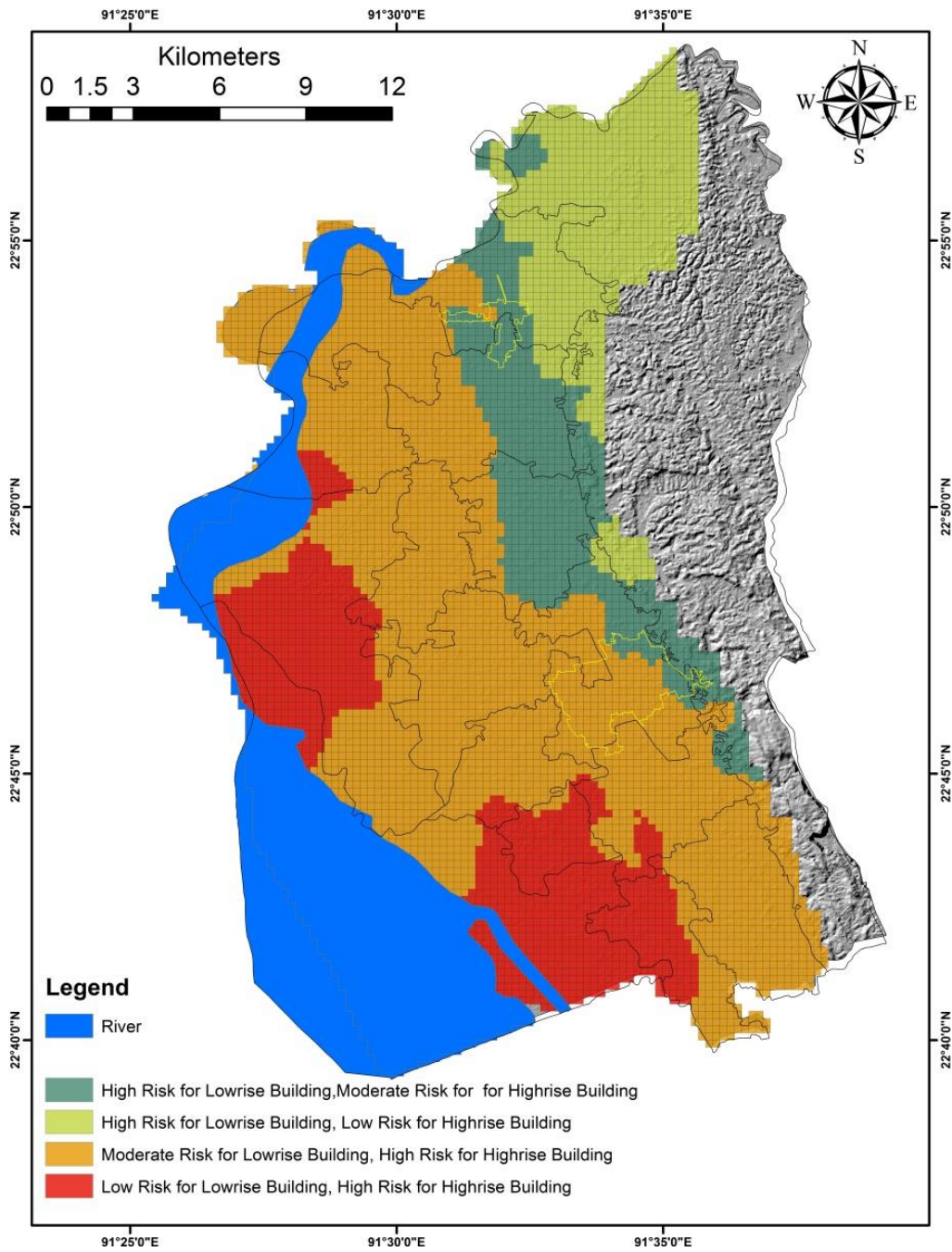


Figure 4.18 Building Height Map of Mirsharai Upazila

From the map it can be observed that the light green colored areas of Karerhat, Hinguli, Zorwarganj and Mirsharai unions area high risk sensitive zones for low rise building but low risk sensitive for high rise buildings. The map also shows that the grey colored areas of Hinguli, Zorwarganj, Durgapur, Mirsharai Paurashave and Mirsharai unions are High risk sensitive for low rise buildings but moderately sensitive for high rise buildings. The red colored zones of Osmanpur, Ichhakhali, Katachara, Saherkhali, Mayani, Haitkandi and Khaiyachara unions are Low risk sensitive for low rise buildings but High risk for high rise

buildings. Rest of the study area with orange color is Moderately sensitive for low rise buildings but high risk sensitive for high rise buildings.

5. LANDSLIDE SUSCEPTIBILITY ASSESSMENT

Landslide is a geological hazard which results in various types of mass movement such as rock falls, slope failure and debris flow down the slope (*Cruden, 1991; Cruden & Varnes, 1996; Crozier, 1999; Abbott, 2004*) when shear stress exceeds the shear strength of the slope materials (*Duncan, 1996*). Many factors act as triggering factors contributing to slope instability either by decreasing the shear strength of the soil or increasing the shear stress (*Duncan, 1996; Goudie, 2004*). Geomorphic and geological aspects such as topography, lithology, soil type, tectonic activities, erosional activities etc. combined with prolonged rainfall, deforestation, changes in land-cover and oversteepening of slope due to human interventions (*Kienholz et al., 1983*) were recognized as some of the causative and triggering factors (*C.J. Van Westen, 2000*) of landslides.

Landslide poses a significant threat to development and the collective damages incurred by landslides in terms of human and property loss have a widespread impact on the economic system of a country (*Schuster & Fleming, 1986; Dai et al., 2002; H.A.Nefeslioglu, C.Gokceoglu, 2008*). According to the *World Disaster report of 2016*, landslide alone was responsible for 9,477 casualties and affected 3,031 thousand population globally which altogether cost 1935 million USD during the period of 2006-2015. Because of the devastating nature of the hazard, several studies (*C J Van Westen et al., 2011; Lin et al., 2010; IFRC, 2016*) identified landslide as an important natural hazard for which actions need to be taken to reduce the severity of its impact. Adversities of landslides is an important concern for Bangladesh since reported cases of devastating landslides have claimed lives of hundreds of people in hilly regions of the country (*DDM, 2017*). In 2007, about 127 people were killed (*IFRC, 2007; Reuters, 2007*) and 5,072 families were displaced by the landslide that severely affected Lalkaan Bazaar, Chittagong (*Anwar Hussain, 2017*). The event recurred again in 2008 and 2012, causing the death of 11 people (*Sarwar, 2008*) and 90 people, respectively. Cox's Bazaar district was also highly affected by landslides in 2010 and 2015 killing 47 and 15 people, respectively, and causing injuries to many people along with huge infrastructural loss (*Ahmed & Forte, 2016*). Moreover, the incident which took place in 2017 has exceeded the past records. It had a widespread impact on the south-eastern region of Bangladesh, affecting Rangamati, Chittagong, and Bandarban. The disaster claims lives of a total of 152 people. About USD 223 million economic loss has been incurred along with the destruction of about 6,000 dwellings (*UN RC, 2017*), road infrastructure, interruption of the telecommunication system and power supply etc. (*Tusher & Minhaz, 2017; reliefweb, 2017*).

Damages to these infrastructures have caused averting of transportation and supply of food and relief aid to the victims, which has aggravated the situation further. Among all the affected districts Rangamati were the worst, where about 118 people died, 77 were injured and 2900 were relocated to safe location (*Nirapad, 2017*).

The frequency of landslide disaster had increased greatly in recent years and is expected to intensify further in near future (*Kanungo et al., 2009; Ahmed, 2015*). On the other hand, anthropogenic activities that result in environmental degradation and factors contributing to slope instability has intensified over time (*Rahman, 2012; Chisty, 2014*) as a result of population growth by several folds. The current project is very much concerned about the occurrence of landslides in the Kutupalong-Balukhali Rohingya Refugee Camp in Bangladesh. The refugees have changed the land cover of the whole project area by erasing the forest and changing the natural slope. In the coming monsoon, the project area may suffer from heavy damage and loss due to the occurrence of numerous landslides.

In order to reduce the damaging effects of landslides, it is crucial to map areas with their degrees of susceptibility to landslides, so that appropriate mitigation measures can be taken and proper land-use plan can be designed to ensure an effective and efficient disaster management. Landslide susceptibility mapping, therefore, involves the determination of the spatial extent of a particular type of landslides and the probability of its occurrence over a period of time and space (*D M Cruden & Varnes, 1996; Soeters, 1996*). Many studies, therefore, describes the best possible methods, techniques, and approaches used to develop landslide susceptibility map. Studies also outline the advantages and disadvantages of using each technique depending on the data quality, availability, accuracy, uncertainty, and interaction with the causal factors. Landslide susceptibility maps, therefore, can be produced using both quantitative and qualitative approach (*Park et al., 2013*). Qualitative maps, which is derived from landslide inventory and knowledge-driven methods, involves in zoning of hazard-prone areas into different categories using descriptive terms (high, moderate, low) (*Carrara et al., 1991*). On the other hand, data-driven probabilistic and deterministic methods are used to produce quantitative maps with the help of computer models, programming, geospatial technologies quantifying the severity of the possible landslide areas (*Thanh & de Smedt, 2012; Ahmed, 2015*). The most commonly used approaches are heuristic, statistical probabilistic, and deterministic models.

In the heuristic analysis, geo-morphologists identify the causal factors of landslides such as geology, slope, aspect, vegetation, rainfall etc. and degrees of their influence by analyzing field data, aerial photographs, satellite images etc. Based on the knowledge of past events, experience, and expertise, they assign weights to each factor accordingly (Yilmaz & Yildirim, 2006; Ahmed, 2015). In other words, it involves both direct and indirect methods to carry out this GIS-based Multi-Criteria Decision Analysis (GISMCDA). Saaty (1980) developed a decision tool named Analytical Hierarchical Process (AHP) to make the analysis easier and more flexible (Westen et al., 2011). This process involves the construction of a hierarchically structured matrix of all relevant factors and information, based on three principles of decomposition, comparative judgment, and synthesis of priorities (Malczewski, 1999). Then a pair-wise comparison between the factors is carried out, where weights are assigned according to their importance and expert judgment (Pradhan & Lee, 2010a), through which inconsistencies in the decision process can be addressed. Despite disadvantages due to subjectivity, this method results in site and landslide specific evaluations and avoids generalization of the causal factors (Malczewski, 1999).

Statistical analysis is another approach to predict the future possible spatial distribution of landslides based on a landslide inventory (Carrara et al., 1991; Nandi & Shakoor, 2006; Firman & Wahono, 2010; Ahmed, 2015). Landslide inventory, which is derived from field survey, aerial photo and satellite image interpretation, is a map showing recent and past historic landslide areas, date of its occurrence and type of activities involved (Wieczorek, 1983; McCalpin, 1984; Guzzetti et al., 2000). Future landslides are quantified by overlaying the causal factors with presence or absence of landslides (Nandi & Shakoor, 2006; Ahmed, 2015) assuming that the past is the key to the future (Carrara et al., 1991; Kanungo et al., 2009). This method provides good results with high accuracy and validation rates (Zêzere et al., 2004; Petrea et al., 2014) and is reproducible (Huang, 2014) but the disadvantages are, it is complex, time-consuming and costly process as it requires large number of variables to be considered (C. J. van Westen, 1994; C.J. Van Westen, 2000) and problem arises with the scale of analysis, which involves calibration (Fressard et al., 2014). Most commonly used methods are multivariate and bivariate statistical analysis (L Yin et al., 1988; Brunori et al., 1996). In bivariate statistics the factor maps are categorized, overlaid and weighted (P. Gupta, R & C. Joshi, 1990; C. J. van Westen et al., 1997) using some of the methods such as information value method, weight-of-evidence modelling (Bathrellos et al., 2009; Ahmed & Dewan, 2017) and landslide nominal susceptibility factor (LNSF) etc. (Adhikari, 2011). On

the other hand, multivariate statistical analysis, which involves methods like logistic regression (*Bui et al., 2011; Francipane et al., 2014*), multiple regression (*Ahmed & Dewan, 2017*), discriminant analysis (*Nandi & Shakoor, 2006*), and Artificial Neural Network (ANN) (*Chalkias et al., 2014*) etc., considers contribution of each causal factors in occurrence of landslides to provide weighting values (*Firman & Wahono, 2010; Zhou et al., 2016*).

Deterministic analysis, on the other hand, is a detailed approach, used to quantify landslide hazards in individual slope with the help of slope stability model (*Intarawichian & Dasananda, 2010*) and calculation of factors of safety (*Van Westen, 2000; Van Westen et al., 2005*). It considers variables such as normal stress, the angle of friction, pore water pressure, antecedent rainfall etc. and various hydrological and stability models are used together to calculate the probability of slope failure (*Montgomery & Dietrich, 1994; Van Westen, 2000; Iverson, 2000*). It is also known as geotechnical engineering analysis (*Huang, 2014*) and provides a sound physical models (*Van Westen, 2000*), which can be used to forecast for different scenarios, depending on the future changes of environmental conditions, land use pattern and climatic factors (*Van Westen et al., 2005*). Complexity arises (*Nandi & Shakoor, 2006*) as the model requires large amount of input data for a region with homogeneous geologic and geomorphic properties (*Hammond et al., 1991; Soeters, 1996*), which therefore, limits the study area to a fairly small or large region due to inadequate data availability and budgetary constraints (*Van Westen, 1993; C. Lee, 2015*). The success of the model further depends on the correct identification of failure and triggering mechanism which is a difficult procedure and several uncertainties result from the parameterization of the model (*Van Westen et al., 2005*).

However, despite all these available methods for landslide mapping, statistical-probabilistic approach, particularly weights-of-evidence (WoE) is chosen to carry out this research because of its simplicity and higher accuracy to perform landslide susceptibility assessment particularly when the spatial extent and distribution of pre-existing landslides are known.

5.1. Methodology

5.1.1. Method Introduction

The landslide susceptibility assessment necessitates the spatial extent and distribution of pre-existing landslides and to map the landslide triggering factors. In the next two sections *i.e.*

section 5.1.2 and 5.2, the methods to derive the pre-existing landslide and the landslide triggering factors are explained, respectively.

5.1.2. Landslide Inventory Preparation

The inventory of landslide i.e. the spatial distribution and location of pre-existing landslides (figure 5.1) was prepared from the provided digital elevation model (DEM) and orthophoto image by Urban Development Directorate (UDD).

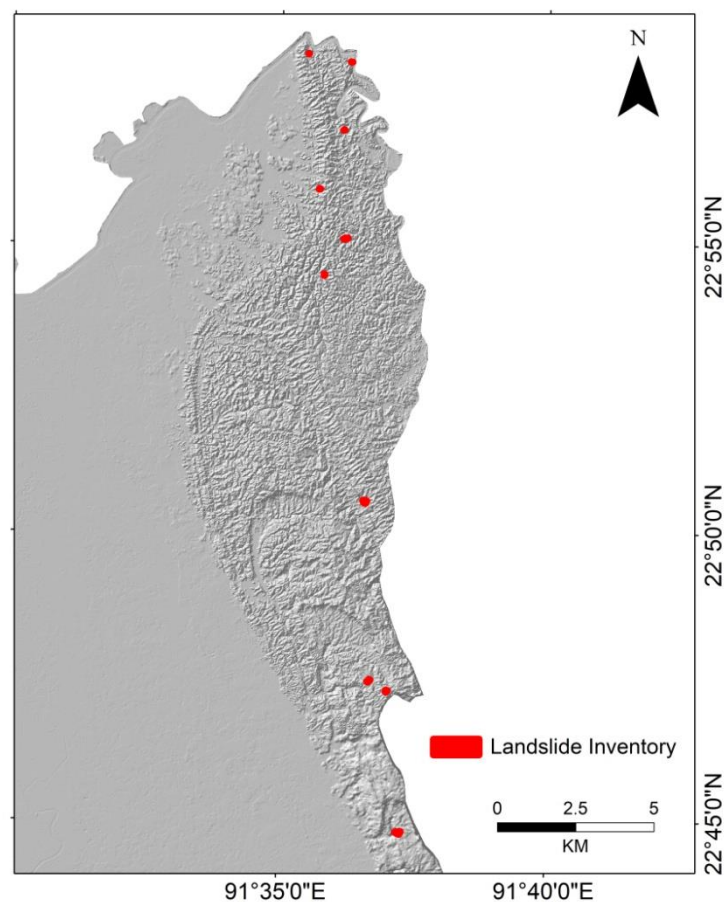


Figure 5.1 Landslide Inventory has been overlaid the hill shade map

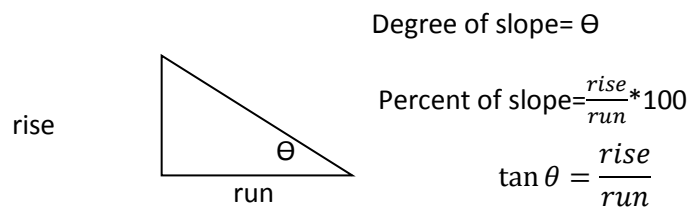
5.2. Landslide Hazard Analysis

Landslide hazard analysis has been conducted to see the relation of previous landslide occurrence with different triggering factors. We have analyzed rainfall, local surface geology, slope, aspect, vegetation cover, proximity to stream and land use-land cover change of the project area. These triggering factors have been mapped as factor maps.

Factor Maps

Slope Map- Slope angle is a significant factor for triggering landslides. Slope map was prepared from the 10meter resolution DEM produced provided by Urban Development and Directorate. Slope map was prepared using ArcGIS tool. In ArcMap slope was calculated using slope tool of surface analysis for each cell in the raster DEM. The slope represents the inclination or steepness of a surface. Slope or gradient is actually the rate of changes in z-values (elevation) between adjacent cells. The steepness is identified by the maximum change in elevation over the distance between a cell and its eight neighbors. Conceptually, the tool fits a plane to the z-values of a block of 3 x 3 cells neighborhood around the processing or center cell. The slope value of this plane is calculated using the average maximum technique. The direction the plane faces is the aspect of the processing cell. Every cell in the output raster has a slope value. The lower slope value represents the flatter terrain; the higher slope value represents the steeper terrain.

The output slope raster can be calculated as a percent of slope or degree of slope. The difference in elevation between points is called the rise. The distance between the points is called the run. The percent rise can be better understood if it is considered that the rise is divided by the run and multiplied by 100. When the slope angle equals 45 degrees, the rise is equal to the run. Expressed as a percentage, the slope of this angle is 100 percent. As the slope approaches vertical (90 degrees), the percentage slope approaches infinity.



The slope tool is most frequently run on an elevation dataset, as the following diagrams show. Steeper slopes are shaded red on the output slope raster.

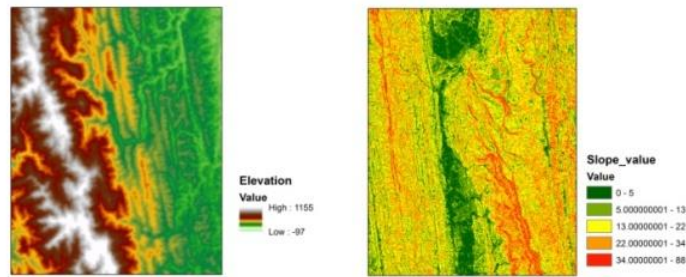


Figure 5.1 Example of Slope Angle

The rates of change (delta) of the surface in the horizontal (dz/dx) and vertical (dz/dy) directions from the center cell determine the slope. The basic algorithm used to calculate the slope is:

$$slope_radians = ATAN (\sqrt{[dz/dx]^2 + [dz/dy]^2})$$

The slope is commonly measured in units of degrees, which uses the algorithm:

$$slope_degrees = ATAN (\sqrt{[dz/dx]^2 + [dz/dy]^2}) * 57.29578$$

The slope algorithm can also be interpreted as:

$$slope_degrees = ATAN (rise_run) * 57.29578$$

Where $rise_run = \sqrt{[dz/dx]^2 + [dz/dy]^2}$ (Moser et al., 1989)

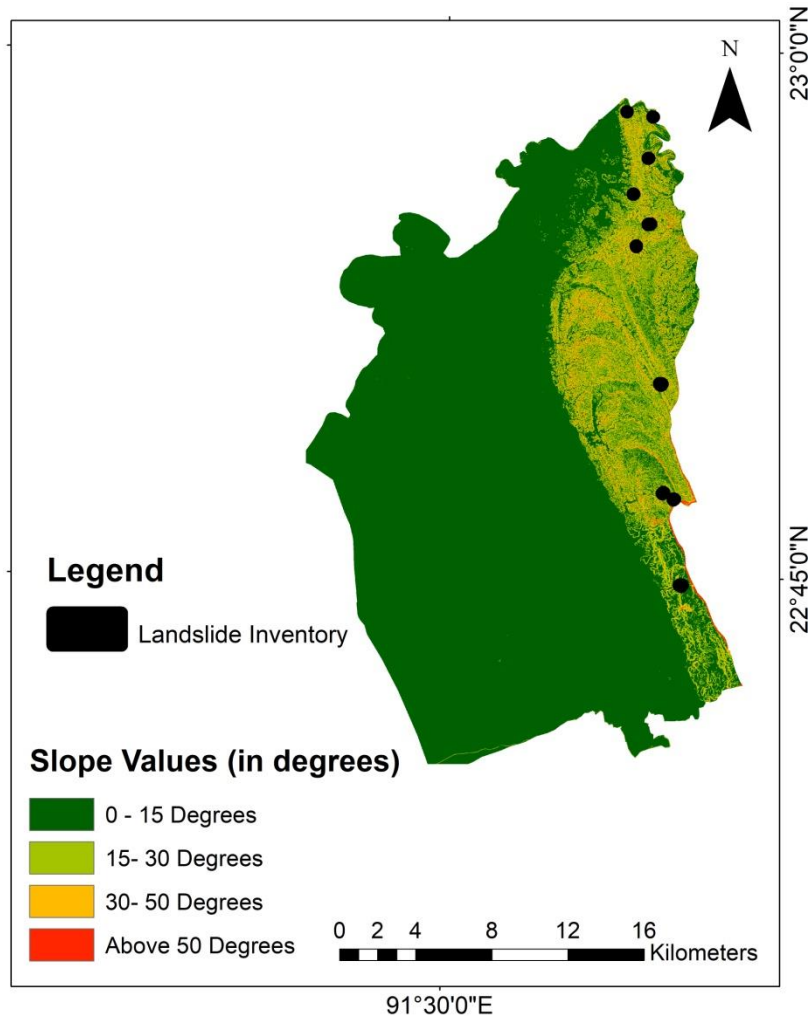


Figure 5.2 Slope Map has been produced from the 10m resolution DEM

Aspect Map: In physical geology, aspect is the compass direction that a slope faces. Aspect identifies the downslope movement of the maximum rate of change in value from a cell to its neighbors. It is considered as the direction of the slope. The value of each cell in the output raster indicates the compass direction that the surface faces at that location.

Aspect is measured clockwise and in degrees ranging from 0 (due north) to 360 (again due north) coming full circle. Flat areas are assigned value -1 as they have no downslope direction. The value of each cell in the aspect dataset represents the direction of the slope of the cell.

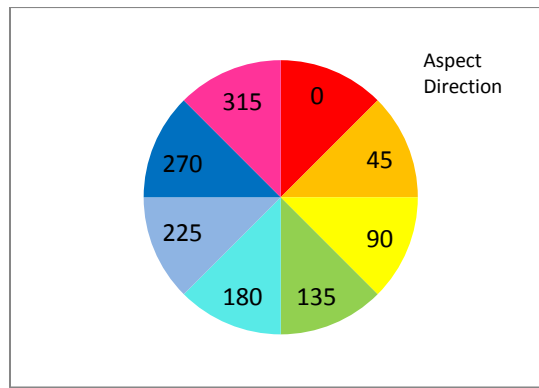


Figure 5.3 Example of Aspect

The aspect map is also produced from the aforementioned high-resolution DEM.

Conceptually the aspect tool fits a plane to the z- values of a 3 x 3 cell neighborhood around the processing or center cell. The direction at which the plane faces represents the aspect of the processing cell.

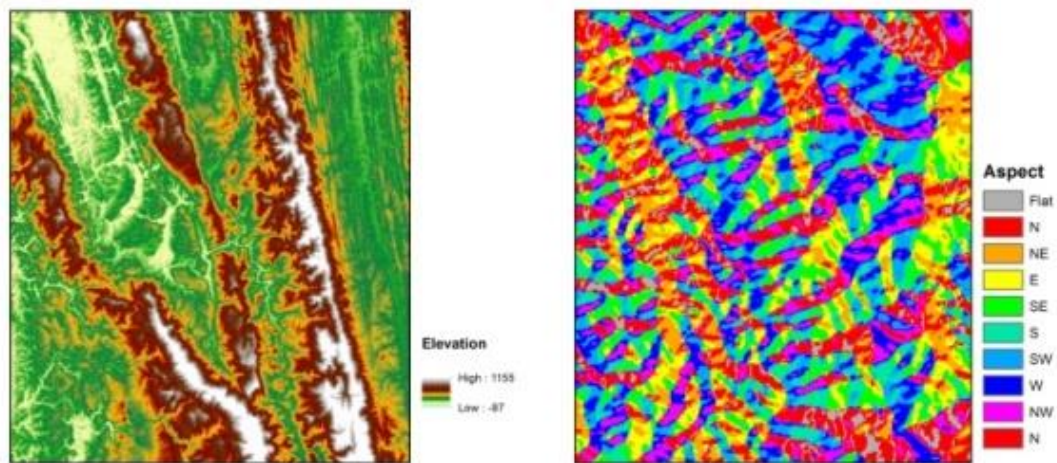


Figure 5.4 Example of Aspect Classes

Aspect value in each cell is calculated using an algorithm that incorporates the values of the cell's eight neighbors. The cells are defined as letters a to i with e which represents the cell for which the aspect value is being calculated.

a	b	c
d	e	f
g	h	i

The rate of change in the x-direction for cell e is calculated with the following algorithm:

$$[dz/dx] = ((c + 2f + i) - (a + 2d + g)) / 8$$

The rate of change in the y-direction for cell e is calculated with the following algorithm:

$$[dz/dy] = ((g + 2h + i) - (a + 2b + c)) / 8$$

Taking the rate of change in both the x and y-direction for cell e, aspect is calculated using:

$$aspect = 57.29578 * atan2 ([dz/dy], -[dz/dx])$$

The aspect-value is then converted to compass direction values (0-360 degrees), according to the following rule:

$$\begin{aligned} & \text{if } aspect < 0 \\ & \text{cell} = 90.0 - aspect \\ & \text{if } aspect > 90.0 \\ & \text{cell} = 360.0 - aspect + 90.0 \\ & \text{else, cell} = 90.0 - aspect \end{aligned}$$

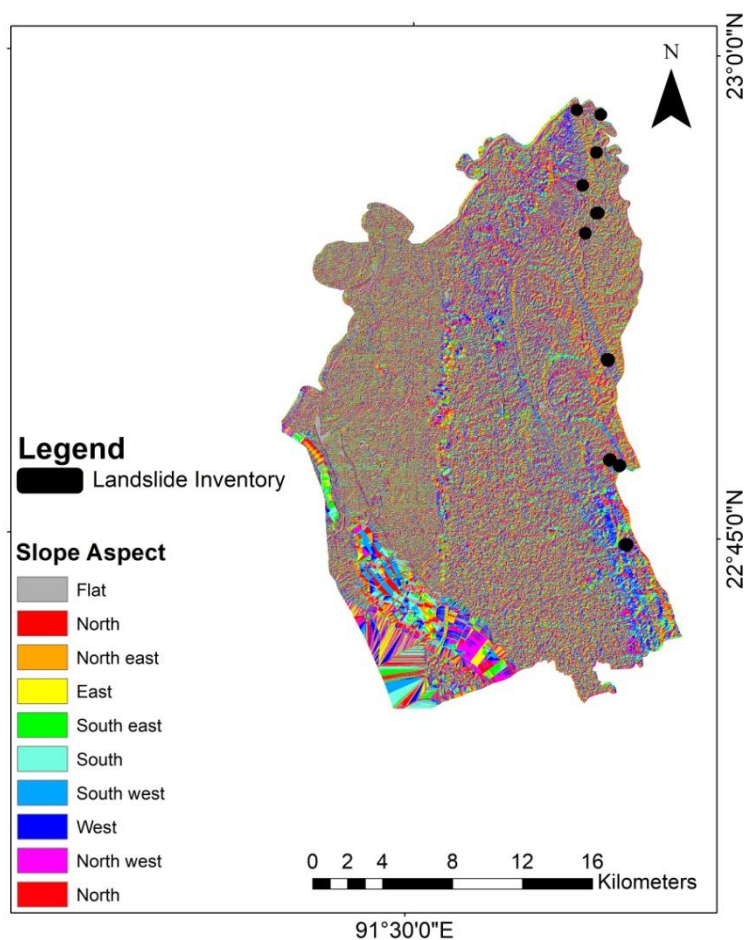


Figure 5.5 Aspect Map of the Study Area

Vegetation Map: Vegetation is another important factor in landslide initiation mechanism. Vegetation covers the top of the soil and reduces erosion as well as increases infiltration through the soil. Vegetation and slope stability are interrelated. The relationship between vegetation and slope stability is a combination of soil type, rainfall, plant type, slope aspect and the steepness of the slope. Vegetation cover provides a considerable contribution to the stability of slope through enhancing soil cohesion (*ECOLOGICAL RESTORATION SPECIALISTS, n.d.*)

A vegetation map is prepared as the Normalized Difference Vegetation Index (NDVI) map. The NDVI is a standardized index that allows generating an image displaying greenness. The index is made from the contrast of the characteristics of two bands from a multispectral raster dataset. Chlorophyll pigment is absorbed in the red band and the plant materials highly reflect in the near-infrared (NIR) band.

The vegetation index map has been prepared from LANDSAT 8 image which has been resampled to 10 meters. The NDVI difference has been retrieved from the image dated 2001 and 2017. This NDVI difference map has also been used as one of the landslide triggering factor maps.

The differential reflection in the red and near-infrared (NIR) bands enables to monitor density and intensity of green vegetation growth using the spectral reflectivity of solar radiation. Green leaves show better reflection in the NIR wavelength range than in visible wavelength ranges. The NDVI process creates a single band dataset that represents greenery. The negative values represent clouds, water, snow and values near 0 represent rock or bare soil. The documented and default NDVI equation is as follows:

$$NDVI = ((IR - R)/(IR + R))$$

Where IR = pixel values from the infrared band and R = pixel values from the red band.

The equation ArcGIS uses to generate the output is as follows:

$$NDVI = ((IR - R)/(IR + R)) * 100 + 100$$

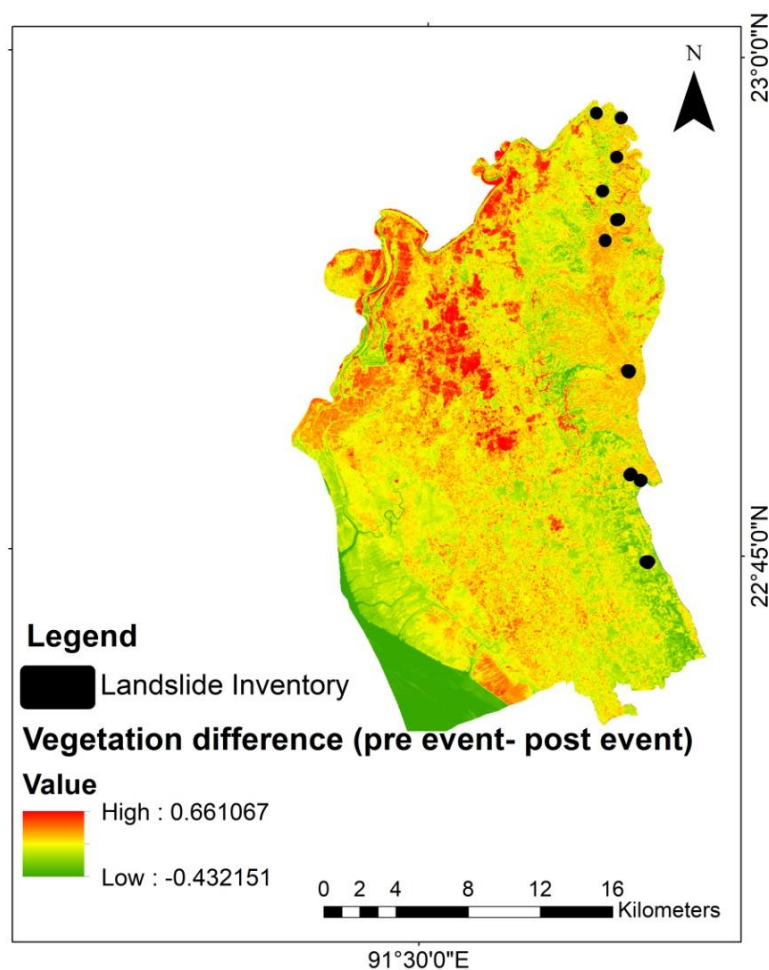


Figure 5.6 NDVI difference map of the project area

Land cover Classification Map preparation: The land cover classification map has been prepared using LANDSAT 8 satellite imagery. Two different time series data were acquired considering the land use change. Both the images were analyzed by supervised classification.

The image classification process involves the conversion of multi-band raster imagery into a single band raster with several categorical classes that represent different land covers. Classification of remotely sensed data is done to assign corresponding levels with respect to homogenous groups to discriminate multiple objects from each other within the image. Raster classification is a process of classifying imagery into different land use/ land cover classes based on pixel values of image bands. It allows for analysis of land use/ land cover change, identification of features, suitability analysis. The resulting raster from the image classification can be used to create thematic maps (Nagi, 2015).

In ArcGIS Spatial Analyst. (*Rebecca Richman, Raster Classification Using ArcGIS Desktop*), there is a full set of tools in the Multivariate toolset to perform supervised classification. Maximum Likelihood Classification tool uses the algorithm based on two principles- The cells in each class sample in the multidimensional space are normally distributed and Bayes' theorem of decision making.

The Maximum Likelihood Classification tool involves the use of training sample variance and covariance to create a multi-band class signature and assigns a class to each pixel based on the maximum likelihood that they belong to that particular class. This process assumes that the training data are normally distributed in multiband space. The image classified by the Maximum Likelihood Classification tool may misclassify certain cells and can create small regions that may be invalid. Those misclassified cells need to be reclassified to improve classification. There are several techniques to clean up the classified image. Filtering process removes single isolated pixels from the classified image. Smoothing class boundaries clumps the classes and smoothest the ragged edges of the classes by increasing the spatial coherence of the classified image. The third one is the generalization output by removing small isolated regions. It is done when there are some small isolated regions even after filtering and smoothing the classified image (*ArcGIS Desktop, 2017*).

Using the Maximum Likelihood classification tool, the images were classified into four major classes- vegetation, water body, built up the area and bare soil. The map has been prepared using 4, 3, 2 bands composite. These three bands are used because they are visible in the EM spectrum and easily differentiate objects.

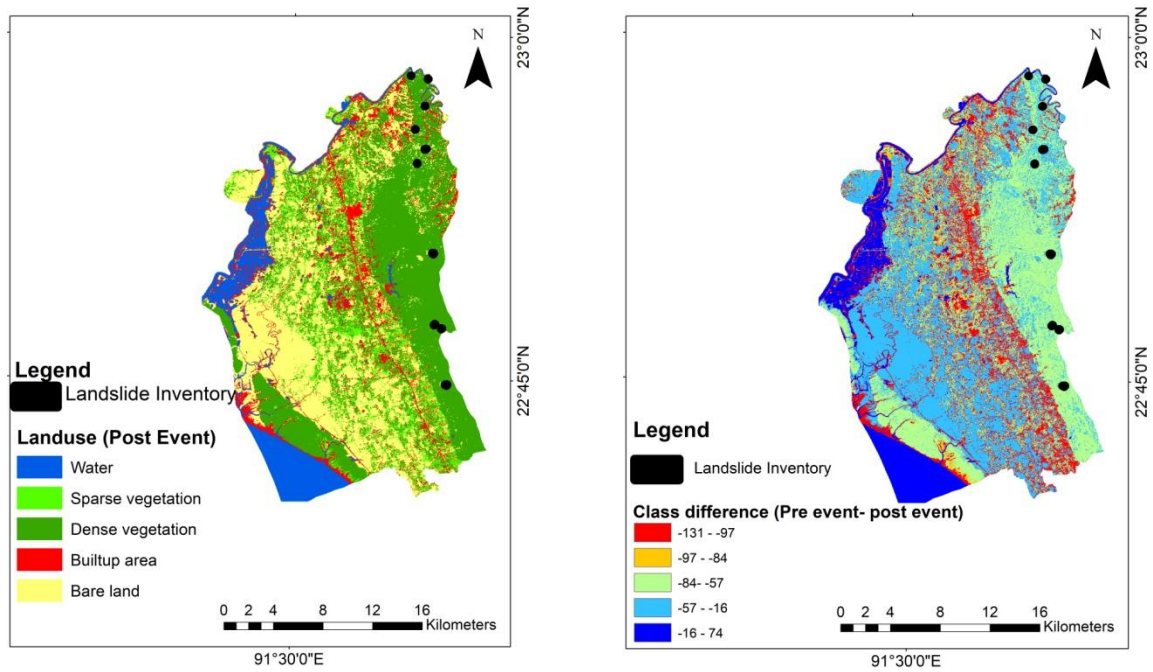


Figure 5.7 Existing land cover and land cover difference map

Drainage Map: The drainage pattern of the study area was extracted from DEM using Hydrology tools of ArcGIS software 10.3. The flow direction and accumulated flow are then calculated. Latter accumulation value greater than 5000 is taken for the study area using raster calculator. In order to link this, stream link operation is used to assign values between the intersections.

In addition to drainage map, the local chorus is being digitized and this kmz file has been exported as ARC GIS shapefile. Later, streams are then converted to a feature class and then Euclidean Distance is used to calculate the distance from the drainage.

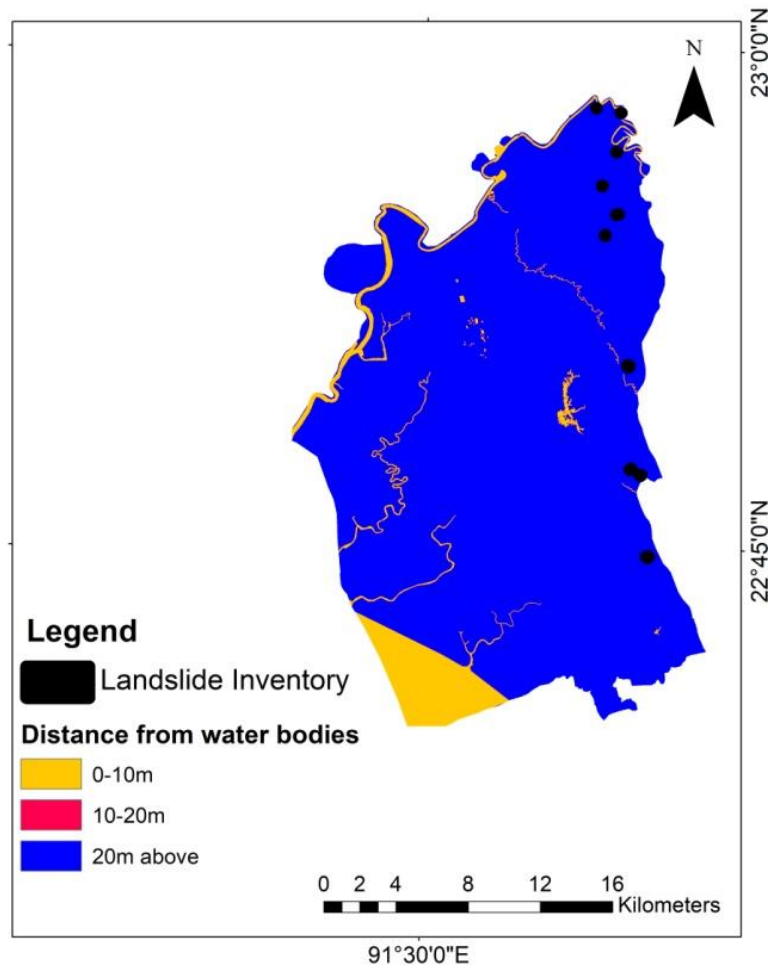


Figure 5.8 Drainage and distance from the water body

Road Map: existing roads maps have been downloaded and if required have been digitized from the orthophoto and Euclidean distance was used to calculate the distances from the road.

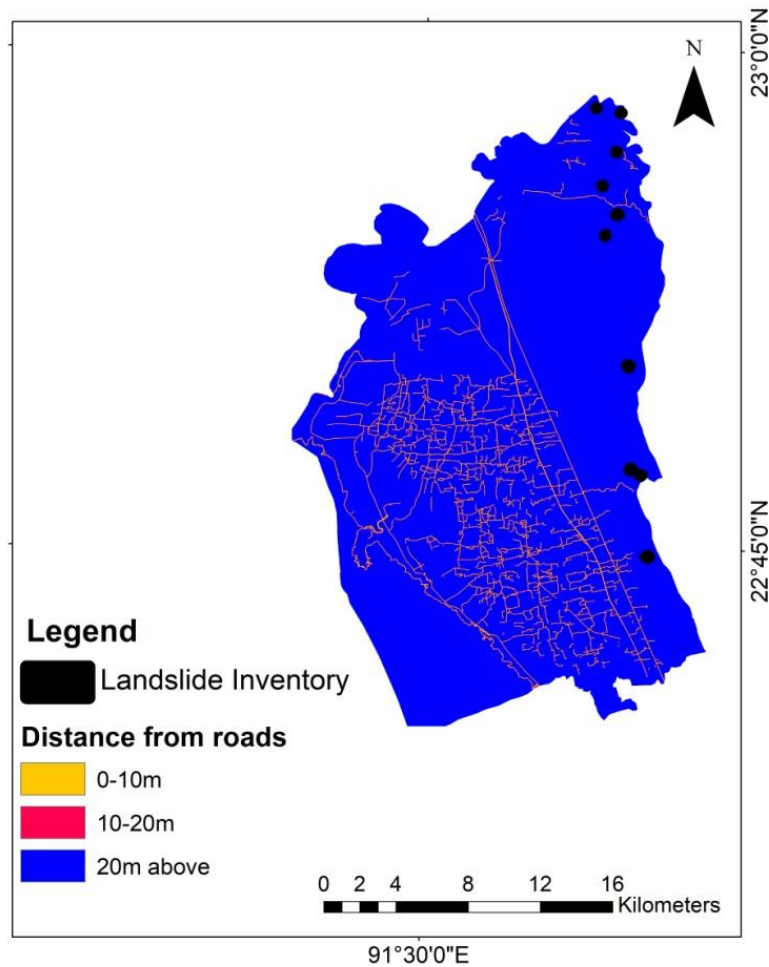


Figure 5.9 Road and Distance from the road

Surface Geology

According to the available geological map (GSB and USGS), there are five different surface geologic units in the project area, namely, Beach and Dune Sand, Bhuban Formation, Bokabil Formation, Tipam and Valley Alluvium.

Rainfall

The rainfall is one of the most important triggering factors for landslide initiation. Particularly, antecedent rainfall is more critical to make slope unstable. The rainfall infiltration increases pore water pressure which decreases the shear strength of the slope forming materials. The consecutive rainfall days and average rainfall have increased critically due to climate change, which results in intense rainfall within a short period of time (*IPCC, 2007*). Rainwater, therefore, reduces the shear strength of the soil as it infiltrates and heightens the erosional activities through rapid runoff, reducing frictions between the soil particles and loosening them (*Horelli, 2005*). The project area is characterized by about 3123

mm annual rainfall. As the project area has limited spatial coverage the rainfall will slightly vary over the whole area.

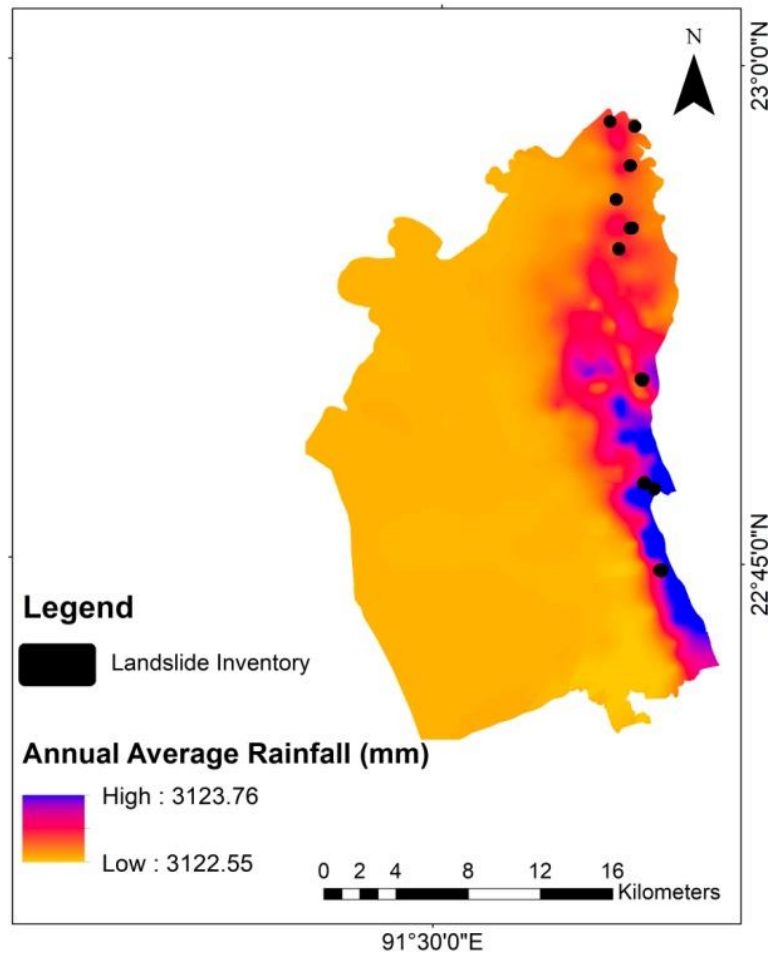


Figure 5.10 Figure showing average rainfall (Data Source: BMD)

Elevation

Elevation is another important factor for landslide occurrence. Digital Elevation model has been provided by Urban Development Directorate. The study area is characterized by 254 meter highest elevation.

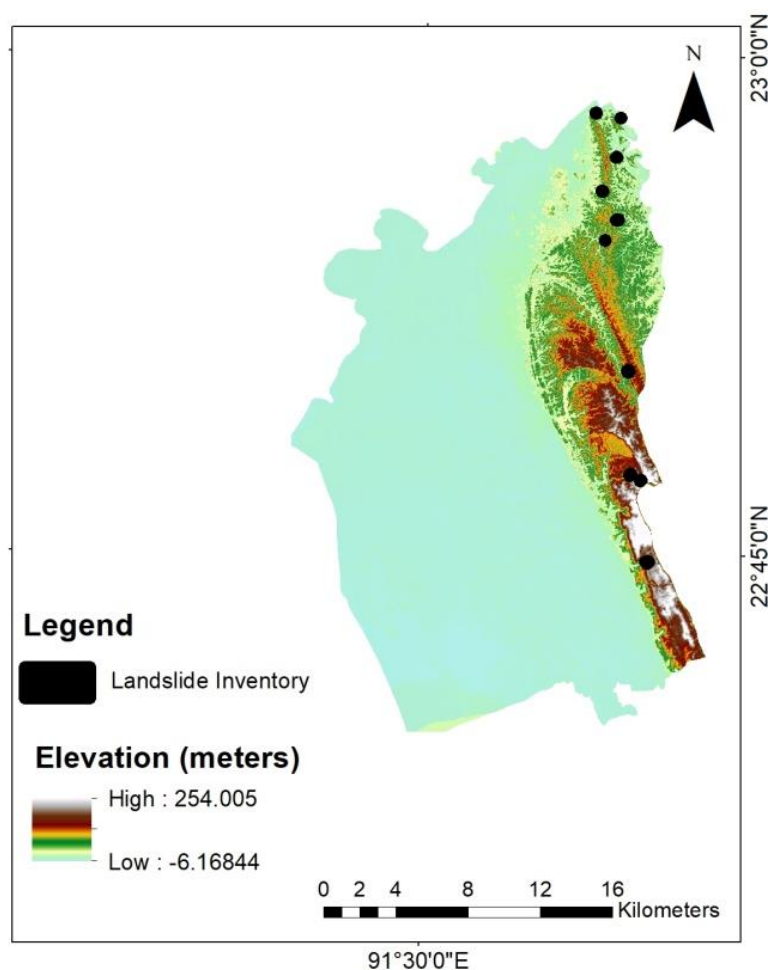


Figure 5.11 Digital Elevation Model

5.3. Landslide Susceptibility Mapping

Introduction to Landslide Susceptibility Mapping

As it is mentioned earlier the landslide susceptibility map has been produced following weight of evidence (WOE) bi-variate statistical method. Weights of evidence (WoE) is a Bayesian probability model which uses a log-linear form of the theorem to map future landslide susceptible areas (*Bonham-Carter, 1994*). It is a data-driven method where prediction is made from prior and conditional probability when the factor maps are overlaid with past landslide events (inventory) (*Bonham-Carter et al., 1989; Agterberg, F.P et al., 1990; Bonham-Carter, 2002*). This bivariate method is commonly used to define the statistical association between the factors and landslide events in several studies (*C.J. van Westen, N. Rengers, 2003; S. Lee & Choi, 2004; Neuhäuser & Terhorst, 2007; Pradhan et al., 2010*). The problems of heterogeneity in ground conditions, lack of detailed maps and inadequate data are solved by using this method. It can be used for large areas having varying data types and information (*Neuhäuser, 2014*). Many researchers consider the method as

robust (*Kanungo et al., 2009*) and reliable as it avoids subjectivity and measures uncertainty associated with estimates of probability values (error and relative error values) (*Neuhäuser, 2014*). After application of this method, it is necessary to find its degree of reliability. This can be done by several ways, which includes field visit to see if the model coincides with the reality or by using mathematical and statistical tools to calculate relative landslide density (RLD), Chi-squared test (*Zhou et al., 2016*), density graph (*Vakhshoori & Zare, 2016*), and the most commonly used method receiver operating curve (ROC) (*Vakhshoori & Zare, 2016; Ahmed & Dewan, 2017*). The success rate and prediction rate method is used in this study for easy understanding where the percentage of landslide susceptibility index rank is plotted against the percentage of cumulative landslide occurrence (*Mezughhi et al., 2011; Jebur et al., 2015; Rossi & Reichenbach, 2016*).

Weight of Evidence Method

In this method, the prior probability is calculated on the basis of past landslides assuming that it will trigger future hazardous event due to unstable nature of the slope resulting from the slope failure. When additional information about the factors are not available, prior probability give a good estimation about the possibility of landslide occurrence by dividing the number of pixels having landslides with a total number of pixels in the map (*Bonham-Carter, 1994*).

$$P_{prior} = P\{S\} = \frac{Area(Slide)}{Area(Total)}$$

But when information such as presence or extent of causal factors of landslides is available, then the prior probability is further modified to obtain a conditional probability. This is done by producing a binary map (B) for that particular factor depending on the presence and absence of the variable in the map. A relationship is then established between the binary maps with the landslide inventory, to calculate the conditional probability for a certain condition. According to *Bonham-Carter(1994)*, the factors are conditionally independent of each other, and the conditional probability of occurring a landslide given that a particular factor unit is present there is expressed as:

$$P\{S|B\} = \frac{P\{S \cap B\}}{P\{B\}}$$

$$= \frac{Npix \{S \cap B\}}{Npix \{B\}}$$

In the equation landslide and the factor, the variable is denoted by S and B respectively. Pixel area in each map is used in the analysis to find out the four possible combinations of probability, which are; when landslides occur in presence of a potential conditioning factor (Npix1) or absence of it (Npix2), when there is no landslide in the map area but the factor is present (Npix3) and absence of both landslide and that particular factor (Npix4). This is obtained by crossing the inventory of landslides with each factor map to calculate:

$$Npix1 = nslide$$

$$Npix2 = nslide - nslide$$

$$Npix3 = nclass - nslide$$

$$Npix4 = nmap - nslide - nclass + nslide$$

The above variables thereby means

slide = Number of pixels with landslides in the map

nclass = Number of pixels in the class

nslide = Number of pixels with landslides in the class

nmap = Total number of pixels in the map

Both positive and negative weighted values of each variable are then estimated to find a degree of correlation in presence or absence of the factor using the formula describes by (Bonham-Carter et al., 1989; Bonham-Carter, 2002):

$$W^+ = \ln\left(\frac{P\{B|S\}}{P\{B|\bar{S}\}}\right)$$

$$W^+ = \ln\left(\frac{Npix1 * (Npix3 + Npix4)}{(Npix1 + Npix2) * Npix3}\right)$$

$$W^- = \ln\left(\frac{P\{\bar{B}|S\}}{P\{\bar{B}|\bar{L}\}}\right)$$

$$W^- = \ln\left(\frac{Npix2 * (Npix3 + Npix4)}{(Npix1 + Npix2) * Npix4}\right)$$

In presence of factor (B) in landslide areas (S) gives a positive weighted value (W^+), defining the correlation between them. On the other hand, a negative weight (W^-) indicates the absence of the factor. Then a Weighted Contrast factor (C) is obtained to see how much the conditioning factor is spatially associated with the landslides. A final susceptibility map (LSI) hence, is produced by combining the weighted map of each factor through an overlay operation.

$$C = W^+ - W^-$$

$$W_{map} = W^+ - W^- + \Sigma W^-$$

$$LSI = \Sigma W_{map}$$

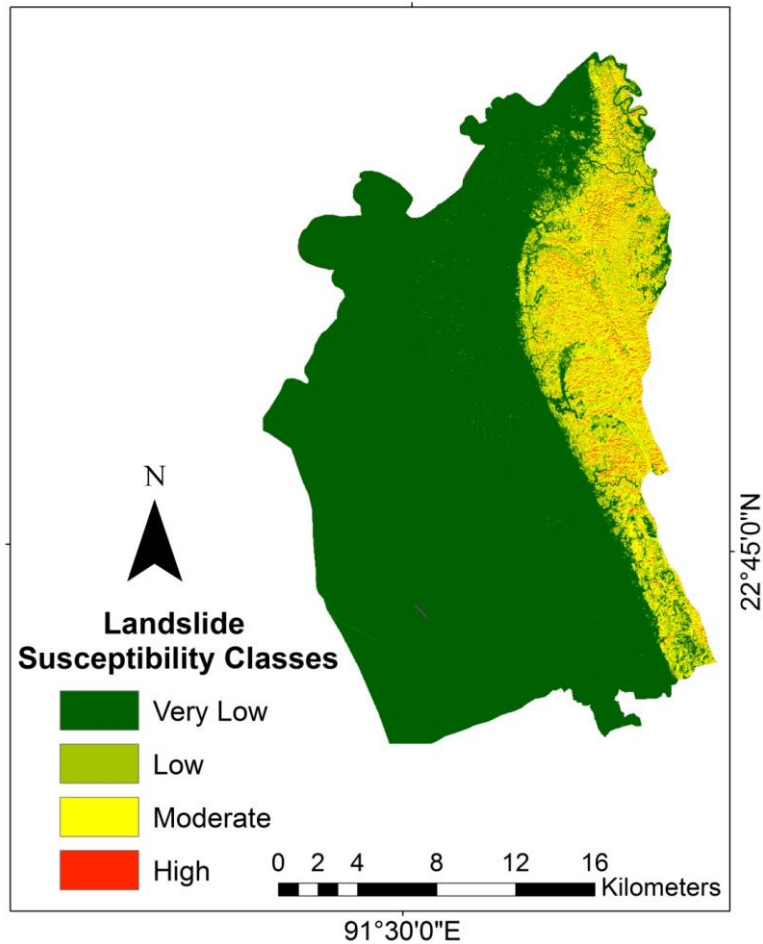
Performance of Weight of Evidence Method

The models are verified to see how well it fits and can predict future landslide areas (*Dietrich et al., 1995; Chung & Fabbri, 2003; Pradhan & Lee, 2010a*) described by the success rate (*Chung et al., 1999*). When the validation is done with the same dataset that was used in a statistical model, we call the resulting curve a success rate curve, because what is tested is only whether the model explains the landslides that were used to make it. When you use a landslide data set that is different from the data set used for making the model, we can actually test the prediction capability of the map, and the resulting curve is called a prediction rate curve. The two sets are called training data set and test datasets.

5.4. Results and Discussions

Results

Landslide susceptibility map is produced by the weight of evidence method in order to show the degree of influence of each causal factors with past landslide occurrence. Nine causal factors have been considered in this study *i.e.* present land use, land-use difference, distance from the major drainage, NDVI difference, slope, aspect, elevation, surface geology, and rainfall. The future landslide-prone areas are classified as high, moderate, low and very low susceptible zones as shown by different color representation in the map (figure 5.13).



5.13 Landslide susceptibility map of the Project Area

In order to establish a clear relationship, each factor was divided into several classes to see which class has the highest influence on landslide occurrence. The weight value for different classes of each factor map for Weights of Evidence (WoE) model is also provided in Appendix II. In case of WoE method, W^+ , W^- and C factor describes the correlation and spatial association of the landslides with the factors. The positive contrast factor indicates positive association that is more occurrences fall in the domain than the expected possibility and vice versa for negative contrast factor. The higher weighted value indicates higher degree of influence on landslide occurrence.

Overall the area lies in low to moderate landslide susceptible prone area. Most of the area lies within very low to low landslide susceptible area (about 85%). The remaining project area is mostly in moderate landslide prone zone (table 5.1).

Table 5.1 Susceptibility zone wise Landslide prone area

SUSCEPTIBLE CLASSES	Pixel COUNT	AREA(sq. meters)	TOTAL (sq. meters)	PERCENTAGE (%)
Very low	3794979	379497900	492871431.5	77
Low	401048	40104800	492871431.5	8
Moderate	623029	62302900	492871431.5	13
High	99369	9936900	492871431.5	2

Result Evaluation

The most important aspect of hazard assessment is the degree of accuracy. The accuracy will tell whether the hazard map perfectly distinguishes the hazard-prone and hazard-free areas. Therefore, the models need to be validated to see how well the susceptible classes are defined by the models used. This is done by finding out the success rate which is a statistical method to determine how well the resulting hazard map has classified the areas of existing landslides as high hazard areas. The method first divides the area of the hazard map in equal classes of the histogram, ranging from the highest to the lowest scores. Then for each of these classes, the percentage of the landslides that occur in that class is calculated. The result is plotted as the percentage of the map on the X-axis, and the percentage of the landslides on the Y-axis (figure 5.13). To do this, 75% of the landslide inventory is used for susceptibility assessment and the remaining 25% of the polygons are used in the analysis to training the dataset to produce the prediction rate. The objective of the prediction rate is to check how well the hazard map can predict the future occurrence of landslides. About 5% of the susceptible areas include more than 80% of the total landslide area. Almost all the pre-existing landslides have fallen into mostly in the high susceptible zone and partly in the moderate susceptible zone (figure 5.14). Therefore, the project area Mirsharai is not that much landslide prone. Prediction rate is also showing the similar trend which means the arbitrarily taken training data sets is also explaining well the prepared susceptibility map.

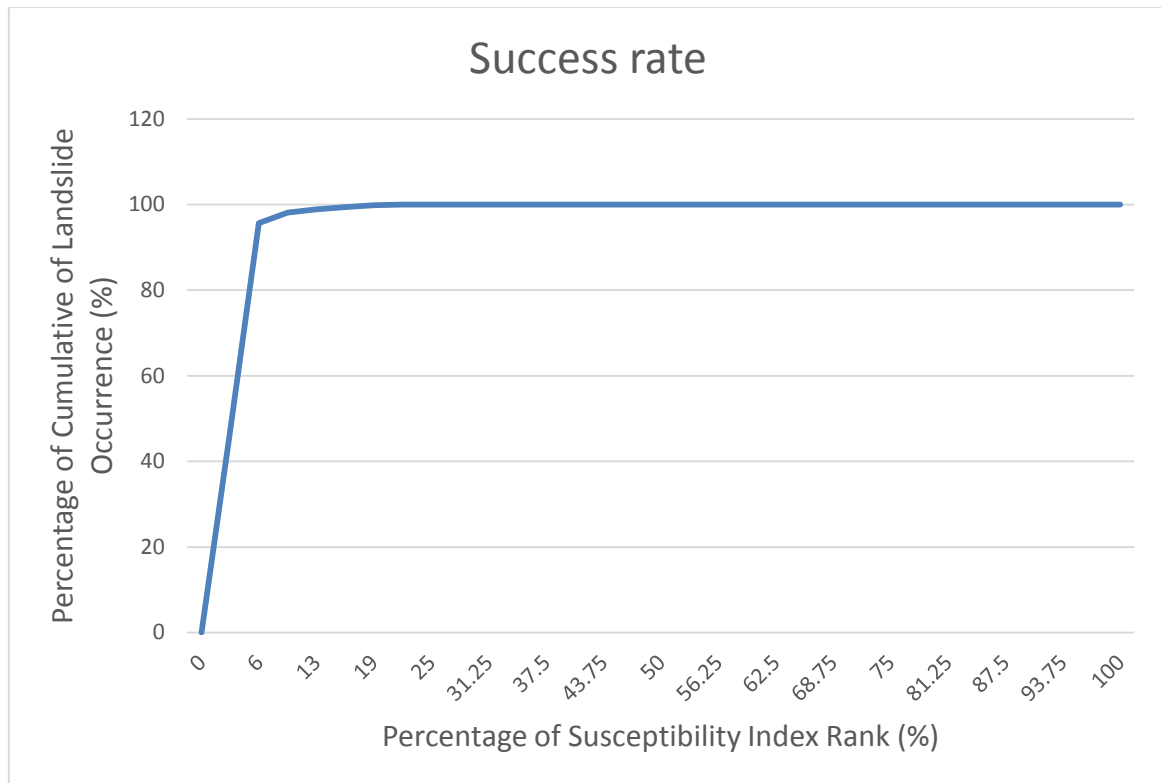


Figure 5.112 Success and Prediction Rate

6. CONCLUSION

Earthquakes are related to faulting and tectonic instability of an area. The overall tectonics of Bangladesh and adjoining region is conducive for the frequent and recurring earthquakes. The geo tectonic setting of the country is very active seismically. These are Himalayan Arc, Shillong Plateau and Dauki fault system in the North, Burmese arc and accretionary wedges in the East, Naga-Disang-Haflong thrust zone in the Northeast. Threatened earthquake disaster inside Bangladesh may be expected from these active seismic zones outside the national boundary.

Seismically, Bangladesh is divided into three zones i.e. less risk zone (zone 1), moderate risk zone (zone2) and highly risk zone (zone3). Mirsharai Upazila at Chittagong district of Bangladesh is situated in zone 2. Besides these, this area is located between Arakan Megathrust and Sagaing fault. So, Mirsharai is moderately vulnerable to earthquake. To propitiate the risk of earthquake some initiatives have been taken by the concerned authorities. One of the projects works named “Geological Study And Seismic Hazard Assessment Under Preparation of Development Plan for Mirsharai Upazila, Chittagong District: Risk Sensitive Landuse Plan (MUDP)” which has been initiated by Urban Development Directorate.

This study is an attempt towards refinement in seismic hazard calculation of Bangladesh using PSHA methods. New approaches in seismic source zone delineations, consideration for local site effects and incorporating inherent certainties in different source parameters as well as attenuation relationship are some of the improvements applied in this study.

Results are presented in form of hazard maps and curves showing PGA and SA. Peak ground acceleration has been computed with 2% and 10% probability exceedance in 50 years. In this study both peak ground acceleration (PGA) and peak spectral acceleration (PSA) have been estimated considering with and without site effect. However, the ground motion has found much higher than all other previous studies. The reason might be due to the utilization of appropriate Ground Motion Prediction Equation for different fault zones and utilization of Vs30 information of Mirsharai to account for the site effect.

It should be noted that there is room for further improvement in tackling the uncertainties of many other source parameters and attenuation models. This study will contribute towards

further seismic hazard assessments in Bangladesh and also facilitate in reducing seismic risk in structures by updating building codes in the country.

However, the project area Mirsharai is not that much landslide prone. Landslide susceptibility map is produced by the weight of evidence method in order to show the degree of influence of each causal factors with past landslide occurrence. Overall the area lies in low to moderate landslide susceptible prone area. Most of the area lies within very low to low landslide susceptible area (about 85%). The remaining project area is mostly in moderate landslide prone zone.

7. REFERENCES

- i. Anbazhagan P, Sitharam TG. Mapping of average shear wave velocity for Bangalore region: a case study. *Journal of Environmental & Engineering Geophysics* 2008;13(2):69–84.
- ii. Anbazhagan P, Sitharam TG. Seismic microzonation of Bangalore. *Journal of Earth System Science* 2008; 117(S2):833–52.
- iii. Anbazhagan P, Sitharam TG. Spatial variability of the weathered and engineering bed rock using multichannel analysis of surface wave survey. *Pure and Applied Geophysics* 2009;166(3):409–28.
- iv. Auld, B., 1977, Cross-Hole and Down-Hole Vs by Mechanical Impulse, *Journal of Geotechnical Engineering Division, ASCE*, Vol. 103, No. GT12, pp. 1381-1398
- v. Abrahamson, N.A. & Silva, W., Empirical Responce Spectral Attenuation Relations for Shallow Crustal Earthquakes.
- vi. Abbott, P. L. (2004). *Natural Disasters* (4th ed.). Boston: McGraw Hill.
- vii. Adhikari, M. (2011). *Bivariate Statistical Analysis of Landslide Susceptibility in Western Nepal*. University of Oslo.
- viii. Agterberg, F.P., Bonham-Carter, G.F. & Wright, D. F. (1990). Statistical pattern integration for mineral exploration. In D. F. Gaal, G. & Merriam (Ed.), *Computer application in resource estimation: prediction and assessment for metals and petroleum* (pp. 1–21). Oxford: Pergamon.
- ix. Ahmed, B. (2015). Landslide susceptibility mapping using multi-criteria evaluation techniques in Chittagong Metropolitan. *Journal of the International Consortium on Landslides, Springer Link*, 12(2015), 1077–1095. <http://doi.org/10.1007/s10346-014-0521-x>
- x. Ahmed, B., & Dewan, A. (2017). Application of Bivariate and Multivariate Statistical Techniques in Landslide Susceptibility Modeling in Chittagong City Corporation , Bangladesh. *Remote Sensing*, (May 2014). <http://doi.org/10.3390/rs9040304>
- xi. Ahmed, B., & Forte, R. (2016). Landslide Risk Zoning Applying Kohonen ' s Self-Organizing Map Neural Network Technique. In *Bangladesh Planning Research Conference (BPRC)*. <http://doi.org/10.13140/RG.2.1.2748.7766/1>
- xii. Alberto Refice & Domenico Capolongo. (2002). Probabilistic modeling of uncertainties in earthquake-induced landslide hazard assessment. *Computers & Geosciences*, 28(6), 735–749. [http://doi.org/10.1016/S0098-3004\(01\)00104-2](http://doi.org/10.1016/S0098-3004(01)00104-2)
- xiii. Anwar Hussain. (2017). No govt initiatives yet to stop rising landslide deaths | Dhaka Tribune.
- xiv. ADPC and OYO, 2009. *Time-Predictable fault Modeling of Bangladesh*,
- xv. Aki, K., 1965. Maximum Likelihood Estimate of b in the formula $\log N = a - b M$ and its Confidence Limits. *Bulletin of the Earthquake Research Institute*, pp.237–239.
- xvi. Al-hussaini, T.M. & Al-noman, M.N., 2010. PROBABILISTIC ESTIMATES OF PGA AND SPECTRAL ACCELERATION IN BANGLADESH.
- xvii. Al-hussaini, T.M., Al-noman, M.N. & Chowdhury, I.N., 2015. SEISMIC HAZARD ASSESSMENT FOR BANGLADESH - OLD AND NEW PERSPECTIVES.
- xviii. Ali, M.H. & Choudhury, J.R., 1994. Seismic Zoning of Bangladesh. In *International Seminar on Recent Developments in Earthquake Disaster Mitigation*. Dhaka. Available at: <papers3://publication/uuid/D1250C05-2FC7-4954-A734-E33EBBEECB95>.
- xix. Ambraseys, N.N., 2004. Three little known early earthquakes in India. *Current Science*, 86(4), pp.506–508.
- xx. Anon, 2015. *Bangladesh National Building Code*, Housing and Building Research Institute.

- xxi. Atkinson, G.M. & Boore, D.M., 2006. Earthquake ground-motion prediction equations for eastern North America. *Bulletin of the Seismological Society of America*.
- xxii. Atkinson, G.M. & Boore, D.M., 2003. Empirical ground-motion relations for subduction-zone earthquakes and their application to Cascadia and other regions. *Bulletin of the Seismological Society of America*, 93(4), pp.1703–1729.
- xxiii. Atkinson, G.M. & Boore, D.M., 1995. Ground-motion relations for eastern north America. *Bulletin of the Seismological Society of America*, 85(1), pp.17–30.
- xxiv. Bender, B., 1983. Maximum likelihood estimation of b values for magnitude grouped data. *Bulletin of the Seismological Society of America*.
- xxv. Bilham, R., 2004. Historical Studies of Earthquakes in India. *Annals of Geophysics*, pp.1–26.
- xxvi. Bathrellos, G. D., Kalivas, D. P., & Skilodimou, H. D. (2009). GIS-based landslide susceptibility mapping models applied to natural and urban planning in Trikala, Central Greece. *Estudios Geológicos*, 65(1), 49–65. <http://doi.org/10.3989/egeol.08642.036>
- xxvii. Bonham-Carter, G. F. (1994). *Geographic Information Systems for Geoscientists, Modeling with GIS*. Oxford: Pergamon Press.
- xxviii. Bonham-Carter, G. F. (2002). Geographic information systems for geoscientist: Modelling with GIS., 302–334.
- xxix. Bonham-Carter, G.F., Agterberg, F.P. & Wright, D. F. (1989). Weights of evidence modelling: A new approach to mapping mineral potential. *Statistical Applications in Earth Science*, 89(9), 171–183.
- xxx. Brunori, F., N. Casagli, S. Fiaschi, C. A. Garzonio, and S. M. (1996). Landslide hazard mapping in Tuscany, Italy: an example of automatic evaluation. In *Geomorphic Hazards* (pp. 56–67). Chichester and New York: Wiley.
- xxxi. Bui, D. T., Lofman, O., Revhaug, I., & Dick, O. (2011). Landslide susceptibility analysis in the Hoa Binh province of Vietnam using statistical index and logistic regression. *Natural Hazards*, 59(3), 1413–1444. <http://doi.org/10.1007/s11069-011-9844-2>
- xxxii.
- xxxiii. Bommer, J.J. & Abrahamson, N.A., 2006. Why do modern probabilistic seismic-hazard analyses often lead to increased hazard estimates? *Bulletin of the Seismological Society of America*.
- xxxiv. Boore, D.M. & Atkinson, G.M., 2008. Ground-motion prediction equations for the average horizontal component of PGA, PGV, and 5%-damped PSA at spectral periods between 0.01 s and 10.0 s. *Earthquake Spectra*.
- xxxv. Banglapedia 2015 - http://en.banglapedia.org/index.php?title=Dohar_Upazila
- xxxvi. C.J. Van Westen. (2000). The Modelling Of Landslide Hazards Using Gis (PDF Download Available). *Surveys in Geophysics*, 21, 241–255.
- xxxvii. C.J. van Westen, N. Rengers, R. S. (2003). *Use of geomorphological information in indirect landslide susceptibility assessment. Natural hazards* (Vol. 30). Kluwer Academic Publishers.
- xxxviii. Carrara, A., Cardinali, M., Detti, R., Guzzetti, F., Pasqui, V., & Reichenbach, P. (1991). GIS techniques and statistical models in evaluating landslide hazard. *Earth Surface Processes and Landforms*, 16(5), 427–445. <http://doi.org/10.1002/esp.3290160505>
- xxxix. Chalkias, C., Ferentinou, M., & Polykretis, C. (2014). GIS-Based Landslide Susceptibility Mapping on the Peloponnese Peninsula, Greece. *Geosciences*, 4(3), 176–190. <http://doi.org/10.3390/geosciences4030176>
- xl. Chisty, K. U. (2014). Landslide in Chittagong City : A Perspective on Hill Cutting. *Journal of Bangladesh Institute of Planners*, 7(December), 1–17.
- xli. Chung, C.-J. F., & Fabbri, A. G. (2003). Validation of Spatial Prediction Models for Landslide Hazard Mapping. *Natural Hazards*, 30(3), 451–472.

- <http://doi.org/10.1023/B:NHAZ.0000007172.62651.2b>
- xlii. Chung, C. -J. F.; Fabbri, A. G. (1999). Probabilistic Prediction Models for Landslide Hazard Mapping. *Photogrammetric Engineering & Remote Sensing*, 65(12), 1389–1399.
- xliiii. Cleary, P. W., Prakash, M., & Rothauge, K. (2010). Combining digital terrain and surface textures with large-scale particle-based computational models to predict dam collapse and landslide events. *International Journal of Image and Data Fusion*, 1(4), 337–357. <http://doi.org/10.1080/19479832.2010.491801>
- xliv. Crozier, M. J. (1999). Landslides. In *Environmental Geology* (pp. 371–375). Dordrecht: Kluwer Academic Publishers. http://doi.org/10.1007/1-4020-4494-1_200
- xl. Cruden, D. M. (1991). A simple definition of a landslide. *Bulletin of the International Association of Engineering Geology - Bulletin de l'Association Internationale de Géologie de l'Ingénieur*, 43(1), 27–29. <http://doi.org/10.1007/BF02590167>
- xlvi. Cruden, D. M., & Varnes, D. J. (1996). Landslide types and processes. In: Turner AK, Schuster, RL (eds) *Landslides Investigation and Mitigation, Special Report 247*. <http://doi.org/Fact Sheet 2004-3072>
- xlvii. Campbell, K.W. & Bozorgnia, Y., 2003. Updated near-source ground-motion (attenuation) relations for the horizontal and vertical components of peak ground acceleration and acceleration response spectra. *Bulletin of the Seismological Society of America*.
- xlviii. Chiou, B.S.J. & Youngs, R.R., 2008. An NGA model for the average horizontal component of peak ground motion and response spectra. *Earthquake Spectra*, 24(1), pp.173–215.
- xlix. Chowdhury, I.N., 2016. Neo-Deterministic Studies for Seismic Hazard Assessment of Bangladesh. , (June).
- I. Cornell, C.A., 1968. Engineering seismic risk analysis. *Bulletin of the Seismological Society of America*, 58(5), pp.1583–1606. Available at: <http://bssa.geoscienceworld.org/cgi/content/abstract/58/5/1583%5Cnhttp://bssaonline.org/cgi/content/abstract/58/5/1583>.
 - li. Dai, F. ., Lee, C. ., & Ngai, Y. . (2002). Landslide risk assessment and management: an overview. *Engineering Geology*, 64(1), 65–87. [http://doi.org/10.1016/S0013-7952\(01\)00093-X](http://doi.org/10.1016/S0013-7952(01)00093-X)
 - lii. Dănuț Petrea, Ștefan Bilașco, Sanda Roșca, I. V. I. F. (2014). The determination of the Landslide occurrence probability by spatial analysis of the Land Morphometric ... *Carpathian Journal of Earth and Environmental Sciences*, 9(May), 91–102.
 - liiii. DDM. (2017). *Bangladesh Needs Assessment Working Group (NAWG) Report on Landslides* (Vol. 2017).
 - liv. Dhakal, A. S., Amada, T., & Aniya, M. (1999). Landslide Hazard Mapping and the Application of GIS in the Kulekhani Watershed, Nepal. *Mountain Research and Development*, 19(1), 3. <http://doi.org/10.2307/3674109>
 - lv. Dietrich, W. E., Reiss, R., Hsu, M. -L, & Montgomery, D. R. (1995). A process-based model for colluvial soil depth and shallow landsliding using digital elevation data. *Hydrological Processes*, 9(3-4), 383–400. <http://doi.org/10.1002/hyp.3360090311>
 - lvi. Duncan, J. M. (1996). Soil Slope Stability Analysis. In R. L. Keith, T. and Schuster (Ed.), *Landslides: Investigation and Mitigation* (pp. 337–371). Washington, D.C: Transportation Research Board National Research Council.
 - lvii. ECOLOGICAL RESTORATION SPECIALISTS. (n.d.). Role of Vegetation. *Sound Native Plants*, p. 98507.
 - lviii. Firman, B., & Wahono, D. (2010). *APPLICATIONS OF STATISTICAL AND HEURISTIC METHODS FOR LANDSLIDE SUSCEPTIBILITY ASSESSMENTS A case study in Wadas Lintang Sub District , Wonosobo Regency , Central Java Province , Indonesia*. Gadjah Mada

University.

- lix. Francipane, A., Arnone, E., Lo Conti, F., Puglisi, C., & Noto, L. V. (2014). A Comparison Between Heuristic, Statistical, And Data-Driven Methods In Landslide Susceptibility Assessment: An Application To The Briga And Giampileri Catchments. In *11^o International Conference on Hydroinformatics* (p. 9).
- lx. Fressard, M., Thiery, Y., & Maquaire, O. (2014). Which data for quantitative landslide susceptibility mapping at operational scale case study of the pays d'auge plateau hillslopes (Normandy, France). *Natural Hazards and Earth System Sciences*, 14(3), 569–588. <http://doi.org/10.5194/nhess-14-569-2014>
- lxi. G.Zhou,T.Esaki,Y.Mitani, M.Xie, J. M. (2003). Spatial probabilistic modeling of slope failure using an integrated GIS Monte Carlo simulation approach. *Engineering Geology*, 68(3-4), 373–386. [http://doi.org/10.1016/S0013-7952\(02\)00241-7](http://doi.org/10.1016/S0013-7952(02)00241-7)
- lxii. Goudie, A. S. (2004). Encyclopedia of Geomorphology. In *Encyclopedia of Geomorphology* (Vol. 1, p. 1156). Routledge. <http://doi.org/10.4324/9780203381137>
- lxiii. Guzzetti, Cardinali, Reichenbach, & Carrara. (2000). Comparing Landslide Maps: A Case Study in the Upper Tiber River Basin, Central Italy. *Environmental Management*, 25(3), 247–263.
- lxiv. Garnder, J.K. & Knopoff, L., 1974. Bulletin of the Seismological Society of America. *Bulletin of the Seismological Society of America*, 64(5), pp.1271–1302. Available at: <http://www.bssaonline.org/cgi/content/abstract/66/3/639>.
- lxv. Ghosh, B. et al., 2012. Seismic Hazard Assessment in India. *15th World Conference on Earthquake Engineering*. Available at: http://www.iitk.ac.in/nicee/wcee/article/WCEE2012_2107.pdf.
- lxvi. GSB, 1979. *Final report by the Committee of Experts on Earthquake Hazard Minimization*,
- lxvii. Gutenberg, B. & Richter, C.F., 1944. Frequency of earthquakes in California. *Bulletin of the Seismological Society of America*, 34, pp.185–188.
- lxviii. Hanks, T.C. & Kanamori, H., 1979. A moment magnitude scale. In *Journal of Geophysical Research B: Solid Earth*. pp. 2348–2350.
- lxix. Heaton, T.H. & Tajima, F., 1986. Estimating Ground Motions Using Recorded Accelerograms. , 8, pp.25–83.
- lxx. H.A.Nefeslioglu, C.Gokceoglu, H. S. (2008). An assessment on the use of logistic regression and artificial neural networks with different sampling strategies for the preparation of landslide susceptibility maps. *Engineering Geology*, 97(3-4), 171–191. <http://doi.org/10.1016/J.ENGGE0.2008.01.004>
- lxxi. Hammond, C.J.; Prellwitz, R.W.; Miller, S. . (1991). Landslide hazard assessment using Monte Carlo simulation. In *Proceedings 6th International symposium of landslides* (pp. 959–964). New Zealand.
- lxxii. Hasan Jahid Tusher, Minhaj Uddin, P. D. and A. C. (2017, June). Fuel crisis hits Rangamati, search underway. *The Daily Star*.
- lxxiii. Horelli, J. A. (2005). *Landslides in Hong Kong*. University of Helsinki.
- lxxiv. Huang, J. (2014). *Investigation on landslide susceptibility using remote sensing and GIS methods*. Hong Kong Baptist University.
- lxxv. IFRC. (2007). *Landslides and Slopes-479.pdf*.
- lxxvi. IFRC. (2016). *World Disasters Report 2016*. IFRC.
- lxxvii. Intarawichian, N., & Dasananda, S. (2010). ANALYTICAL HIERARCHY PROCESS FOR LANDSLIDE SUSCEPTIBILITY MAPPING IN LOWER MAE CHAEM WATERSHED, NORTHERN THAILAND. *Suranaree J. Sci. Technol*, 7(3).
- lxxviii. IPCC. (2007). *IPCC Fourth Assessment Report: Climate Change 2007 (AR4)*.

- lxxix. Iverson, R. M. (2000). Landslide triggering by rain infiltration. *Water Resources Research*, 36(7), 1897–1910. <http://doi.org/10.1029/2000WR900090>
- lxxx. Islam, M.S. et al., 2010. ATTENUATION OF EARTHQUAKE INTENSITY IN BANGLADESH. In *Proceedings, 3rd International Earthquake Symposium, Bangladesh, Dhaka, March.5-6 2010*.
- lxxxi. Jebur, M. N., Pradhan, B., Shafri, H. Z. M., Yusoff, Z. M., & Tehrany, M. S. (2015). An integrated user-friendly ArcMAP tool for bivariate statistical modelling in geoscience applications. *Geoscientific Model Development*, 8(3), 881–891. <http://doi.org/10.5194/gmd-8-881-2015>
- lxxxii. Kanungo, D. P., Arora, M. K., Sarkar, S., & Gupta, R. P. (2009). Landslide Susceptibility Zonation (LSZ) Mapping - A Review. *Journal of South Asia Disaster Studies*, 2(1), 81–106.
- lxxxiii. Kienholz, H., Hafner, H., Schneider, G., & Tamrakar, R. (1983). Mountain Hazards Mapping in Nepal's Middle Mountains Maps of Land Use and Geomorphic Damages (Kathmandu-Kakani Area). *Mountain Research and Development*, 3(3), 195–220.
- lxxxiv. L Yin, K & Z Yan, T. (1988). Statistical Prediction models for slope instability of metamorphosed rocks. In *Proceedings of 5th Int Symp on Landslides*. Lausanne.
- lxxxv. Lee, C. (2015). Review and Perspectives on Methodology for Landslide Hazard Analysis. 10th Asian Regional Conference of IAEG, 1–6.
- lxxxvi. Lee, S., & Choi, J. (2004). Landslide susceptibility mapping using GIS and the weight-of-evidence model. *International Journal of Geographical Information Science*, 18(8), 789–814. <http://doi.org/10.1080/13658810410001702003>
- lxxxvii. Lin, Y.-P., Chu, H.-J., & Wu, C.-F. (2010). Spatial pattern analysis of landslide using landscape metrics and logistic regression: a case study in Central Taiwan. *Hydrology and Earth System Sciences Discussions*, 7(3), 3423–3451. <http://doi.org/10.5194/hessd-7-3423-2010>
- lxxxviii. Kitsunezaki, C., N. Goto, Y. Kobayashi., T. Ikawa, M. Horike, T. Saito, T. Kurota, K. Yamane, and K. Okuzumi, 1990, Estimation of P- and S- wave velocities in Deep Soil Deposits for Evaluating Ground Vibrations in Earthquake, SIZEN-SAIGAI-KAGAKU,9-3,1-17 (in Japanese).
- lxxxix. Ludwig, W.J., Nafe, J.E., and Drake, C.L., 1970, Seismic refraction, in *The Sea*, A.E. Maxwell (Editor), Vol. 4, Wiley-Interscience, New York, pp. 53-84
- xc. Miller RD, Xia J, Park CB, Ivanov J. Multichannel analysis of surface waves to map bedrock. *The Leading Edge* 1999;18(12):1392–6.
- xc. Makropoulos, K.C. & Burton, P.W., 1983. Seismic risk of circum-pacific earthquakes I. Strain energy release. *Pure and Applied Geophysics PAGEOPH*.
- xcii. Musson, R.M.W., 1999. Probabilistic seismic hazard maps for the north Balkan region. *Annals of Geophysics*.
- xciii. Malczewski, J. (1999). *GIS and multicriteria decision analysis. Engineering* (Vol. 31).
- xciv. McCalpin, J. (1984). Preliminary age classification of landslides for inventory mapping. *Annual Symposium on Engineering Geology and Soil Engineering 21*, (January 1984), 99–111.
- xcv. Mezughi, T. H., Akhir, J. M., Rafek, A. G., & Abdullah, I. (2011). Landslide susceptibility assessment using frequency ratio model applied to an area along the E-W highway (Gerik-Jeli). *American Journal of Environmental Sciences*, 7(1), 43–50. <http://doi.org/10.3844/ajessp.2011.43.50>
- xcvi. Montgomery, D. R., & Dietrich, W. E. (1994). A physically based model for the topographic control on shallow landsliding. *Water Resources Research*, 30(4), 1153–1171. <http://doi.org/10.1029/93WR02979>

- xcvii. Moser, H., Morgenschweis, G., Hydro-, H. Z. I., & Hallsworth, E. G. (1989). Book reviews, *14*, 361–362.
- xcviii. Nandi, A., & Shakoor, A. (2006). Preparation of a landslide susceptibility map of Summit County, Ohio, USA, using numerical models. In *Proceedings of the 10th IAEG Congress, Nottingham, UK* (Vol. 610).
- xcix. Neuhäuser, B. (2014). *Landslide Susceptibility and Climate Change Scenarios in Flysch Areas of the Eastern Alps*.
- c. Neuhäuser, B., & Terhorst, B. (2007). Landslide susceptibility assessment using “weights-of-evidence” applied to a study area at the Jurassic escarpment (SW-Germany). *Geomorphology*, 86(1-2), 12–24. <http://doi.org/10.1016/j.geomorph.2006.08.002>
- ci. Nirapad. (2017). *Hazard Incidents in Bangladesh , April 2017*.
- cii. P. Gupta, R & C. Joshi, B. (1990). Landslide Hazard Zonation using the GIS Approach - A case Study from the Ramganga Catchment Himalayas. *Engineering Geology*, 28, 119–131.
- ciiii. Nath, S.K. & Thingbaijam, K.K.S., 2012. Probabilistic Seismic Hazard Assessment of India. *Seismological Research Letters*, 83(1), pp.135–149. Available at: <https://pubs.geoscienceworld.org/srl/article/83/1/135-149/143990>.
- civ. Noor, M.A., Yasin, M. & Ansary, M.A., 2005. Seismic Hazard Analysis of Bangladesh. In *First Bangladesh Earthquake Symposium*. Dhaka.
- cv. Okada, H., 2003, The microtremor survey method, Society of Exploration Geophysicist, Tulsa
- cvi. Park CB, Miller RD, Xia J. Multi-channel analysis of surface waves. *Geophysics* 1999; 64(3):800–8.
- cvii. Scordilis, E.M., 2006. Empirical global relations converting MSand mbto moment magnitude. *Journal of Seismology*, 10(2), pp.225–236.
- cviii. Silva, V. et al., 2014. Development of the OpenQuake engine, the Global Earthquake Model’s open-source software for seismic risk assessment. *Natural Hazards*, 72(3), pp.1409–1427.
- cix. Sipkin, S.A., 2003. A Correlation to Body-wave magnitude mb Based on Moment Magnitude Mw. *Seismological Research Letters*, 74(6), pp.739–742.
- cx. Steckler, M.S. et al., 2016. Locked and loading megathrust linked to active subduction beneath the Indo-Burman Ranges. *Nature Geoscience*, 9(8), pp.615–618.
- cxii. Stepp, J.C., 1972. Analysis of completeness of the earthquake sample in the Puget Sound area and its effect on statistical estimates of earthquake hazard. *Proc. of the 1st Int. Conf. on Microzonation, Seattle, Vol. 2*, (July), pp.897–910.
- cxiii. Strasser, F.O., Arango, M.C. & Bommer, J.J., 2010. Scaling of the Source Dimensions of Interface and Intraslab Subduction-zone Earthquakes with Moment Magnitude. *Seismological Research Letters*, 81(6), pp.941–950.
- cxiiii. U.S. Geological Survey, USGS. Available at: <https://earthquake.usgs.gov/earthquakes/search/> [Accessed June 13, 2018].
- cxv. Wang, Y., 2014. Active tectonic and earthquake Myanmar region. *Journal of Geophysical Research: Solid Earth*, pp.3576–3822.
- cxvi. Wang, Y. et al., 2014. Active tectonic and earthquake Myanmar region. *Journal of Geophysical Research: Solid Earth*, 119, pp.3576–3822.
- cxvii. Weatherill, G.A., 2014. *OpenQuake Hazard Modeller ’s Toolkit-User Guide*,
- cxviii. Youngs, R., 1997. Youngs et al_Strong Ground Motion Attenuation Relationships for Subduction Zone Earthquakes.pdf. *Seismological Research Letters*, 68(1), pp.58–73.
- cxix. Yu, W. & Sieh, K., 2013. *Active tectonic features that pose a seismic threat to Bangladesh*, Dhaka.
- cxix. Abbott, P. L. (2004). *Natural Disasters* (4th ed.). Boston: McGraw Hill.

- cxx. Adhikari, M. (2011). Bivariate Statistical Analysis of Landslide Susceptibility in Western Nepal. University of Oslo.
- cxxi. Agterberg, F.P., Bonham-Carter, G.F. & Wright, D. F. (1990). Statistical pattern integration for mineral exploration. In D. F. Gaal, G. & Merriam (Ed.), Computer application in resource estimation: prediction and assessment for metals and petroleum (pp. 1–21). Oxford: Pergamon.
- cxxii. Ahmed, B. (2015). Landslide susceptibility mapping using multi-criteria evaluation techniques in Chittagong Metropolitan. *Journal of the International Consortium on Landslides*, Springer Link, 12(2015), 1077–1095. <http://doi.org/10.1007/s10346-014-0521-x>
- cxxiii. Ahmed, B., & Dewan, A. (2017). Application of Bivariate and Multivariate Statistical Techniques in Landslide Susceptibility Modeling in Chittagong City Corporation , Bangladesh. *Remote Sensing*, (May 2014). <http://doi.org/10.3390/rs9040304>
- cxxiv. Ahmed, B., & Forte, R. (2016). Landslide Risk Zoning Applying Kohonen ' s Self-Organizing Map Neural Network Technique. In Bangladesh Planning Research Conference (BPRC). <http://doi.org/10.13140/RG.2.1.2748.7766/1>
- cxxv. Alberto Refice & Domenico Capolongo. (2002). Probabilistic modeling of uncertainties in earthquake-induced landslide hazard assessment. *Computers & Geosciences*, 28(6), 735–749. [http://doi.org/10.1016/S0098-3004\(01\)00104-2](http://doi.org/10.1016/S0098-3004(01)00104-2)
- cxxvi. Anwar Hussain. (2017). No govt initiatives yet to stop rising landslide deaths | Dhaka Tribune.
- cxxvii. Bathrellos, G. D., Kalivas, D. P., & Skilodimou, H. D. (2009). GIS-based landslide susceptibility mapping models applied to natural and urban planning in Trikala, Central Greece. *Estudios Geológicos*, 65(1), 49–65. <http://doi.org/10.3989/egol.08642.036>
- cxxviii. Bonham-Carter, G. F. (1994). *Geographic Information Systems for Geoscientists, Modeling with GIS*. Oxford: Pergamon Press.
- cxxix. Bonham-Carter, G. F. (2002). *Geographic information systems for geoscientist: Modelling with GIS.*, 302–334.
- cxxx. Bonham-Carter, G.F., Agterberg, F.P. & Wright, D. F. (1989). Weights of evidence modelling: A new approach to mapping mineral potential. *Statistical Applications in Earth Science*, 89(9), 171–183.
- cxxxi. Brunori, F., N. Casagli, S. Fiaschi, C. A. Garzonio, and S. M. (1996). Landslide hazard mapping in Tuscany, Italy: an example of automatic evaluation. In *Geomorphic Hazards* (pp. 56–67). Chichester and New York: Wiley.
- cxxxii. Bui, D. T., Lofman, O., Revhaug, I., & Dick, O. (2011). Landslide susceptibility analysis in the Hoa Binh province of Vietnam using statistical index and logistic regression. *Natural Hazards*, 59(3), 1413–1444. <http://doi.org/10.1007/s11069-011-9844-2>
- cxxxiii. C.J. Van Westen. (2000). The Modelling Of Landslide Hazards Using Gis (PDF Download Available). *Surveys in Geophysics*, 21, 241–255.
- cxxxiv. C.J. van Westen, N. Rengers, R. S. (2003). Use of geomorphological information in indirect landslide susceptibility assessment. *Natural hazards* (Vol. 30). Kluwer Academic Publishers.
- cxxxv. Carrara, A., Cardinali, M., Detti, R., Guzzetti, F., Pasqui, V., & Reichenbach, P. (1991). GIS techniques and statistical models in evaluating landslide hazard. *Earth Surface Processes and Landforms*, 16(5), 427–445. <http://doi.org/10.1002/esp.3290160505>
- cxxxvi. Chalkias, C., Ferentinou, M., & Polykretis, C. (2014). GIS-Based Landslide Susceptibility Mapping on the Peloponnese Peninsula, Greece. *Geosciences*, 4(3), 176–190. <http://doi.org/10.3390/geosciences4030176>
- cxxxvii. Chisty, K. U. (2014). Landslide in Chittagong City : A Perspective on Hill Cutting. *Journal of Bangladesh Institute of Planners*, 7(December), 1–17.

- cxviii. Chung, C.-J. F., & Fabbri, A. G. (2003). Validation of Spatial Prediction Models for Landslide Hazard Mapping. *Natural Hazards*, 30(3), 451–472. <http://doi.org/10.1023/B:NHAZ.0000007172.62651.2b>
- cxviii. Chung, C. -J. F.; Fabbri, A. G. (1999). Probabilistic Prediction Models for Landslide Hazard Mapping. *Photogrammetric Engineering & Remote Sensing*, 65(12), 1389–1399.
- cxix. Cleary, P. W., Prakash, M., & Rothauge, K. (2010). Combining digital terrain and surface textures with large-scale particle-based computational models to predict dam collapse and landslide events. *International Journal of Image and Data Fusion*, 1(4), 337–357. <http://doi.org/10.1080/19479832.2010.491801>
- cxli. Crozier, M. J. (1999). Landslides. In *Environmental Geology* (pp. 371–375). Dordrecht: Kluwer Academic Publishers. http://doi.org/10.1007/1-4020-4494-1_200
- cxlii. Cruden, D. M. (1991). A simple definition of a landslide. *Bulletin of the International Association of Engineering Geology - Bulletin de l'Association Internationale de Géologie de l'Ingénieur*, 43(1), 27–29. <http://doi.org/10.1007/BF02590167>
- cxliii. Cruden, D. M., & Varnes, D. J. (1996). Landslide types and processes. In: Turner AK, Schuster, RL (eds) *Landslides Investigation and Mitigation*, Special Report 247. <http://doi.org/Fact Sheet 2004-3072>
- cxliv. Dai, F. ., Lee, C. ., & Ngai, Y. . (2002). Landslide risk assessment and management: an overview. *Engineering Geology*, 64(1), 65–87. [http://doi.org/10.1016/S0013-7952\(01\)00093-X](http://doi.org/10.1016/S0013-7952(01)00093-X)
- cxlv. Dănuț Petrea, Ștefan Bilașco, Sanda Roșca, I. V. I. F. (2014). The determination of the Landslide occurrence probability by spatial analysis of the Land Morphometric ... *Carpathian Journal of Earth and Environmental Sciences*, 9(May), 91–102.
- cxlvi. DDM. (2017). *Bangladesh Needs Assessment Working Group (NAWG) Report on Landslides (Vol. 2017)*.
- cxlvii. Dhakal, A. S., Amada, T., & Aniya, M. (1999). Landslide Hazard Mapping and the Application of GIS in the Kulekhani Watershed, Nepal. *Mountain Research and Development*, 19(1), 3. <http://doi.org/10.2307/3674109>
- cxlviii. Dietrich, W. E., Reiss, R., Hsu, M. -L, & Montgomery, D. R. (1995). A process-based model for colluvial soil depth and shallow landsliding using digital elevation data. *Hydrological Processes*, 9(3-4), 383–400. <http://doi.org/10.1002/hyp.3360090311>
- cxlix. Duncan, J. M. (1996). Soil Slope Stability Analysis. In R. L. Keith, T. and Schuster (Ed.), *Landslides: Investigation and Mitigation* (pp. 337–371). Washington, D.C: Transportation Research Board National Research Council.
- cl. ECOLOGICAL RESTORATION SPECIALISTS. (n.d.). Role of Vegetation. *Sound Native Plants*, p. 98507.
- cli. Firman, B., & Wahono, D. (2010). APPLICATIONS OF STATISTICAL AND HEURISTIC METHODS FOR LANDSLIDE SUSCEPTIBILITY ASSESSMENTS A case study in Wadas Lintang Sub District , Wonosobo Regency , Central Java Province , Indonesia. Gadjah Mada University.
- clii. Francipane, A., Arnone, E., Lo Conti, F., Puglisi, C., & Noto, L. V. (2014). A Comparison Between Heuristic, Statistical, And Data-Driven Methods In Landslide Susceptibility Assessment: An Application To The Briga And Giampileri Catchments. In 11o International Conference on Hydroinformatics (p. 9).
- cliii. Fressard, M., Thiery, Y., & Maquaire, O. (2014). Which data for quantitative landslide susceptibility mapping at operational scale case study of the pays d'auge plateau hillslopes (Normandy, France). *Natural Hazards and Earth System Sciences*, 14(3), 569–588. <http://doi.org/10.5194/nhess-14-569-2014>

- cliv. G.Zhou,T.Esaki,Y.Mitani, M.Xie, J. M. (2003). Spatial probabilistic modeling of slope failure using an integrated GIS Monte Carlo simulation approach. *Engineering Geology*, 68(3-4), 373–386. [http://doi.org/10.1016/S0013-7952\(02\)00241-7](http://doi.org/10.1016/S0013-7952(02)00241-7)
- clv. Goudie, A. S. (2004). *Encyclopedia of Geomorphology*. In *Encyclopedia of Geomorphology* (Vol. 1, p. 1156). Routledge. <http://doi.org/10.4324/9780203381137>
- clvi. Guzzetti, Cardinali, Reichenbach, & Carrara. (2000). Comparing Landslide Maps: A Case Study in the Upper Tiber River Basin, Central Italy. *Environmental Management*, 25(3), 247–263.
- clvii. H.A.Nefeslioglu, C.Gokceoglu, H. S. (2008). An assessment on the use of logistic regression and artificial neural networks with different sampling strategies for the preparation of landslide susceptibility maps. *Engineering Geology*, 97(3-4), 171–191. <http://doi.org/10.1016/J.ENGGE0.2008.01.004>
- clviii. Hammond, C.J.; Prellwitz, R.W.; Miller, S. . (1991). Landslide hazard assessment using Monte Carlo simulation. In *Proceedings 6th International symposium of landslides* (pp. 959–964). New Zealand.
- clix. Hasan Jahid Tusher, Minhaj Uddin, P. D. and A. C. (2017, June). Fuel crisis hits Rangamati, search underway. *The Daily Star*.
- clx. Horelli, J. A. (2005). *Landslides in Hong Kong*. University of Helsinki.
- clxi. Huang, J. (2014). *Investigation on landslide susceptibility using remote sensing and GIS methods*. Hong Kong Baptist University.
- clxii. IFRC. (2016). *World Disasters Report 2016*. IFRC.
- clxiii. Intarawichian, N., & Dasananda, S. (2010). ANALYTICAL HIERARCHY PROCESS FOR LANDSLIDE SUSCEPTIBILITY MAPPING IN LOWER MAE CHAEM WATERSHED, NORTHERN THAILAND. *Suranaree J. Sci. Technol*, 7(3).
- clxiv. IPCC. (2007). *IPCC Fourth Assessment Report: Climate Change 2007 (AR4)*.
- clxv. Iverson, R. M. (2000). Landslide triggering by rain infiltration. *Water Resources Research*, 36(7), 1897–1910. <http://doi.org/10.1029/2000WR900090>
- clxvi. Jebur, M. N., Pradhan, B., Shafri, H. Z. M., Yusoff, Z. M., & Tehrany, M. S. (2015). An integrated user-friendly ArcMAP tool for bivariate statistical modelling in geoscience applications. *Geoscientific Model Development*, 8(3), 881–891. <http://doi.org/10.5194/gmd-8-881-2015>
- clxvii. Kanungo, D. P., Arora, M. K., Sarkar, S., & Gupta, R. P. (2009). Landslide Susceptibility Zonation (LSZ) Mapping - A Review. *Journal of South Asia Disaster Studies*, 2(1), 81–106.
- clxviii. Kienholz, H., Hafner, H., Schneider, G., & Tamrakar, R. (1983). Mountain Hazards Mapping in Nepal's Middle Mountains Maps of Land Use and Geomorphic Damages (Kathmandu-Kakani Area). *Mountain Research and Development*, 3(3), 195–220.
- clxix. L Yin, K & Z Yan, T. (1988). Statistical Prediction models for slope instability of metamorphosed rocks. In *Proceedings of 5th Int Symp on Landslides*. Lausanne.
- clxx. Lee, C. (2015). Review and Perspectives on Methodology for Landslide Hazard Analysis. 10th Asian Regional Conference of IAEG, 1–6.
- clxxi. Lee, S., & Choi, J. (2004). Landslide susceptibility mapping using GIS and the weight-of-evidence model. *International Journal of Geographical Information Science*, 18(8), 789–814. <http://doi.org/10.1080/13658810410001702003>
- clxxii. Lin, Y.-P., Chu, H.-J., & Wu, C.-F. (2010). Spatial pattern analysis of landslide using landscape metrics and logistic regression: a case study in Central Taiwan. *Hydrology and Earth System Sciences Discussions*, 7(3), 3423–3451. <http://doi.org/10.5194/hessd-7-3423-2010>
- clxxiii. Malczewski, J. (1999). GIS and multicriteria decision analysis. *Engineering* (Vol. 31).

- clxxiv. McCalpin, J. (1984). Preliminary age classification of landslides for inventory mapping. *Annual Symposium on Engineering Geology and Soil Engineering* 21, (January 1984), 99–111.
- clxxv. Mezughi, T. H., Akhir, J. M., Rafek, A. G., & Abdullah, I. (2011). Landslide susceptibility assessment using frequency ratio model applied to an area along the E-W highway (Gerik-Jeli). *American Journal of Environmental Sciences*, 7(1), 43–50. <http://doi.org/10.3844/ajessp.2011.43.50>
- clxxvi. Montgomery, D. R., & Dietrich, W. E. (1994). A physically based model for the topographic control on shallow landsliding. *Water Resources Research*, 30(4), 1153–1171. <http://doi.org/10.1029/93WR02979>
- clxxvii. Moser, H., Morgenschweis, G., Hydro-, H. Z. I., & Hallsworth, E. G. (1989). Book reviews, 14, 361–362.
- clxxviii. Nandi, A., & Shakoor, A. (2006). Preparation of a landslide susceptibility map of Summit County, Ohio, USA, using numerical models. In *Proceedings of the 10th IAEG Congress*, Nottingham, UK (Vol. 610).
- clxxix. Neuhäuser, B. (2014). Landslide Susceptibility and Climate Change Scenarios in Flysch Areas of the Eastern Alps.
- clxxx. Neuhäuser, B., & Terhorst, B. (2007). Landslide susceptibility assessment using “weights-of-evidence” applied to a study area at the Jurassic escarpment (SW-Germany). *Geomorphology*, 86(1-2), 12–24. <http://doi.org/10.1016/j.geomorph.2006.08.002>
- clxxxi. Nirapad. (2017). Hazard Incidents in Bangladesh , April 2017.
- clxxxii. P. Gupta, R & C. Joshi, B. (1990). Landslide Hazard Zonation using the GIS Approach - A case Study from the Ramganga Catchment Himalayas. *Engineering Geology*, 28, 119–131.
- clxxxiii. Park, S., Choi, C., Kim, B., & Kim, J. (2013). Landslide susceptibility mapping using frequency ratio, analytic hierarchy process, logistic regression, and artificial neural network methods at the Inje area, Korea. *Environmental Earth Sciences*, 68(5), 1443–1464. <http://doi.org/10.1007/s12665-012-1842-5>
- clxxxiv. Pradhan, B., & Lee, S. (2010). Delineation of landslide hazard areas on Penang Island, Malaysia, by using frequency ratio, logistic regression, and artificial neural network models. *Environmental Earth Sciences*, 60(5), 1037–1054. <http://doi.org/10.1007/s12665-009-0245-8>
- clxxxv. Pradhan, B., Oh, H., Buchroithner, M., & Buchroithner, M. (2010). Weights-of-evidence model applied to landslide susceptibility mapping in a tropical hilly area. *Geomatics, Natural Hazards and Risk*, 1(3). <http://doi.org/10.1080/19475705.2010.498151>
- clxxxvi. Rahman, T. (2012). LANDSLIDE RISK REDUCTION OF THE INFORMAL FOOTHILL SETTLEMENTS OF CHITTAGONG CITY THROUGH STRATEGIC DESIGN MEASURE A Dissertation for the Degree of Master in Disaster Management Tanvia Rahman Summer 2012 Postgraduate Programs in Disaster Management (PPDM. BRAC University.
- clxxxvii. reliefweb. (2017). Bangladesh: Floods and Landslides - Jun 2017 | ReliefWeb.
- clxxxviii. Reuters. (2007). Bangladesh landslide toll reaches 128.
- clxxxix. Rossi, M., & Reichenbach, P. (2016). LAND-SE: A software for statistically based landslide susceptibility zonation, version 1.0. *Geoscientific Model Development*, 9(10), 3533–3543. <http://doi.org/10.5194/gmd-9-3533-2016>
- cxc. Sarwar, M. G. M. (2008). Landslide Tragedy of Bangladesh. In *The First World Landslide Forum*. Tokyo.
- cxci. Schuster, R. L., & Fleming, R. W. (1986). Economic Losses and Fatalities Due to Landslides. *Environmental & Engineering Geoscience*, xxiii(1). <http://doi.org/10.2113/gseegeosci.xxiii.1.11>
- cxcii. Shahabi, H., Ahmad, B. B., & Khezri, S. (2013). Evaluation and comparison of bivariate and

- multivariate statistical methods for landslide susceptibility mapping (case study: Zab basin). *Arabian Journal of Geosciences*, 6(10), 3885–3907. <http://doi.org/10.1007/s12517-012-0650-2>
- cxci. Soeters, R. & W. C. (1996). Slope instability Recognition, analysis and zonation (PDF Download Available). (R. L. Turner, A.K., Schuster, Ed.) *Landslide: Investigations and Mitigation*. Washington, D.C.
- cxci. Thanh, L. N., & de Smedt, F. (2012). Application of an analytical hierarchical process approach for landslide susceptibility mapping in A Luoi district, Thua Thien Hue Province, Vietnam. *Environmental Earth Sciences*, 66(7), 1739–1752. <http://doi.org/10.1007/s12665-011-1397-x>
- cxci. UN RC. (2017). Bangladesh: HCTT Response Plan (June-December 2017) - Bangladesh | ReliefWeb.
- cxci. Vakhshoori, V., & Zare, M. (2016). Landslide susceptibility mapping by comparing weight of evidence, fuzzy logic, and frequency ratio methods. *Geomatics, Natural Hazards and Risk*, 7(5), 1731–1752. <http://doi.org/10.1080/19475705.2016.1144655>
- cxci. van Westen, C. J. (1994). GIS in landslide hazard zonation: a review, with examples from the Andes Colombia. *Mountain Environment and Geographic Information Systems*, (January 1994), 135–165.
- cxci. Van Westen, C. J., Ghosh, S., Jaiswal, P., Martha, T. R., & Kuriakose, S. L. (2011). From landslide inventories to landslide risk assessment; an attempt to support methodological development in India. In the *Second World Landslide Forum* (Vol. 1, pp. 3–20). <http://doi.org/10.1007/978-3-642-31325-7-1>
- cxci. van Westen, C. J., van Asch, T. W. J., & Soeters, R. (2005). Landslide hazard and risk zonation - Why is it still so difficult? *Bulletin of Engineering Geology and the Environment*, 65(2), 167–184. <http://doi.org/10.1007/s10064-005-0023-0>
- cc. Westen, C. J. va., Alkema, D., Kerle, N., & Kingma, N. C. (2011). Multi-hazard risk assessment. The Netherlands: United Nations University—ITC School on Disaster Geo-Information Management.
- cci. Westen, C. J. Van. (1993). Application of Geographic Information Systems to Landslide Hazard Zonation (PDF Download Available). Technical University of Delft.
- ccii. Westen, C. J. Van, Alkema, D., Damen, M. C. J., Kerle, N., & Kingma, N. C. (2011). Multi-hazard risk assessment. Distance education course. Guide book, 371.
- cciii. Westen, C. J. van, Rengers, N., Terlien, M. T. J., & Soeters, R. (1997). Prediction of the occurrence of slope instability phenomenal through GIS-based hazard zonation. *Geologische Rundschau*, 86(2), 404–414. <http://doi.org/10.1007/s005310050149>
- cciv. Wieczorek, G. F. (1983). PREPARING A DETAILED LANDSLIDE-INVENTORY MAP FOR HAZARD EVALUATION AND REDUCTION. *Bulletin of the Association of Engineering Geologists*, 21(3), 337–342.
- ccv. Yilmaz, I., & Yildirim, M. (2006). Structural and geomorphological aspects of the Kat landslides (Tokat-Turkey) and susceptibility mapping by means of GIS. *Environmental Geology*, 50(4), 461–472. <http://doi.org/10.1007/s00254-005-0107-y>
- ccvi. Zêzere, J. L.; Reis, E.; Garcia, R.; Oliveira, S.; Rodrigues, M. L.; Vieira, G.; Ferreira, A. B. (2004). Integration of spatial and temporal data for the definition of different landslide hazard scenarios in the area north of Lisbon (Portugal). *Natural Hazards and Earth System Science*, 4(1), 133–146. <http://doi.org/10.5194/nhess-4-133-2004>
- ccvii. Zhou, S., Chen, G., Fang, L., & Nie, Y. (2016). GIS-based integration of subjective and objective weighting methods for regional landslides susceptibility mapping. *Sustainability (Switzerland)*, 8(4). <http://doi.org/10.3390/su8040334>